CORA Cork Open Research Archive
Cartlann Taighde Oscailte Chorcaí

Title	Modelling the tumour microenvironment and reversible and irreversible chemotherapy resistance
Authors	Quinlan, Thomas
Publication date	2024
Original Citation	Quinlan, T. 2024. Modelling the tumour microenvironment and reversible and irreversible chemotherapy resistance. MRes Thesis, University College Cork.
Type of publication	Masters thesis (Research)
Rights	© 2024, Thomas Quinlan. - https://creativecommons.org/licenses/by/4.0/
Download date	2026-11-06 12:21:42
Item downloaded from	https://hdl.handle.net/10468/17027



UCC
University College Cork, Ireland
Coláiste na hOllscoile Corcaigh

Ollscoil na hÉireann, Corcaigh
National University of Ireland, Cork



University College Cork, Ireland
Coláiste na hOllscoile Corcaigh

Modelling the Tumour Microenvironment and Reversible and Irreversible Chemotherapy Resistance

Thesis presented by

Thomas Quinlan, BSc

for the degree of

Masters by Research

University College Cork
School of Mathematical Sciences

Head of School:	Dr Kevin Hayes
Primary Supervisor:	Prof. Sebastian Wieczorek
Secondary Supervisors:	Dr Hassan Alkhayuon
	Dr Kieran Mulchrone

2024

Contents

1 Introduction **1**

1.1 Cancer Research and the Role of Mathematical Modelling 1

1.2 The Tumour Microenvironment 1

1.2.1 Cancer Cells 2

1.2.2 The Tumour Stroma 2

1.2.3 The Immune System 3

1.2.4 Cancer Immunoediting: The Extinction Threshold 3

1.3 Mathematical Modelling of Cancer 4

1.4 Aims and Objectives 6

1.5 Thesis Outline 6

2 Model Derivation and Sanity Checks **7**

2.1 Model Flowchart 7

2.2 Cancer Equations 11

2.2.1 Sensitive Cancer Equation ($\dot{x}_1$) 11

2.2.2 Resistant Cancer Equation ($\dot{x}_2$) 17

2.2.3 $\dot{x}_1$ and $\dot{x}_2$ System Sanity Check. 20

2.3 Active & Inactive Stroma Equations ($\dot{x}_3$ & $\dot{x}_4$) 29

2.3.1 $\dot{x}_3$ and $\dot{x}_4$ System Sanity Check. 37

2.4 Immune System Equation ($\dot{x}_5$) 41

2.4.1 $\dot{x}_5$ Sanity Check. 50

2.4.2 $\dot{x}_5$ and $\dot{x}_1$ with No Treatment System Sanity Check. 53

3 Complete Model Equations **64**

3.1 Simplifying Assumptions and Non-Dimensionalisation 64

4 Model Simulations Without Treatment: **67**

4.1 Reduced Model A: Cancer Growth without the Stroma, the Immune System or Treatment. 67

4.2 Reduced Model B: Cancer Growth without the Immune System or Treatment. 69

4.3 Complete Model: Cancer Growth without Treatment. 73

5 Model Simulations With Treatment: **77**

5.1 Treatment Regimens and Pharmacokinetics 80

5.2 Simulations 82

6 Conclusions and Results: **89**

A Calculations **91**

A.1 Calculations for the Sanity Check of the $\frac{d\tilde{x}_1}{dt}$ and $\frac{d\tilde{x}_2}{dt}$ Equations. . 91

A.1.1 Solving for the equilibrium points. 91

A.1.2 Computing the eigenvalues and eigenvectors corresponding to e_0, e_1 and e_2. 93

A.1.3 Proving that the lines passing through the points e_0 and e_1, e_0 and e_2, and e_1 and e_2 are invariant sets. 100

A.2 Showing Conditions (1) and (2) Both Hold if $\frac{a_3}{e^{a_3}-1} < \frac{\delta_3}{\nu_3} < 1$. 103

A.3 Showing $\tilde{x}_3^e$ is non-decreasing when $\tilde{C} = 0$ or $\tilde{D} = 0$. 103

A.4 Solving for $\tilde{D}_{\text{opt},5}$. 105

A.5 Reparameterising the Immune Response to Cancer. 106

A.6 Solving for the Condition that $\tilde{d} > \tilde{M}$ for the Existence of $\tilde{x}_5^e$. . . 110

A.7 Behaviour of $\tilde{x}_5^e$ on separate intervals of $\tilde{C}$. 113

A.8 Solving for $\psi_{0,1,2,3}$. 114

B Complete Model Equations Prior to Any Rescalings. **116**

C Code Availability Statement **117**

This is to certify that the work I am submitting is my own and has not been submitted for another degree, either at University College Cork or elsewhere. All external references and sources are clearly acknowledged and identified within the contents. I have read and understood the regulations of University College Cork concerning plagiarism and intellectual property.

Thomas Quinlan
September 2024

Acknowledgements

First and foremost, I would like to sincerely thank my supervisors, Prof. Sebastian Wieczorek, Dr Hassan Alkhayuon and Dr Kieran Mulchrone, for their unwavering support and guidance over the course of this year. Their support not only helped me elevate the standard of my thesis far beyond what I could have achieved alone, but also provided me with invaluable advice for my future career.

I would also like to thank a number of other academic and medical professionals whose expert advice made the completion of this thesis possible. I deeply appreciate the help of Dr Sharon McKenna, Principal Investigator at Cancer Research UCC, who met with me on several occasions to discuss the effects of chemotherapy on the stroma and immune system, and who emphasised the critical role of the immune population within the tumour microenvironment. I would also like to express my gratitude to Dr Micheal O'Riordain, Clinical Professor of Surgery at UCC and Chair of the Department of Surgery at Mercy University Hospital Cork. Dr O'Riordain's expert feedback helped both validate and challenge some of the early modelling assumptions I made, ultimately improving the model. Finally, I am particularly grateful to Dr Noemi Picco, Senior Lecturer in Mathematical Biology at Swansea University, who first inspired me to explore mathematical models of the tumour stroma and who subsequently answered my many questions on the subject.

Last but not least I would like to thank my parents, family, and friends for their endless support throughout the year and for helping to keep me motivated.

Abstract

The tumour microenvironment (TME) comprises various cell types, including cancer cells, immune cells, and stromal cells, which all engage in complex, dynamical interactions. Understanding these interactions, particularly their role in promoting cancer growth and the emergence of drug resistance, is crucial for developing effective treatment strategies. This project constructs a comprehensive mathematical model of the TME that incorporates the effects of chemotherapy. We systematically derive a series of process-based equations to describe the tripartite interactions between cancer cells, immune cells and stromal cells within the TME, as well as their response to chemotherapy. Throughout the model development, we analyse sub-models to ensure we capture key qualitative behaviours. Finally, we conduct a qualitative study by simulating our model under various hypothetical TME scenarios and different chemotherapy dosing schedules. Our simulations demonstrate how variations in stromal activity and treatment regimens can lead to diverse patient outcomes, highlighting the need for personalised treatment strategies.

1 Introduction

1.1 Cancer Research and the Role of Mathematical Modelling

Cancer is a disease characterised by the uncontrolled growth of a population of malignant cells and it impacts the lives of millions every year. Europe's Beating Cancer Plan projects that without proactive measures, cancer-related deaths will surge by over 24% by 2035, making it the leading cause of death in the EU [15]. According to the 'vital statistics yearly summary' published by the Irish Central Statistics Office (CSO), cancer overtook circulatory diseases as the leading cause of death in Ireland in 2022, accounting for 29% of all mortalities [58]. Stark facts like these underscore the importance and necessity of interdisciplinary research that enhances our understanding of cancer and leads to the optimisation of treatment strategies.

Mathematical modelling is an excellent tool to aid in this research. Models can make both qualitative and quantitative predictions about cancer growth and its response to different types of treatment. Scientists can use computer simulations to guide decision-making when designing laboratory experiments, which saves time, money and resources [3]. Mathematical models can also be used to identify the optimal way to administer a given treatment [77], even in a patient specific manner if personalised data is incorporated into the model [57, 28]. The biological components and cellular interactions that contribute to the growth of cancer cells are highly complex and mathematical models are well equipped to describe these interactions and often elucidate unexpected outcomes. In this work, we aim to model the interactions that occur between key elements of the tumour microenvironment (TME): cancer cells, stromal cells and immune cells, with the aim of gaining an improved understanding of the outcomes of these complex interactions and how they impact the efficacy of chemotherapy.

1.2 The Tumour Microenvironment

The TME refers to that which resides in the spatial vacinity of the cancer cell population [40]. It consists of the cancer cells themselves, stromal cells, immune cells, vasculature and a non-cellular protein network called the extra-cellular matrix (ECM).

1.2.1 Cancer Cells

Cellular proliferation is a tightly controlled process and the population sizes of cells within various tissues are carefully maintained. Mistakes during cell-division, or damage from carcinogens, can lead to alterations in one or more of the growth-controlling genes of an otherwise healthy cell. This can cause the cell to become cancerous; it divides uncontrollably and can invade surrounding tissue. This eventually gives rise to tumours, large groups of cancer cells, that can metastasise to distant parts of the body [86].

There are many different types of cancer and they are classified by the type of tissue in which they originate. Carcinomas, such as breast, lung and colon cancer, arise from epithelial tissues which form the lining of organs and body cavities. Sarcomas are rare cancers that originate in connective tissue, bone, fat and muscle. Hematologic cancers, such as Leukemia, are cancers of the blood. These do not form a solid tumour mass; rather, cancerous cells circulate through the blood, lymphatic system or bone marrow [5]. Our focus will be on solid tumours, such as carcinomas, that have dense stromal compartments.

There are many different treatments that aim to reduce the size of a cancer cell population, but chemotherapy remains the main treatment modality [10]. Chemotherapeutic drugs are cytotoxic chemicals that arrest the growth of or induce apoptosis (programmed cell death) in actively proliferating cells, primarily targeting cancer cells [56]. Chemotherapy can initially stimulate an immune response but high doses can be toxic, resulting in immune supression. Chemotherapy also has dose dependent effects on the stroma which we discuss in detail during the model derivation.

1.2.2 The Tumour Stroma

The stroma is the connective and supportive tissue of an organ, that does not perform the function of that organ [20, p.2017-2019]. It consists of the basement membrane, fibroblasts and vasculature cells that are all surrounded by the ECM [34, 8]. The stroma can undergo physiological changes as a healing response to a wound or cancer at which point it is termed the active stroma. Here we are interested in cancer activated stroma.

Fibroblasts, a major component of the stroma, are ordinarily in a dormant state; however, in response to a wound, they may 'activate' and become myofibroblasts. As myofibroblasts, they are more biologically 'active,' secreting cell signalling proteins and restructuring the ECM. At the end of the wound healing process, the number of myofibroblasts reduces through apoptosis [34, 17]. This same wound healing response is triggered in the context of cancer, however

the cancerous lesion never heals leading to the perpetual activation of fibroblasts which are then termed 'cancer associated fibroblasts' (CAFs) [34]. CAFs are abundant in the tumour stroma and strongly influence tumour growth [21]. Many of the dynamical processes involving the stroma that we will model are mediated through CAFs.

Emerging evidence suggests that CAFs are a heterogeneous population of cells with both tumour promoting and tumour restraining types. Tumour promoting CAFs have been thoroughly investigated but study of tumour restraining CAFs is still in its infancy [4, 45]. Here we focus on the tumour promoting CAFs.

1.2.3 The Immune System

Cells of the immune system make up another important component of the TME. They can be divided into two groups, innate and adaptive. The innate immune system consists of non-specific immune cells which react rapidly to any pathogen or infection. Cells of the innate immune response include neutrophils, natural killer cells and dendritic cells. Neutrophils and natural killer cells can kill tumour cells without needing to be activated, and dendritic cells help to activate the adaptive immune response. The adaptive immune response consists of cells that are primed to respond to specific threats. These cells include both cytotoxic and regulatory T-cells. Cytotoxic T-cells recognise antigens on cancer cells and kill them by injecting proteins that induce apoptosis. Regulatory T-cells restrain the activity of cytotoxic T-cells to prevent auto-immune diseases [79, 18]. The innate and adaptive arms of the immune system play critical roles in preventing the onset of cancer by seeking and eliminating early neoplasms. This process is known as immunosurveillance [82].

An important area of ongoing research is that of immunotherapy. Immunotherapy aims to generate a potent anti-tumour response of the patient's own immune system [6]. We do not model such treatment here but, by including the immune system in our model, future work can easily extend it to include the effects of an immunotherapy regimen.

1.2.4 Cancer Immunoediting: The Extinction Threshold

The process of immunosurveillance can eventually fail. This occurs either due to changes in the cancer cell population or through cancer-induced immune suppression [82]. The transition from immunosurveillance to cancer progression is known as the process of 'cancer immunoediting' and it consists of three distinct stages: elimination, equilibrium and escape. **Elimination:** Healthy cells transform into cancerous cells as described in Section 1.2.1. Innate and adaptive immune cells

detect and eliminate the vast majority of these cancerous cells through immunosurveillance. This occurs before the cancer cells have time to form a clinically relevant tumour. **Equilibrium:** A state in which there is a balance between immune system control and tumour growth, resulting in a small, dormant cancer cell population. **Escape:** The cancer cells escape the immune system's control through various immune suppressing mechanisms which leads to uncontrolled growth [83]. When modelling this process it will be important to ensure that there exists an 'extinction threshold' in the cancer population. This is a small population size below which cancer cells are 'eliminated' by the immune system and above which cancer cells 'escape' and proliferate to a lethal size.

1.3 Mathematical Modelling of Cancer

Altrock et al. [3] provide an overview of the wide range of mathematical modelling techniques used in cancer research. These include stochastic branching processes, which have been used to model the accumulation of random mutations during cell divisions over discrete cellular generations. Such models are easy to work with, but often lack spatial information and the other elements of the TME. Ordinary and partial differential equations, (ODEs) and (PDEs), are also often used. ODEs can describe the dynamics of cancer and its environment over time; PDEs can additionally incorporate how the variables of the system vary across space. Another modelling approach is that of evolutionary game theory (EGT). EGT frames cancer treatment as a strategic game played by a 'rational physician' and an 'adaptive cancer population' which evolves resistance strategies to combat the physicians treatment strategies. Such models are useful for finding optimal treatment strategies to overcome drug resistance [77].

Byrne et al. [11] outline the need for a suite of mathematical models, each capturing biological phenomena at different scales. The outputs of models at one scale can serve as inputs for models at another, which helps to break down the modelling problem while maintaining both tractability and understanding at every level. The focus of our work will be to build a high-level ODE model of the TME at the macro scale which can fit into this suite of models. There are some foundational considerations to be made when constructing such a model, such as which underlying cancer growth model to use and how to model the effects of chemotherapy.

The simplest cancer growth models include:

1. The logistic growth model: $\dot{x} = rx\left(1 - \frac{x}{K}\right)$.
2. The generalised logistic growth model: $\dot{x} = rx\left(1 - \left(\frac{x}{K}\right)^{\nu}\right)$.

3. The gompertz growth model: $\dot{x} = rx \ln\left(\frac{K}{x}\right)$.

In each case x denotes the size of the cancer cell population, $r > 0$ is a growth rate parameter, $\nu > 0$ determines whether the maximum growth rate occurs for population sizes closer to $x = 0$ or $x = K$, and $K > 0$ is the population carrying capacity, i.e. the maximum size of the population that can be sustained given the environmental constraints. Our model will build upon the simplest of these models, the logistic growth model. However, future work could explore how using other growth models as a base might affect our model's output.

There are two fundamental approaches to incorporate the effects of chemotherapy into such models and these are:

1. The log-kill hypothesis: $\dot{x} = rx\left(1 - \frac{x}{K}\right) - \delta D(t)x$.
2. The Norton-Simon hypothesis: $\dot{x} = r\left(1 - \delta D(t)\right)x\left(1 - \frac{x}{K}\right)$.

Here $\delta > 0$ is a constant that determines the rate of drug induced death and $D(t) > 0$ represents the concentration/intensity of the drug over time. The log-kill hypothesis assumes that a given dose of chemotherapy will kill the same fraction of the tumour regardless of its size at treatment onset. The Norton-Simon hypothesis assumes that the rate of cell kill becomes small for large tumours due to their slowing growth [55]. The cancer growth rate in our model will be influenced by numerous interactions between elements of the TME and as such we opt to work with the simpler log-kill hypothesis.

There exist many ODE models of tumour-stroma and tumour-immune interaction in the literature. Picco et al. [64] investigate how therapy-induced activation of the stroma can lead to the emergence of reversible resistance to targeted therapy, however they omit the activation of the stroma in response to cancer growth itself. Flach et al. [25] on the other hand construct a compartment model that does account for such cancer induced activation. Their model is very simple and resultantly misses a number of key features such as the spatial competition between cancer and stromal cells and the tendency of cancer to develop irreversible, genetic resistance to treatment. Kuznetsov et al. [38] develop a predator-prey model of cancer and immune cell interaction, but their work does not consider the effects of any treatment regimen.

Seager et al. [72] underline the importance of understanding the dynamic, tripartite interaction between cancer cells, immune cells and the stroma in order to fully understand the mechanisms of cancer progression. There is less mathematical work covering the interactions of all three of these TME components and that is what we hope to address. We aim to build upon the models developed by Picco et al., Flach et al., and Kuznetsov et al. to create a more comprehensive model of the TME.

1.4 Aims and Objectives

The aims of our research are as follows:

1. Develop a high-level, macro-scale model of the TME that incorporates the tripartite interaction between cancer cells, immune cells and the stroma as well as their response to chemotherapeutic treatment.

2. Validate our model's ability to reproduce key qualitative behaviour.

Our objectives are as follows:

1. Derive our process-based equations term by term.

2. Analyse submodels throughout model development to confirm its validity.

3. Identify rough parameter estimates from the literature and use them in a qualitative study of our model's behaviour across various biological scenarios and treatment approaches.

1.5 Thesis Outline

The structure of the remainder of this thesis is as follows:

1. At the beginning of Section 2 and throughout Section 2.1, we introduce our model variables and provide flowcharts that give a high-level overview of how these variables interact.

2. Throughout Sections 2.2.1 to 2.4.2 we derive the equations of our model, term by term.

3. Throughout the model derivation, in Sections 2.2.3, 2.3.1, 2.4.1, and 2.4.2, we carry out sanity checks of our model's equations. We fix certain variables in time and analyse the resultant simple systems. Doing this provides insight into the outcomes of various processes and helps us to identify areas for future improvement of the model.

4. In Section 3, we provide the complete system of model equations and subsequently non-dimensionalise them.

5. In Section 4, we simulate our model without treatment across various biological scenarios.

6. In Section 5, we simulate our model for two chemotherapy regimens: a maximum-tolerated dose regimen and low-dose metronomic regimen.

7. Finally in Section 6, we state our results and provide an outlook for future work.

2 Model Derivation and Sanity Checks

Our process-based model consists of the following five variables:

1. x_1 - Chemotherapy-sensitive cancer.
2. x_2 - Chemotherapy-resistant cancer.
3. x_3 - The active stroma.
4. x_4 - The inactive stroma.
5. x_5 - The immune system.

$x_i \geq 0$ for all $i \in \{1, ..., 5\}$. $D(t) \in [0, D_{\text{MTD}}]$ is the intensity of chemotherapy at time t. $D(t) = 0$ implies chemotherapy is not being applied and $D(t) = D_{\text{MTD}}$ corresponds to the maximum tolerated dose (MTD). We follow [64] and assume the total amount of stroma remains fixed over time and simply switches from inactive to active and vice versa. This implies $x_3(t) + x_4(t) = T > 0$ with $T \in \mathbb{R}$ constant for all time t. Flowcharts of the model processes are given in Subsection 2.1 and detailed derivations of the model terms are provided in Subsections 2.2.1-2.4. Throughout this derivation, all parameters we introduce can be assumed to be greater than or equal to zero unless otherwise stated.

2.1 Model Flowchart

The model flowcharts consists of boxes and links.

Boxes:

- Each red box represents a certain cell type or variable within our model and they are labelled accordingly.
- Each green boxes represents chemotherapy, a time dependent parameter of our model.

Blue, Arrow-Tipped Links:

1. Links pointing to the same box from which they originate represent the birth of cells in that box.

2. Links pointing to a different box from which they originate indicate a change of cell type in that link's direction. The cell type from which the arrow originates experiences a reduction in its growth rate that is equal to the increase in the growth rate of the cell type the arrow points to.

3. Links originating from an empty circle represent an external influx of cells in the box they point to.

4. Links pointing from a box to a link represent enhancement of the process they point to.

Red, Flat-Tipped Links:

1. Links pointing to the same box from which they originate represent the death of cells in that box.

2. Links pointing to a different box from which they originate, indicate the death of cells in the box they point to, due to cells/chemotherapy in the originating box.

3. Links pointing from a box to a link represent suppression of the process they point to.

Flowcharts

The numbering of the links in each flowchart correspond to the numbering of the equation terms derived in subsections 2.2.1-2.4. The complete model involves a large number of processes. To ensure clarity, we introduce the model flowchart in stages through [Fig. 1-4]. [Fig. 1] illustrates the model processes with only sensitive cancer cells present, excluding the stroma, the immune system and chemotherapy. Processes involving these excluded components are faded out. [Fig. 2] extends the model flowchart by including the stroma, while processes involving the immune system and chemotherapy remain faded. [Fig. 3] further includes the immune system. Finally, [Fig. 4] presents the complete model, including all processes when chemotherapy is also applied.

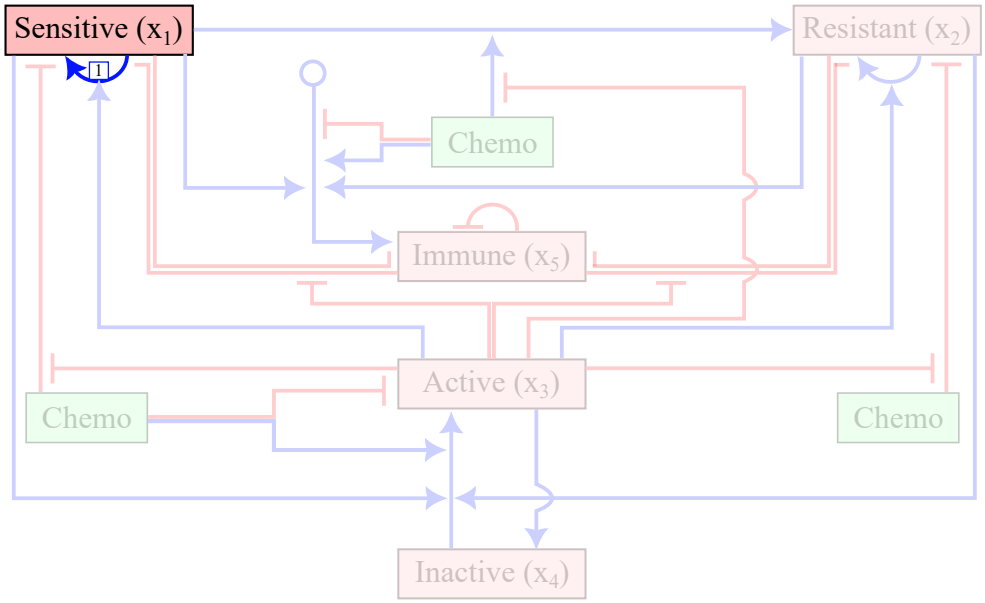


Figure 1: Flowchart of model processes without the stroma, immune system or chemotherapy (these processes are faded out). Chemotherapy-sensitive cancer cells grow without interacting with any other cells.

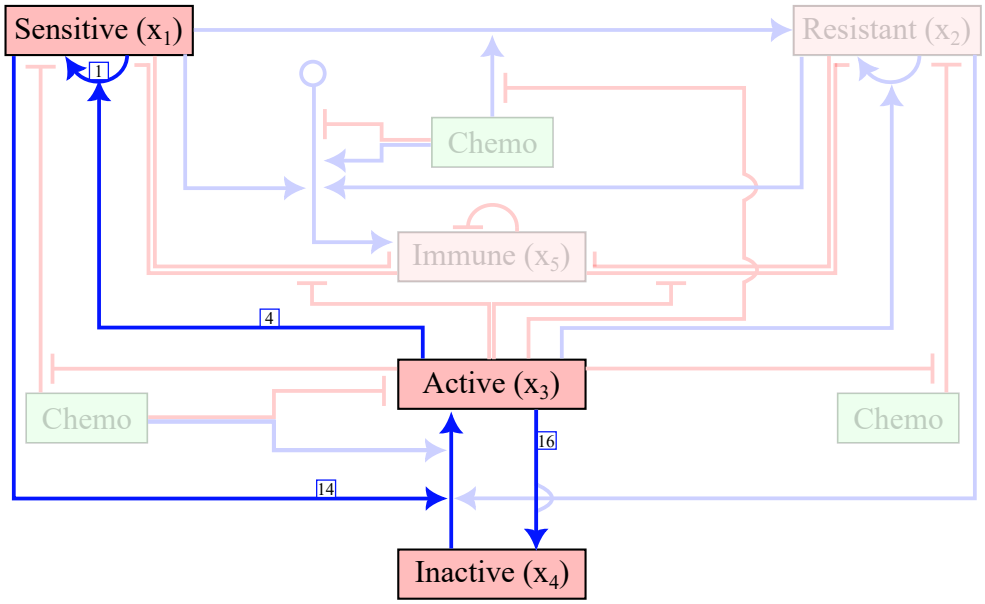


Figure 2: Flowchart of model processes without the immune system or chemotherapy. Chemotherapy-sensitive cancer cells grow and cooperate with the active stroma.

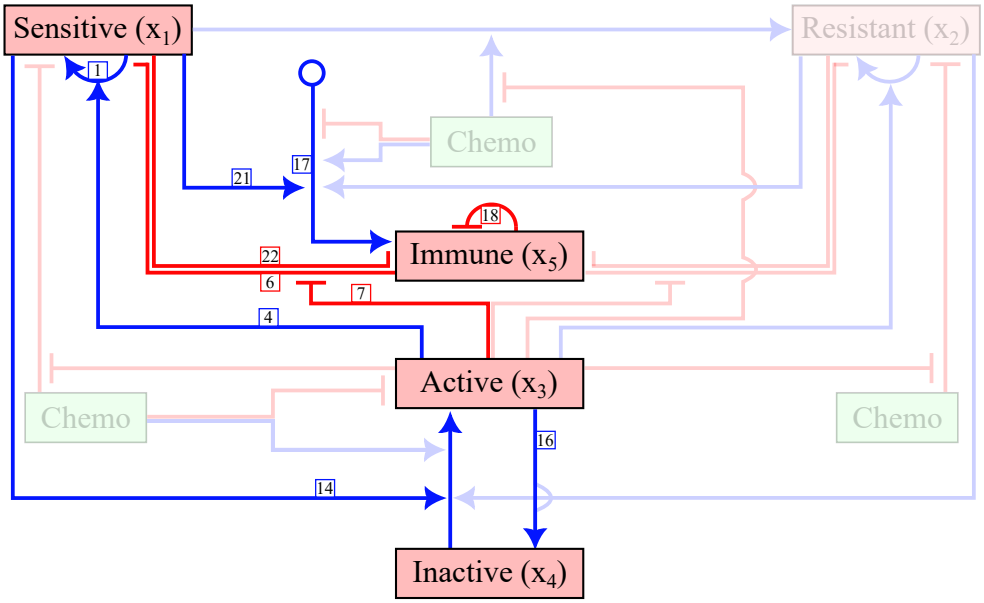


Figure 3: Flowchart of model processes without chemotherapy. Chemotherapy-sensitive cancer cells grow and cooperate with the active stroma. Competition exists between cancer and the immune system; the active stroma helps protect the cancer from immune attack.

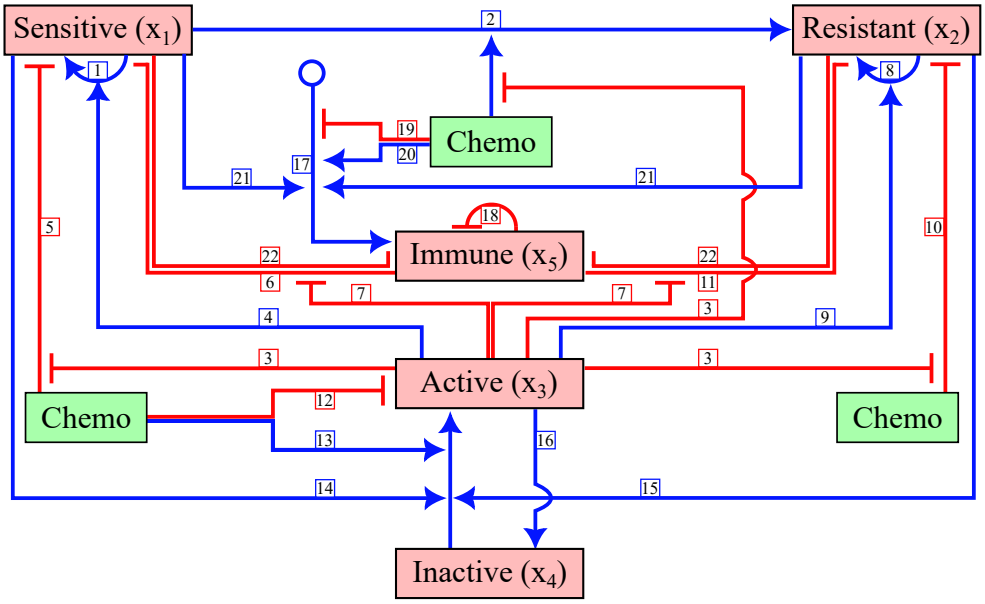


Figure 4: Complete flowchart of all model processes. Chemotherapy-sensitive cancer cells grow and cooperate with the active stroma. Competition exists between cancer and the immune system; the active stroma helps protect the cancer from immune attack. Chemotherapy attacks cancer, leading to the emergence of irreversible resistance. Chemotherapy exerts non-linear, dose-dependent effects on the immune system and the active stroma.

2.2 Cancer Equations

2.2.1 Sensitive Cancer Equation ($\dot{x}_1$)

We follow [1, p.1206] and define "invasive" cancer as a cluster of mutated cells which posses the following heritable properties:

(1) They continue reproducing past the normal limits on cell division.

(2) They invade surrounding tissue.

Our model of sensitive cancer growth will have the following form,

$$\begin{aligned}\dot{x}_1 =&\{\text{Growth}\} - \{\text{Competition}\} - \{\text{Chemotherapy Induced Death}\} \\ &- \{\text{Immune Induced Death}\}. \end{aligned} \tag{1}$$

(1) Proliferation of sensitive cancer. In the absence of treatment, we model unabated cellular division with the term,

$$r_1 x_1,$$

where r_1 is the per-capita growth rate of a small population of sensitive cancer cells in the absence of chemotherapy, the stroma and the immune system. This is the first growth term and our equation becomes,

$$\begin{aligned}\dot{x}_1 =&r_1 x_1 - \{\text{competition}\} - \{\text{Chemotherapy Induced Death}\} \\ &- \{\text{Immune Induced Death}\}.\end{aligned}$$

So far, this equation only describes exponential growth of the sensitive cancer cell population in time. We will proceed to add additional terms that account for other biological processes.

(2) Acquired irreversible drug resistance. Chemotherapy damages cancer cell DNA which can result in genetic mutations [37]. These mutations may provide cancer cells with irreversible, genetic resistance to chemotherapy. This type of resistance is called 'acquired resistance' since it develops during treatment [85].

To include such chemotherapy associated effects in our model, we define and work with the normalised chemotherapy intensity,

$$\tilde{D}(t) = \frac{D(t)}{D_{\text{MTD}}} \in [0, 1].$$

We will derive the remainder of our model in terms of the normalised quantity

$\tilde{D}(t)$. The complete model equations in terms of $D(t)$, prior to any rescaling, are provided in appendix B.

To model the development of chemotherapy resistance, we assume that during treatment, $\tilde{D}(t) \neq 0$, a proportion of sensitive cancer's daughter cells are born resistant. This results in a reduction of the per-capita growth rate of sensitive cells and we thus include the term,

$$-\lambda \tilde{D}(t) x_1,$$

in the $\dot{x}_1$ equation. Here, $\lambda \tilde{D}(t)$ is the per-capita birth rate of resistant cells born from parent sensitive cells and is proportional to chemotherapy intensity. This is the second growth term and our equation becomes,

$$\dot{x}_1 = \left(r_1 - \lambda \tilde{D}(t)\right) x_1 - \{\text{competition}\} - \{\text{Chemotherapy Induced Death}\} - \{\text{Immune Induced Death}\}.$$

(3) Reversible drug resistance Chemotherapy induced DNA damage drives resistance conferring mutations in cancer cells but CAFs offer protection from such damage. CAFs thicken the ECM, which limits effective drug diffusion, and secrete cytokines that impair cancer cell drug sensitivity [16, 24, 31]. This is termed 'reversible resistance' as it is lost when the stroma becomes inactive. These processes dampen the rate at which resistance conferring mutations occur. In the interest of model simplicity, we combine these effects into a single term,

$$e^{-\kappa_D x_3}.$$

We use this term to modulate drug intensity $\tilde{D}(t)$ as follows,

$$\tilde{D}(t) e^{-\kappa_D x_3}$$

such that the effect of a given drug intensity weakens as the stroma activates. The maximum reduction in drug intensity occurs for $x_3 = T$, in which case $\tilde{D}(t)$ is scaled by,

$$\mu = e^{-\kappa_D T}.$$

To visualise the reduction of $\tilde{D}(t)$ due to x_3, we will introduce the rescaling,

$$\tilde{x}_3 = \frac{x_3}{T},$$

and plot,

$$\tilde{D}(t) e^{-\tilde{\kappa}_D \tilde{x}_3} \tag{2}$$

against $\tilde{x}_3$ for various fixed values of $\tilde{D}(t) = \tilde{D}$ and $\tilde{\kappa}_D = \kappa_D T$ [Fig. 5].

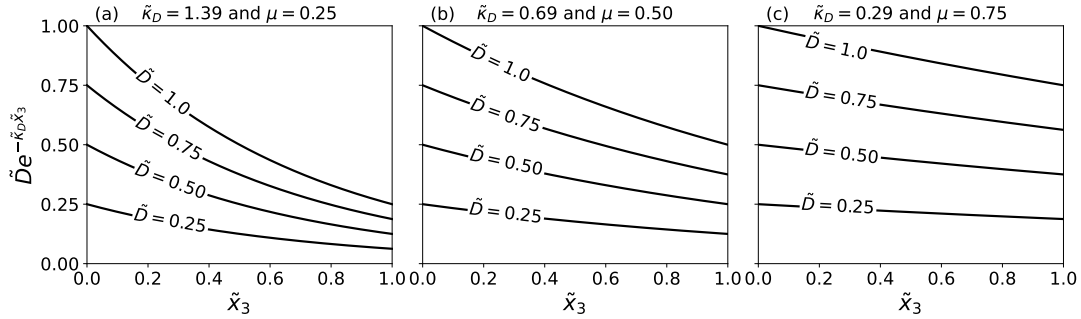


Figure 5: Plots of $\tilde{D}e^{-\tilde{\kappa}_D\tilde{x}_3}$ vs. $\tilde{x}_3$ [Eq. 2] for various $\tilde{D}$ and $\tilde{\kappa}_D$.

At times throughout the model derivation, we will temporarily rescale variables, as was done above. These rescalings help illustrate the model's terms and behaviour at different stages of its development. The complete set of variable rescalings used are provided in Section 3.1, and these will be permanently introduced prior to simulating the model.

To account for the active stroma mediated protection, the birth rate of resistant cells born from parent sensitive cells can be updated to,

$$-\lambda\tilde{D}(t)e^{-\kappa_D x_3}x_1,$$

and our equation becomes,

$$\dot{x}_1 = \left(r_1 - \lambda\tilde{D}(t)e^{-\kappa_D x_3}\right)x_1 - \{\text{competition}\} - \{\text{Chemotherapy Induced Death}\} - \{\text{Immune Induced Death}\}.$$

(4) Active-stroma enhancement of sensitive cancer growth. In addition to protecting cancer cells from chemotherapy, CAFs also secrete pro-inflammatory and growth cytokines that promote cancer cell proliferation [4, 16]. We model this with the term,

$$\rho_{13}\phi_1(x_3)x_1$$

where

$$\phi_1(x_3) = \frac{x_3(1+a_1)}{x_3 + a_1 T}.$$

This results in an enhancement of the per-capita growth rate of cancer with increasing x_3. We base the inclusion of the functional response term ϕ_1 on the assumption that cancer cells can process a limited amount of growth promoting molecules. As the tumour becomes densely populated with CAFs, most cancer cells will have already reached this limit, and as such the growth promotion must slow down for large x_3. This effect can be seen by plotting ϕ_1 vs. x_3 with various

values of a_1. For this figure we again make use of the rescaling $\tilde{x}_3 = \frac{x_3}{T}$, under which ϕ_1 becomes,

$$\tilde{\phi}_1(\tilde{x}_3) = \phi_1(T\tilde{x}_3) = \frac{\tilde{x}_3(1+a_1)}{\tilde{x}_3 + a_1}. \tag{3}$$

We then plot $\tilde{\phi}_1$ vs. $\tilde{x}_3$ for various values of a_1 [Fig. 6].

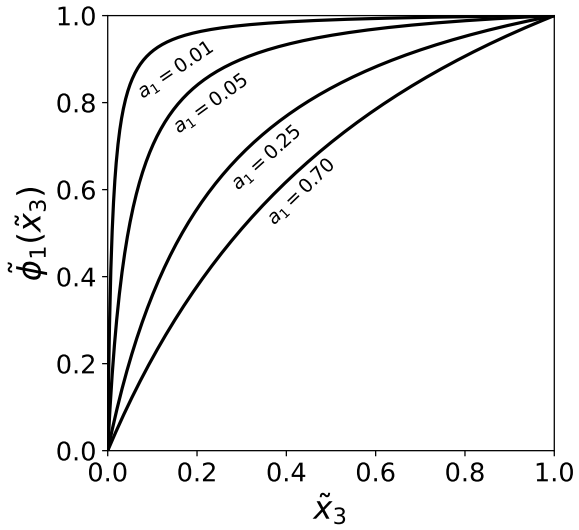


Figure 6: Plots of $\tilde{\phi}_1(\tilde{x}_3)$ vs $\tilde{x}_3$ [Eq. 3] for various $a_1 \in \{0.01, 0.05, 0.25, 0.7\}$.

Note that since $\phi_1(T) = 1$, ρ_{13} is the maximum increase in the per-capita growth rate of sensitive cancer due to the active stroma.

This is the final growth term and the $\dot{x}_1$ equation so far is,

$$\dot{x}_1 = \left(r_1 - \lambda\tilde{D}(t)e^{-\kappa_D x_3} + \rho_{13}\left(\frac{x_3(1+a_1)}{x_3 + a_1 T}\right)\right)x_1 - \{\text{competition}\}$$
$$-\{\text{Chemotherapy Induced Death}\} - \{\text{Immune Induced Death}\}. \tag{4}$$

Competition for resources. We assume cancer cells compete for resources and space between themselves and the stroma, and we follow the Lotka-Volterra model for competing species. We model the growth inhibition of cancer type x_i due to competition with type x_j using the term,

$$-\gamma_{ij}x_i x_j$$

and the growth inhibition of cancer type x_i due to competition with the stroma using the term,

$$-\gamma_{iT}x_i T.$$

These competition terms fit into our equation as follows,

$$\begin{aligned}\dot{x}_1 =&\{\text{Growth}\} - x_1\left[\gamma_{11}x_1 + \gamma_{12}x_2 + \gamma_{1T}T\right]\\ &-\{\text{Chemotherapy Induced Death}\} - \{\text{Immune Induced Death}\}.\end{aligned} \tag{5}$$

(5) Drug-induced death of sensitive cancer. Chemotherapeutic drugs damage cell DNA resulting in apoptosis [56]. To model this we follow the Log-Kill Hypothesis put forward by Skipper, Schabel and Wilcox in the 1960s [73]. This hypothesis proposes that a single dose of chemotherapy kills the same fraction of cancer cells in a tumour regardless of its initial size at the time of treatment [71, p.2537]. We thus model chemotherapy induced death as being proportional to both the size of the sensitive cancer population and the intensity of the treatment. This takes the following form in our model,

$$-\delta_1\tilde{D}(t)e^{-\kappa_D x_3}x_1$$

where $e^{-\kappa_D x_3}\tilde{D}(t)$ is the reduced drug intensity due to active stroma mediated reversible resistance. With this, we can fill in the chemotherapy-induced death term of our equation,

$$\begin{aligned}\dot{x}_1 =&\{\text{Growth}\} - \{\text{Competition}\} - \delta_1\tilde{D}(t)e^{-\kappa_D x_3}x_1\\ &-\{\text{Immune Induced Death}\}.\end{aligned} \tag{6}$$

(6) Immune system-induced death of sensitive cancer. T-cells, NK-cells and macrophages can all kill cancer cells directly. T-cells and NK cells recognise cancerous cells through cell-surface signals and inject proteins that induce apoptosis [66, 50]. Macrophages ingest cancer cells by phagocytosis [44]. Immune system induced death of cancer often requires direct cell-to-cell contact so we follow the law of mass action and model such deaths with the term,

$$-\sigma_{15}x_5x_1,$$

which we include in our equation as follows,

$$\begin{aligned}\dot{x}_1 =&\{\text{Growth}\} - \{\text{Competition}\} - \{\text{Chemotherapy Induced Death}\}\\ &- \sigma_{15}x_5x_1.\end{aligned}$$

This approach assumes that immune cells and cancer cells circulate within the tumour microenvironment, where encounters between them are probabilistic and occur with a likelihood given by x_1x_5. The extent of cancer cell death is then

determined by the parameter σ_{15}. While this is the approach we will take in our model, another approach worth mentioning is to remove the dependency on x_1 and instead use the term,

$$-\sigma_{15}x_5. \tag{7}$$

This formulation assumes that the immune cells attack cancer cells uniformly. The strength of the attack depends solely on the size of the immune cell population, with a fixed number of cancer cells being 'harvested' per unit time based on the immune cell population size. The inclusion of this term will lose the equilibrium at $x_1 = 0$, so to prevent this we must also impose that $\dot{x}_1 = 0$ when $x_1 = 0$. The advantage of this approach is that, for fixed in time values of x_3 and x_5, the cancer population exhibits an 'extinction threshold'; a population size below which the cancer will die out towards extinction due to the immune system. This is a desirable property that agrees with the theory of cancer immunoediting discussed in Section 1.2.4. We will later show that our approach can also attain such a threshold; however, it is more complicated and arises through the coupling between x_1 and x_5 when x_5 is allowed to vary over time. Details are provided later in Section 2.4.2. Future work could involve replacing our approach with the harvesting approach and investigating any resulting changes in the model's behaviour.

(7) Reversible resistance to the immune system.

In addition to supporting cancer growth and protecting cancer cells from the effects of chemotherapy, CAFs can also dampen the ability of the immune system to operate efficiently. CAFs can impair and prevent Natural Killer cell activation, an important component of the innate immune system. Additionally, CAFs attract regulatory T-cells to the tumour site, suppressing T-cell activity, and they directly inhibit T-cell function through the release of various cytokines [30, 45].

To model this suppression of immune cell function by the active stroma we modulate the death rate of sensitive cancer due to the immune system, $-\sigma_{15}x_5x_1$, by,

$$e^{-\kappa_5 x_3},$$

such that the death rate, for fixed x_1 and x_5, reduces as the stroma activates. The full term then becomes,

$$-\sigma_{15}x_5e^{-\kappa_5 x_3}x_1,$$

and we update our equation accordingly,

$$\begin{aligned}\dot{x}_1 =&\{\text{Growth}\} - \{\text{Competition}\} - \{\text{Chemotherapy Induced Death}\} \\ &- \sigma_{15} x_5 e^{-\kappa_5 x_3} x_1. \end{aligned} \tag{8}$$

Combining all of the above processes provides the complete sensitive cancer equation as

$$\begin{aligned}\dot{x}_1 = &\underbrace{\left(r_1 - \lambda \tilde{D}(t) e^{-\kappa_D x_3} + \rho_{13} \frac{x_3(1+a_1)}{x_3 + a_1 T}\right) x_1}_{\text{Growth}} - \underbrace{x_1\left[\gamma_{11} x_1 + \gamma_{12} x_2 + \gamma_{1T} T\right]}_{\text{Competition}} \\ &- \underbrace{\delta_1 \tilde{D}(t) e^{-\kappa_D x_3} x_1}_{\text{Chemotherapy Induced Death}} - \underbrace{\sigma_{15} x_5 e^{-\kappa_5 x_3} x_1}_{\text{Immune Induced Death}} \end{aligned} \tag{9}$$

2.2.2 Resistant Cancer Equation ($\dot{x}_2$)

Our model of resistant cancer growth will have the following form,

$$\begin{aligned}\dot{x}_2 =&\{\text{Sensitive Cell Mutations}\} + \{\text{Growth}\} - \{\text{Competition}\} \\ &- \{\text{Chemotherapy Induced Death}\} - \{\text{Immune Induced Death}\}. \end{aligned} \tag{10}$$

(2) Acquired irreversible drug resistance. Resistant cells, in the first instance, are born from sensitive cells. Chemotherapy induced genetic mutations render some daughters of sensitive cells resistant to chemotherapy. In Section 2.2.1 we modelled such births as a reduction in the birth rate of sensitive cells using the term,

$$-\lambda \tilde{D}(t) e^{-\kappa_D x_3} x_1.$$

The mass lost in the sensitive cell compartment due to such births is gained in the resistant cell compartment, so we include

$$\lambda \tilde{D}(t) e^{-\kappa_D x_3} x_1,$$

to model resistance conferring mutations in the $\dot{x}_2$ equation,

$$\begin{aligned}\dot{x}_2 =&\lambda \tilde{D}(t) e^{-\kappa_D x_3} x_1 + \{\text{Growth}\} - \{\text{Competition}\} \\ &- \{\text{Chemotherapy Induced Death}\} - \{\text{Immune Induced Death}\}. \end{aligned} \tag{11}$$

(8) Proliferation of resistant cancer. Once some cells have mutated and acquired genetic resistance to chemotherapy they, like any cancerous cell, will continue dividing past the normal limits. We again model this unabated cellular

division with the term,

$$r_2 x_2$$

where $r_2 > 0$ is the per-capita growth rate of resistant cancer in the absence of chemotherapy, the stroma and the immune system. This is the first growth term of the $\dot{x}_2$ equation,

$$\begin{aligned}\dot{x}_2 =&\{\text{Sensitive Cell Mutations}\} + r_2 x_2 - \{\text{Competition}\} \\ &-\{\text{Chemotherapy Induced Death}\} - \{\text{Immune Induced Death}\}.\end{aligned}$$

(9) Active-stroma enhancement of resistant cancer growth. CAFs enhance resistant cancer growth via the same mechanisms by which they enhance sensitive cancer growth. We thus include the term,

$$\rho_{23}\phi_2(x_3)x_2$$

with,

$$\phi_2(x_3) = \frac{x_3(1+a_2)}{x_3 + a_2 T},$$

to model the enhancement. For now we use new parameters ρ_{23} and a_2 in order to keep the model as general as possible, however later on we will be making the simplifying assumption that $\rho_{13} = \rho_{23}$ and $a_1 = a_2$. This forms the second and final growth term of the $\dot{x}_2$ equation,

$$\begin{aligned}\dot{x}_2 =&\{\text{Sensitive Cell Mutations}\} + \left(r_2 + \rho_{23}\left(\frac{x_3(1+a_2)}{x_3 + a_2 T}\right)\right) x_2 - \{\text{Competition}\} \\ &-\{\text{Chemotherapy Induced Death}\} - \{\text{Immune Induced Death}\}. \qquad (12)\end{aligned}$$

Competition for resources. We again include resource and space competition terms of the forms,

$$-\gamma_{ij} x_i x_j \quad \text{and} \quad -\gamma_{iT} x_i T$$

with the same interpretations as provided in 2.2.1. This fixes the competition component of the $\dot{x}_2$ equation,

$$\begin{aligned}\dot{x}_2 =&\{\text{Sensitive Cell Mutations}\} + \{\text{Growth}\} - x_2\left[\gamma_{21}x_1 + \gamma_{22}x_2 + \gamma_{2T}T\right] \\ &-\{\text{Chemotherapy Induced Death}\} - \{\text{Immune Induced Death}\}. \qquad (13)\end{aligned}$$

(10) Drug-induced death of resistant cancer. Although these cells have acquired genetic resistance to chemotherapy, it is still possible that some will

be killed during treatment. We again follow the Log-Kill Hypothesis and model chemotherapy induced death of resistant cells as,

$$-\delta_2 \tilde{D}(t) e^{-\kappa_D x_3} x_2.$$

We assume $0 \leq \delta_2 < \delta_1$ so that chemotherapy has a weaker effect on resistant cells compared to sensitive cells. Additionally we assume that resistant cells benefit from the same CAF mediated protection as sensitive cells. With this the $\dot{x}_2$ equation becomes,

$$\begin{aligned}\dot{x}_2 =& \{\text{Sensitive Cell Mutations}\} + \{\text{Growth}\} - \{\text{Competition}\} \\ & - \delta_2 \tilde{D}(t) e^{-\kappa_D x_3} x_2 - \{\text{Immune Induced Death}\}. \end{aligned} \tag{14}$$

(11) Immune system-induced death of resistant cancer. The immune system also targets resistant cancer cells through the same mechanisms as described for sensitive cancer cells. We thus again include the term,

$$-\sigma_{25} x_5 x_2.$$

Some of the genetic mutations that render these cells resistant to chemotherapy may also provide a level of resistance to the immune system [69] and therefore we impose that $\sigma_{25} < \sigma_{15}$.

This forms the immune system-induced death component of the $\dot{x}_2$ equation,

$$\begin{aligned}\dot{x}_2 =& \{\text{Sensitive Cell Mutations}\} + \{\text{Growth}\} - \{\text{Competition}\} \\ & - \{\text{Immune Induced Death}\} - \sigma_{25} x_5 x_2.\end{aligned}$$

(7) Reversible resistance to the immune system.

The active stroma suppresses the ability of the immune system to attack resistant cancer cells through the same mechanisms it uses for sensitive cancer cells. As such we modulate immune system-induced death of resistance cancer with the term,

$$e^{-\kappa_5 x_3},$$

obtaining the complete term as,

$$-\sigma_{25} x_5 e^{-\kappa_5 x_3} x_2.$$

We update the $\dot{x}_2$ equation accordingly,

$$\begin{aligned}\dot{x}_2 =& \{\text{Sensitive Cell Mutations}\} + \{\text{Growth}\} - \{\text{Competition}\} \\ & - \{\text{Chemotherapy Induced Death}\} - \sigma_{25} x_5 e^{-\kappa_5 x_3} x_2. \end{aligned} \tag{15}$$

Together, these processes provide the complete resistant cancer equation as

$$\begin{aligned}\dot{x}_2 = & \underbrace{\lambda \tilde{D}(t) e^{-\kappa_D x_3} x_1}_{\text{Sensitive Cell Mutations}} + \underbrace{\left(r_2 + \rho_{23} \frac{x_3(1+a_2)}{x_3 + a_2 T} \right) x_2}_{\text{Growth}} - \underbrace{x_2 \left[\gamma_{21} x_1 + \gamma_{22} x_2 + \gamma_{2T} T \right]}_{\text{Competition}} \\ & - \underbrace{\delta_2 \tilde{D}(t) e^{-\kappa_D x_3} x_2}_{\text{Chemotherapy Induced Death}} - \underbrace{\sigma_{25} x_5 e^{-\kappa_5 x_3} x_2}_{\text{Immune Induced Death}} \end{aligned} \tag{16}$$

2.2.3 $\dot{x}_1$ and $\dot{x}_2$ System Sanity Check.

Now that we have completely defined both the sensitive and resistant cancer equations, we will analyse their behaviour for various different but fixed in time values of $\tilde{D}(t) = \tilde{D}$, $x_3 = A$ and $x_5 = I$. We use this capital letter notation to denote that the variables are fixed in time. The aim of this analysis is to ensure that the system behaves how we expect. For the purposes of this analysis, as was previously mentioned, we will temporarily rescale the model variables and introduce some simplifying assumptions. After completing the analysis, we will remove these rescalings and assumptions and proceed with the model derivation as before. However, these rescalings and assumptions will be reintroduced permanently before simulating the model. The assumptions we will make are as follows:

1. $\rho_{13} = \rho_{23} = \rho_{C3}$.
2. $a_1 = a_2 = a_C$.
3. $\gamma_{ij} = \gamma_{iT} = \gamma$ for all $i, j \in \{1, 2\}$.

The variable rescalings we will use are as follows:

1. $\tilde{x}_{1/2} = \frac{x_{1/2}}{C^*}$. Here C^* denotes the lethal tumour burden.
2. $\tilde{x}_3 = \frac{x_3}{T}$ (or $\tilde{A} = \frac{A}{T}$). Here T denotes the total amount of active and inactive stroma combined.
3. $\tilde{x}_5 = \frac{x_5}{I_0}$ (or $\tilde{I} = \frac{I}{I_0}$). Here I_0 denotes the strength of the immune system under normal circumstances.

4. $\tilde{t} = r_1 t$. r_1 is the intrinsic per-capita growth rate of a 'small' population of sensitive cancer cells.

For the full details of these simplifying assumptions and variable rescalings, including their interpretations, see Section 3.1.

With these rescalings and assumptions the $\frac{d\tilde{x}_1}{d\tilde{t}}$ and $\frac{d\tilde{x}_2}{d\tilde{t}}$ equations become,

$$\begin{aligned}\frac{d\tilde{x}_1}{d\tilde{t}} =& \left(1 - \tilde{\lambda}\tilde{D}e^{-\tilde{\kappa}_D\tilde{A}} + \tilde{\rho}_{C3}\frac{\tilde{A}(1+a_C)}{\tilde{A}+a_C}\right)\tilde{x}_1 - \tilde{\gamma}\tilde{x}_1\left[\tilde{x}_1+\tilde{x}_2\right] - \tilde{\gamma}_T\tilde{x}_1 \\ & - \tilde{\delta}_1\tilde{D}e^{-\tilde{\kappa}_D\tilde{A}}\tilde{x}_1 - \tilde{\sigma}_{15}\tilde{I}e^{-\tilde{\kappa}_5\tilde{A}}\tilde{x}_1 \qquad (17)\\ \frac{d\tilde{x}_2}{d\tilde{t}} =& \tilde{\lambda}\tilde{D}e^{-\tilde{\kappa}_D\tilde{A}}\tilde{x}_1 + \left(\tilde{r}_2 + \tilde{\rho}_{C3}\frac{\tilde{A}(1+a_C)}{\tilde{A}+a_C}\right)\tilde{x}_2 - \tilde{\gamma}\tilde{x}_2\left[\tilde{x}_1+\tilde{x}_2\right] + \tilde{\gamma}_T\tilde{x}_2 \\ & - \tilde{\delta}_2\tilde{D}e^{-\tilde{\kappa}_D\tilde{A}}\tilde{x}_2 - \tilde{\sigma}_{25}\tilde{I}e^{-\tilde{\kappa}_5\tilde{A}}\tilde{x}_2 \qquad (18)\end{aligned}$$

where: $\tilde{\lambda} = \frac{\lambda}{r_1}$, $\tilde{\rho}_{C3} = \frac{\rho_{C3}}{r_1}$, $\tilde{\kappa}_D = \kappa_D T$, $\tilde{\gamma} = \frac{\gamma C^*}{r_1}$, $\tilde{\gamma}_T = \frac{\gamma T}{r_1}$, $\tilde{\delta}_1 = \frac{\delta_1}{r_1}$ $\tilde{\sigma}_{15} = \frac{\sigma_{15} I_0}{r_1}$, $\tilde{\kappa}_5 = \kappa_5 T$, $\tilde{r}_2 = \frac{r_2}{r_1}$, $\tilde{\delta}_2 = \frac{\delta_2}{r_1}$ and $\tilde{\sigma}_{25} = \frac{\sigma_{25} I_0}{r_1}$.

First we will analyse the case of untreated, chemotherapy-sensitive cancer growth, i.e. $\tilde{D} = 0$ and $\tilde{x}_2 = 0$. In this case we only have one equation,

$$\frac{d\tilde{x}_1}{d\tilde{t}} = \left(1 + \tilde{\rho}_{C3}\frac{\tilde{A}(1+a_C)}{\tilde{A}+a_C} - \tilde{\gamma}_T - \tilde{\sigma}_{15}\tilde{I}e^{-\tilde{\kappa}_5\tilde{A}}\right)\tilde{x}_1 - \tilde{\gamma}\tilde{x}_1^2.$$

This has the form of a logistic growth equation where the coefficient in the linear growth term is,

$$1 + \tilde{\rho}_{C3}\frac{\tilde{A}(1+a_C)}{\tilde{A}+a_C} - \tilde{\gamma}_T - \tilde{\sigma}_{15}\tilde{I}e^{-\tilde{\kappa}_5\tilde{A}}, \qquad (19)$$

which depends on $\tilde{A}$ and $\tilde{I}$. Since these are fixed in time, there are two equilibrium solutions for this equation,

1. $\boldsymbol{e_0}$ **:**

$$\tilde{x}_1 = 0. \qquad (20)$$

2. $\boldsymbol{e_1}$ **:**

$$\tilde{x}_1 = \frac{1 + \tilde{\rho}_{C3}\frac{\tilde{A}(1+a_C)}{\tilde{A}+a_C} - \tilde{\gamma}_T - \tilde{\sigma}_{15}\tilde{I}e^{-\tilde{\kappa}_5\tilde{A}}}{\tilde{\gamma}} \qquad (21)$$

If the linear growth term [Eq. 19] is positive, then e_0 is unstable and e_1 is both positive and stable. Otherwise, if the linear growth term is negative, the opposite is true, e_0 is stable and e_1 is both negative and unstable. Whether [Eq. 19] is positive or negative will depend on $\tilde{A}$ and $\tilde{I}$ and the relative strengths of the

processes that contribute to this term. Namely, it is positive if,

$$1 + \tilde{\rho}_{C3}\frac{\tilde{A}(1+a_C)}{\tilde{A}+a_C} - \tilde{\gamma}_T > \tilde{\sigma}_{15}\tilde{I}e^{-\tilde{\kappa}_5\tilde{A}}. \tag{22}$$

Next we will consider the case where treatment has been or is currently being applied, i.e. $\tilde{D}$ and $\tilde{x}_2$ not simultaneously zero. This is the 2D system defined by [Eq. 17] and [Eq. 18]. There are three equilibrium solutions for this system of equations,

1. $\boldsymbol{e_0}$ **:**

$$(\tilde{x}_1^{e_0}, \tilde{x}_2^{e_0}) = (0, 0) \tag{23}$$

2. $\boldsymbol{e_1}$ **:**

$$(\tilde{x}_1^{e_1}, \tilde{x}_2^{e_1}) = (0, \frac{\zeta_2}{\tilde{\gamma}}) \tag{24}$$

3. $\boldsymbol{e_2}$ **:**

$$(\tilde{x}_1^{e_2}, \tilde{x}_2^{e_2}) = \left(\frac{\zeta_1}{\tilde{\gamma}}\left(\frac{\zeta_1-\zeta_2}{\zeta_1+\tilde{\lambda}\tilde{D}e^{-\tilde{\kappa}_D\tilde{A}}-\zeta_2}\right), \frac{\zeta_1}{\tilde{\gamma}}\left(\frac{\tilde{\lambda}\tilde{D}e^{-\tilde{\kappa}_D\tilde{A}}}{\zeta_1+\tilde{\lambda}\tilde{D}e^{-\tilde{\kappa}_D\tilde{A}}-\zeta_2}\right)\right) \tag{25}$$

where,

$$\zeta_1 = 1 - \tilde{\lambda}\tilde{D}e^{-\tilde{\kappa}_D\tilde{A}} + \tilde{\rho}_{C3}\frac{\tilde{A}(1+a_C)}{\tilde{A}+a_C} - \tilde{\gamma}_T - \tilde{\delta}_1\tilde{D}e^{-\tilde{\kappa}_D\tilde{A}} - \tilde{\sigma}_{15}\tilde{I}e^{-\tilde{\kappa}_5\tilde{A}}$$
$$\zeta_2 = \tilde{r}_2 + \tilde{\rho}_{C3}\frac{\tilde{A}(1+a_C)}{\tilde{A}+a_C} - \tilde{\gamma}_T - \tilde{\delta}_2\tilde{D}e^{-\tilde{\kappa}_D\tilde{A}} - \tilde{\sigma}_{25}\tilde{I}e^{-\tilde{\kappa}_5\tilde{A}}.$$

Calculations obtaining these equilibrium solutions and the analysis to follow are given in appendix A.1.

Evaluating the Jacobian matrix at each of e_0, e_1 and e_2 [Eq. 23-25], we can obtain the following eigenvalues and eigenvectors in terms of ζ_1 and ζ_2. We denote eigenvalues with L instead of λ to avoid a clash of notation with the model parameter λ.

1. e_0:

   The eigenvalues are,

$$L_1^{e_0} = \zeta_1 \quad \text{and} \quad L_2^{e_0} = \zeta_2. \tag{26}$$

The eigenvectors are,

$$\boldsymbol{v_1^{e_0}} = \begin{pmatrix} 1 \\ \frac{\tilde{\lambda}\tilde{D}e^{-\tilde{\kappa}_D\tilde{A}}}{\zeta_1-\zeta_2} \end{pmatrix} \quad \text{and} \quad \boldsymbol{v_2^{e_0}} = \begin{pmatrix} 0 \\ 1 \end{pmatrix}. \tag{27}$$

2. $\boldsymbol{e_1}$ **:**

The eigenvalues are,

$$L_1^{e_1} = \zeta_1 - \zeta_2 \quad \text{and} \quad L_2^{e_1} = -\zeta_2. \tag{28}$$

The eigenvectors are,

$$\boldsymbol{v_1^{e_1}} = \begin{pmatrix} 1 \\ \frac{\tilde{\lambda}\tilde{D}e^{-\tilde{\kappa}_D\tilde{A}}-\zeta_2}{\zeta_1} \end{pmatrix} \quad \text{and} \quad \boldsymbol{v_2^{e_1}} = \begin{pmatrix} 0 \\ 1 \end{pmatrix}. \tag{29}$$

3. $\boldsymbol{e_2}$ **:**

The eigenvalues are,

$$L_1^{e_2} = \zeta_2 - \zeta_1 \quad \text{and} \quad L_2^{e_2} = -\zeta_1. \tag{30}$$

The eigenvectors are,

$$\boldsymbol{v_1^{e_2}} = \begin{pmatrix} 1 \\ \frac{\tilde{\lambda}\tilde{D}e^{-\tilde{\kappa}_D\tilde{A}}-\zeta_2}{\zeta_1} \end{pmatrix} \quad \text{and} \quad \boldsymbol{v_2^{e_2}} = \begin{pmatrix} 1 \\ \frac{\tilde{\lambda}\tilde{D}e^{-\tilde{\kappa}_D\tilde{A}}}{\zeta_1-\zeta_2} \end{pmatrix}. \tag{31}$$

The eigenvectors of each equilibrium, point towards the other two equilibria. In appendix A.1.3, we show that the lines defined by extending the eigenvectors infinitely outwards from each equilibrium point (i.e. the lines passing through each pair of equilibrium points), define invariant sets of the phase space. With this in mind and using the eigenvalues stated above, we can split the qualitative dynamics of the system into six different cases, depending on the relative sizes and signs of ζ_1 and ζ_2.

Case 1 (a): $\boldsymbol{0 < \zeta_1 < \zeta_2 \quad \text{and} \quad \zeta_1 + \tilde{\lambda}\tilde{D}e^{-\tilde{\kappa}_D\tilde{A}} - \zeta_2 > 0.}$

We can examine the signs of the eigenvalues associated to each equilibrium point to determine their stability for this case.

- $\boldsymbol{e_0}$ **:** e_0 is an unstable node since both eigenvalues are real with $L_1^{e_0} > 0$ and $L_2^{e_0} > 0$ [Eq. 26].

- $\boldsymbol{e_1}$ **:** e_1 is a stable node since both eigenvalues are real with $L_1^{e_1} < 0$ and $L_2^{e_1} < 0$ [Eq. 28]. Further we have that $\tilde{x}_2^{e_1} > 0$ since $\zeta_2 > 0$ in this case.

- $\boldsymbol{e_2}$ **:** e_2 is an unstable saddle since both eigenvalues are real with $L_1^{e_2} > 0$ and $L_2^{e_2} < 0$ [Eq. 30].

Using the eigenvectors [Eq. 27], [Eq. 29] and [Eq. 31] along with their corresponding eigenvalues, we can determine the direction of the flow along each of the invariant lines that pass through the equilibrium points in the phase space. In particular, we can find the stable and unstable eigendirections of e_2. The stable eigendirection of e_2 points from e_0 towards e_2 since $L_2^{e_2} = -\zeta_1 < 0$. The unstable eigendirection of e_2 points from e_2 to e_1 since $L_1^{e_2} = \zeta_2 - \zeta_1 > 0$.

The e_2 equilibrium point may exist in the second or fourth quadrant of the phase space. This is because the numerators of $\tilde{x}_1^{e_2}$ and $\tilde{x}_2^{e_2}$ have opposite sign, and the denominators are equal. The location thus depends on the sign of,

$$\zeta_1 + \tilde{\lambda}\tilde{D}e^{-\tilde{\kappa}_D\tilde{A}} - \zeta_2, \tag{32}$$

which may be positive or negative. Here we assume it is positive and e_2 is thus in the second quadrant. We can now sketch a phase portrait of the system for this case [Fig. 7: 1(a)].

Case 1 (b): $\boldsymbol{0 < \zeta_1 < \zeta_2}$ and $\boldsymbol{\zeta_1 + \tilde{\lambda}\tilde{D}e^{-\tilde{\kappa}_D\tilde{A}} - \zeta_2 < 0}$.

In this case we assume $\zeta_1 + \tilde{\lambda}\tilde{D}e^{-\tilde{\kappa}_D\tilde{A}} - \zeta_2 < 0$ and thus e_2 is in the fourth quadrant. The rest of the stability analysis remains the same as in case 1(a) and as such we can now sketch a phase portrait of the system for this case [Fig. 7: 1(b)].

Case 1 (c): $\boldsymbol{0 < \zeta_1 < \zeta_2}$ and $\boldsymbol{\zeta_1 + \tilde{\lambda}\tilde{D}e^{-\tilde{\kappa}_D\tilde{A}} - \zeta_2 = 0}$.

If [Eq. 32] is equal to zero, then the e_2 equilibrium is no longer well defined, and the phase space only contains the equilibrium points e_0 and e_1. In this case we also have that the eigenvectors $\boldsymbol{v_1^{e_0}}$ and $\boldsymbol{v_1^{e_1}}$ coincide,

$$\boldsymbol{v_1^{e_0}} = \boldsymbol{v_1^{e_1}} = \begin{pmatrix} 1 \\ -1 \end{pmatrix}.$$

See [Fig. 7: 1(c)] for a sketch of the phase portrait in this case.

Case 2(a): $\boldsymbol{\zeta_1 < 0 < \zeta_2}$ and $\boldsymbol{\zeta_1 + \tilde{\lambda}\tilde{D}e^{-\tilde{\kappa}_D\tilde{A}} - \zeta_2 > 0}$.

We again examine the signs of the eigenvalues associated to each equilibrium point to determine their stability for this case.

- $\boldsymbol{e_0}$ **:** e_0 is an unstable saddle since the eigenvalues associated to e_0 have opposite signs, $L_1^{e_0} < 0$ and $L_2^{e_0} > 0$ [Eq. 26].

- $\boldsymbol{e_1}$ **:** e_1 remains a stable node since both eigenvalues are real with $L_1^{e_1} < 0$ and $L_2^{e_1} < 0$ [Eq. 28]. Again, we still have that $\tilde{x}_2^{e_1} > 0$ since $\zeta_2 > 0$.

- $\boldsymbol{e_2}$ **:** e_2 becomes an unstable node since both eigenvalues are real with $L_1^{e_2} > 0$ and $L_2^{e_2} > 0$ [Eq. 30].

The stable eigendirection of e_0 points from e_2 to e_1 since $L_1^{e_0} < 0$. The unstable eigendirection of e_0 points from e_0 to e_1 since $L_2^{e_0} > 0$.

If we assume $\zeta_1 + \tilde{\lambda}\tilde{D}e^{-\tilde{\kappa}_D\tilde{A}} - \zeta_2 > 0$, then e_2 is in the fourth quadrant and we can then sketch the phase portrait of the system for this case [Fig. 7: 2(a)].

Case 2(b): $\boldsymbol{\zeta_1 < 0 < \zeta_2}$ **and** $\boldsymbol{\zeta_1 + \tilde{\lambda}\tilde{D}e^{-\tilde{\kappa}_D\tilde{A}} - \zeta_2 < 0.}$

If we assume $\zeta_1 + \tilde{\lambda}\tilde{D}e^{-\tilde{\kappa}_D\tilde{A}} - \zeta_2 < 0$, then e_2 is in the second quadrant. The stability analysis is otherwise the same as in case 2(a), and thus we can also produce the phase portrait for this case [Fig. 7: 2(b)].

Case 2(c): $\boldsymbol{\zeta_1 < 0 < \zeta_2}$ **and** $\boldsymbol{\zeta_1 + \tilde{\lambda}\tilde{D}e^{-\tilde{\kappa}_D\tilde{A}} - \zeta_2 = 0.}$

In the case that [Eq. 32] is zero, we again have that e_2 becomes undefined, leaving just e_0 and e_1. We also again have that $\boldsymbol{v_1^{e_0}}$ and $\boldsymbol{v_1^{e_1}}$ coincide. The phase portrait for this case is sketched in [Fig. 7: 2(c)].

Case 3(a): $\boldsymbol{\zeta_1 < \zeta_2 < 0}$ **and** $\boldsymbol{\zeta_1 + \tilde{\lambda}\tilde{D}e^{-\tilde{\kappa}_D\tilde{A}} - \zeta_2 > 0.}$

As before we examine the eigenvalues to determine the stability of each equilibrium point.

- $\boldsymbol{e_0}$ **:** e_0 is a stable node since the eigenvalues associated to e_0 are both negative, $L_1^{e_0} < 0$ and $L_2^{e_0} < 0$ [Eq. 26].

- $\boldsymbol{e_1}$ **:** e_1 becomes an unstable saddle in this case, since the eigenvalues have opposite signs, $L_1^{e_1} < 0$ and $L_2^{e_1} > 0$ [Eq. 28]. We also now have that $\tilde{x}_2^{e_1} < 0$ since $\zeta_2 < 0$.

- $\boldsymbol{e_2}$ **:** e_2 remains an unstable node since both eigenvalues are again real with $L_1^{e_2} > 0$ and $L_2^{e_2} > 0$ [Eq. 30].

The stable eigendirection of e_1 points from e_2 towards e_1 since $L_1^{e_1} < 0$. The unstable eigendirection of e_1 points from e_1 towards e_0 since $L_2^{e_1} > 0$.

Once again the position of e_2 depends on the sign of [Eq. 32]. If we assume $\zeta_1 + \tilde{\lambda}\tilde{D}e^{-\tilde{\kappa}_D\tilde{A}} - \zeta_2 > 0$, then e_2 is in the fourth quadrant. With this we can draw the phase portrait of the system for this case [Fig. 7: 3(a)].

Case 3(b): $\boldsymbol{\zeta_1 < \zeta_2 < 0}$ **and** $\boldsymbol{\zeta_1 + \tilde{\lambda}\tilde{D}e^{-\tilde{\kappa}_D\tilde{A}} - \zeta_2 < 0.}$

If $\zeta_1 + \tilde{\lambda}\tilde{D}e^{-\tilde{\kappa}_D\tilde{A}} - \zeta_2 < 0$, then e_2 is in the second quadrant. The rest of the stability analysis is unchanged and the phase portrait for this case is given in [Fig. 7: 3(b)].

Case 3(c): $\boldsymbol{\zeta_1 < \zeta_2 < 0}$ **and** $\boldsymbol{\zeta_1 + \tilde{\lambda}\tilde{D}e^{-\tilde{\kappa}_D\tilde{A}} - \zeta_2 = 0.}$

If [Eq. 32] is zero then once again e_2 becomes undefined and $\boldsymbol{v_1^{e_0}}$ and $\boldsymbol{v_1^{e_1}}$ coincide. The phase portrait for this case is given in [Fig. 7: 3(c)].

Case 4: $0 < \zeta_2 < \zeta_1$.

We again use the eigenvalues to determine the stability of the equilibrium points.

- $\boldsymbol{e_0}$ **:** e_0 is an unstable node in this case since the eigenvalues associated to e_0 are both positive, $L_1^{e_0} > 0$ and $L_2^{e_0} > 0$ [Eq. 26].

- $\boldsymbol{e_1}$ **:** e_1 is an unstable saddle in this case, since the eigenvalues have opposite signs, $L_1^{e_1} > 0$ and $L_2^{e_1} < 0$ [Eq. 28]. In this case, we have that $\tilde{x}_2^{e_1} > 0$ since $\zeta_2 > 0$.

- $\boldsymbol{e_2}$ **:** e_2 is a stable node since both eigenvalues are again real with $L_1^{e_2} < 0$ and $L_2^{e_2} < 0$ [Eq. 30].

The stable eigendirection of e_1 points from e_0 towards e_1, since $L_2^{e_1} < 0$. The unstable eigendirection of e_1 points from e_1 towards e_2, since $L_1^{e_1} > 0$.

In this case both $\tilde{x}_1^{e_2} > 0$ and $\tilde{x}_2^{e_2} > 0$, and as such e_2 exists in the first quadrant of the phase portrait. With this we can sketch the phase portrait for this case [Fig. 8: 4].

Case 5: $\zeta_2 < 0 < \zeta_1$.

The stability of the equilibrium points for this case is given below.

- $\boldsymbol{e_0}$ **:** e_0 is an unstable saddle in this case since the eigenvalues associated to e_0 have opposite signs, $L_1^{e_0} > 0$ and $L_2^{e_0} < 0$ [Eq. 26].

- $\boldsymbol{e_1}$ **:** e_1 is an unstable node, since the eigenvalues are both positive, $L_1^{e_1} > 0$ and $L_2^{e_1} > 0$ [Eq. 28]. In this case, we have that $\tilde{x}_2^{e_1} < 0$ since $\zeta_2 < 0$.

- $\boldsymbol{e_2}$ **:** e_2 is a stable node since both eigenvalues are real with $L_1^{e_2} < 0$ and $L_2^{e_2} < 0$ [Eq. 30].

The stable eigendirection of e_0 points from e_1 towards e_0, since $L_2^{e_0} < 0$. The unstable eigendirection of e_0 points from e_0 towards e_2, since $L_1^{e_0} > 0$.

In this case both $\tilde{x}_1^{e_2} > 0$ and $\tilde{x}_2^{e_2} > 0$, and as such e_2 again exists in the first quadrant of the phase plane. We can now produce a sketch of the phase portrait for this case [Fig. 8: 5].

Case 6: $\zeta_2 < \zeta_1 < 0$.

The stability of the equilibrium points for this case can be determined as follows,

- $\boldsymbol{e_0}$ **:** e_0 is a stable node in this case since the eigenvalues associated to e_0 are both negative, $L_1^{e_0} < 0$ and $L_2^{e_0} < 0$ [Eq. 26].

- $\boldsymbol{e_1}$ **:** e_1 is again an unstable node, since the eigenvalues are both positive, $L_1^{e_1} > 0$ and $L_2^{e_1} > 0$ [Eq. 28]. Again, we have that $\tilde{x}_2^{e_1} < 0$ since $\zeta_2 < 0$.

- $\boldsymbol{e_2}$ **:** e_2 is an unstable saddle since both eigenvalues have opposite signs, $L_1^{e_2} < 0$ and $L_2^{e_2} > 0$ [Eq. 30].

The stable eigendirection of e_2 points from e_1 towards e_2, since $L_1^{e_2} < 0$. The unstable eigendirection of e_2 points from e_2 towards e_0, since $L_2^{e_2} > 0$.

In this case both $\tilde{x}_1^{e_2} < 0$ and $\tilde{x}_2^{e_2} < 0$, and as such e_2 exists in the third quadrant of the phase plane. The phase portrait for this case is sketched in [Fig. 8: 6].

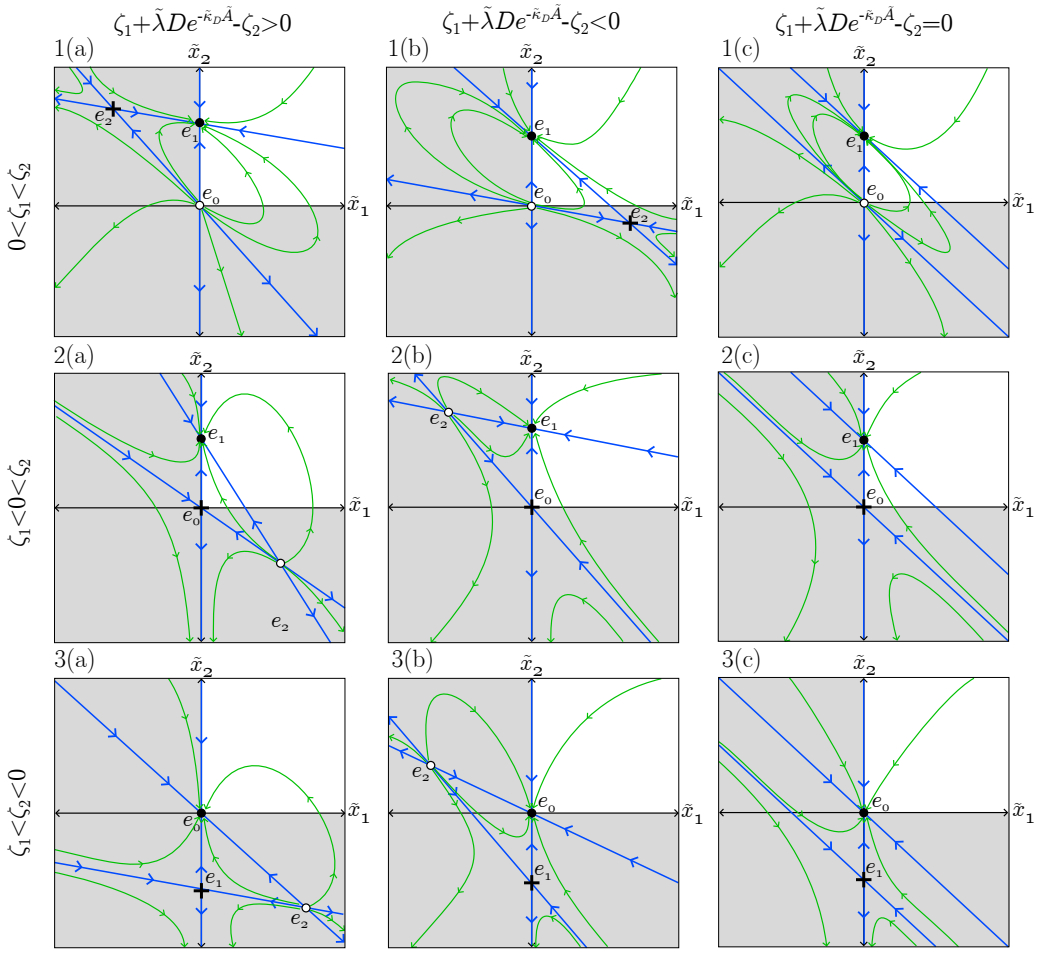


Figure 7: Hand-sketched phase portraits for cases 1(a)-3(c). Solid black dots represent stable nodes, black dots with white centers represent unstable nodes and black plus signs represent saddle points. The blue lines represent invariant sets in the directions of the eigenvectors. The green arrows are sample trajectories. The shaded regions of the phase space correspond to non-physical values of $\tilde{x}_1$ and $\tilde{x}_2$.

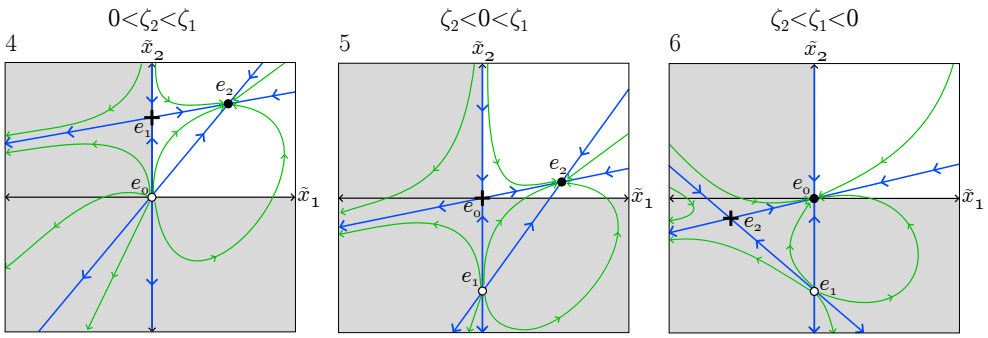


Figure 8: Hand-sketched phase portraits for cases 4-6. Solid black dots represent stable nodes, black dots with white centers represent unstable nodes and black plus signs represent saddle points. The blue lines represent invariant sets in the directions of the eigenvectors. The green arrows are sample trajectories. The shaded regions of the phase space correspond to non-physical values of $\tilde{x}_1$ and $\tilde{x}_2$.

This analysis outlines that the model behaves reasonably. For instance, solutions can never become unphysical ($x_1 < 0$ and/or $x_2 < 0$) if given physical ($x_1 \geq 0$ and $x_2 \geq 0$) initial conditions. If $\tilde{x}_2 = 0$ and $\tilde{x}_1 > 0$ we have that $\frac{d\tilde{x}_2}{dt} \geq 0$, and as such the flow on the positive half of $\tilde{x}_1$ axis points into the first quadrant of the phase space. We also already have that the $\tilde{x}_2$ axis is invariant. Hence the first quadrant of the phase space is invariant. This is well illustrated through the phase diagrams above.

In cases 4-6 we have $\zeta_2 < \zeta_1$, which can be interpreted biologically as the resistant population's growth being dominated by the sensitive population's growth in the presence of both chemotherapy and the immune system. To see this, first assume that $\tilde{x}_1$ and $\tilde{x}_2$ are both very small such that $\tilde{x}_1^2 \approx \tilde{x}_2^2 \approx \tilde{x}_1\tilde{x}_2 \approx 0$. Under this assumption, ζ_1 represents the per-capita growth rate of $\tilde{x}_1$ when the population is small, while ζ_2 is the corresponding per-capita growth rate of $\tilde{x}_2$ minus the additional growth contribution from sensitive cell mutations. This explains why $\zeta_2 < \zeta_1$ implies that resistant cells grow more slowly than sensitive cells under these conditions.

The relative growth rates of the resistant and sensitive populations depend on the specific types of cancer cells and resistance mechanisms involved. For instance, the resistant population's growth rate could be slower due to an evolutionary cost of developing resistance [22], or faster in the case of cancer stem cells (CSCs) [23]. Our model captures both possibilities, allowing cases 1-3 of 4-6 to be selected based on the biological plausibility for a given application.

In this work, we focus on the scenario where $\zeta_1 \leq \zeta_2$, which can be enforced by assuming $r_1 = r_2$ or,

$$\tilde{r}_2 = 1.$$

The above analysis is all based on the assumption that $\tilde{D}$, $\tilde{A}$ and $\tilde{I}$ are all fixed in time. When allowed to vary, the true dynamics of the cancer variables may be different.

We will now continue to derive the model in full generality but we will reintroduce the variable rescalings and simplifying assumptions in Section 3.1 as well as during any further system sanity checks.

2.3 Active & Inactive Stroma Equations ($\dot{x}_3$ & $\dot{x}_4$)

Our model of the active stroma will have the following form,

$$\begin{aligned}\dot{x}_3 =&\{\text{Chemotherapy Induced Activation}\} - \{\text{Chemotherapy Induced Death}\} \\ &+ \{\text{Cancer Induced Activation}\} - \{\text{Natural Inactivation}\}. \end{aligned} \tag{33}$$

Tissue homeostasis. Tissue homeostasis is the process that maintains stability at the tissue level and regulates cell numbers [52]. Cancer cells lose the ability to maintain homeostasis and proliferate uncontrollably whereas healthy stromal cells are relatively stable. Thus, in line with [64], we assume that the total stroma, active and inactive combined, remains constant in time such that,

$$x_3(t) + x_4(t) = T$$

with $T \in \mathbb{R}$ constant. During cancer growth and treatment, a variety of factors cause the stroma to switch from its inactive state to an active state.

(12) & (13) Chemotherapy-induced death and activation of the stroma. Many cells can be damaged by chemotherapy, including CAFs [74]. Cancer cells suffer the most because chemotherapy preferentially targets actively proliferating cells [56]. As a result, the death rate of stromal cells, including active stromal cells, due to chemotherapy is lower than that of cancer cells.

In addition to inducing cell death, chemotherapy can also activate fibroblasts into CAFs [63, 70, 42]. High dose chemotherapy leads to strong stromal activation whereas low dose metronomic chemotherapy curbs such potent chemotherapy-induced activation [42, 13].

The strength of these processes—that is, the death of the active stroma and activation of the inactive stroma—also depends on how much of the stroma is already active. If the stroma is fully inactive, then there are no active stromal cells that chemotherapy can kill. If the stroma is fully active, then there are no inactive cells that chemotherapy can activate. We would like to describe the response of the active stroma to chemotherapy without the behaviour being skewed by how much of the stroma is already active. Therefore, the following

description refers specifically to the per-capita growth rate of the active stroma given an equal proportion of active and inactive stroma.

In the absence of chemotherapy, the growth rate is zero. Then, as chemotherapy intensity increases, the growth rate decreases becoming negative. This is because at low doses, stromal cell death dominates over the very weak stromal cell activation. As chemotherapy intensity continues to increase, it will pass some optimal intensity at which the growth rate attains its most negative value. Beyond this optimal intensity, the growth rate begins to increase, eventually becoming positive beyond some critical intensity. This is because the stromal cell death rate is relatively limited, whereas the stromal cell activation rate becomes very large near the maximum tolerated dose. This response can be summarised in a schematic [Fig. 9].

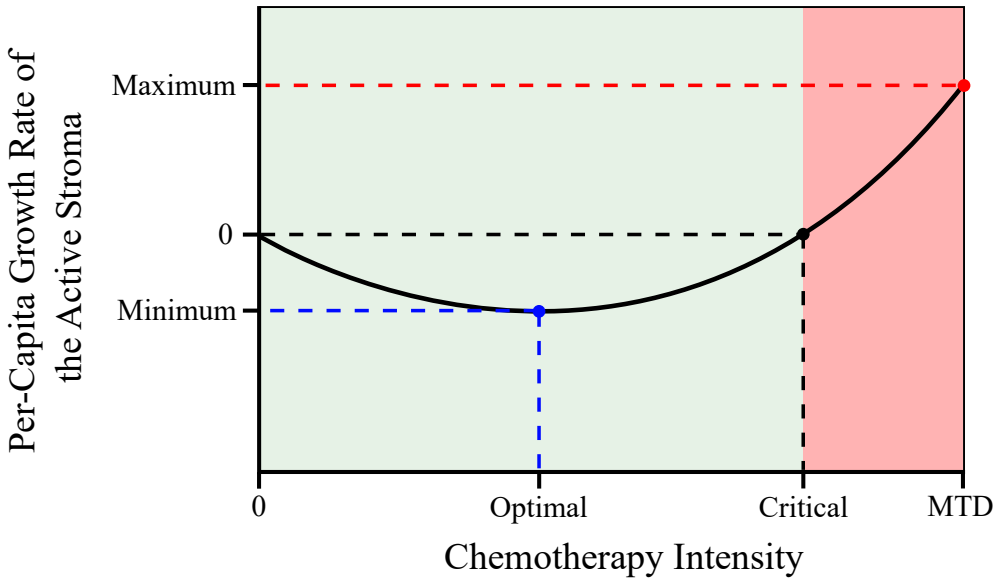


Figure 9: Schematic of the per-capita growth rate of the active stroma in response to chemotherapy, given an equal proportion of active and inactive stroma. The green region represents chemotherapy intensities for which the per-capita growth rate of the active stroma is negative, and the red region indicates the intensities for which it is positive.

To model this behaviour, we assume that chemotherapy induced death of active stromal cells is proportional to $\tilde{D}(t)$, as was done for cancer cells, and include the term,

$$-\delta_3 \tilde{D}(t) x_3, \tag{34}$$

in the $\dot{x}_3$ equation. δ_3 is the maximum per-capita death rate of the active stromal cells due to chemotherapy and since this is more limited for stromal cells than that of cancer cells, we assume $0 \leq \delta_3 < \delta_1$. For the sake of mathematical simplicity

we further assume that in the presence of chemotherapy, inactive stromal cells grow at an equivalent rate to the dying stromal cells (both active and inactive) such that the relationship $x_3(t) + x_4(t) = T \in \mathbb{R}$ is maintained.

To model stromal activation due to chemotherapy we include the term,

$$\nu_3 \, \phi_3 \left(\tilde{D}(t) \right) (T - x_3), \tag{35}$$

in the $\dot{x}_3$ equation, where,

$$\phi_3 \left(\tilde{D}(t) \right) = \frac{e^{a_3 \tilde{D}(t)} - 1}{e^{a_3} - 1}. \tag{36}$$

The functional response ϕ_3 is included to model the fact that stromal activation is most prominent for chemotherapy intensities near the maximum tolerated dose, and is far less prominent at lower doses. This is illustrated through plots of ϕ_3 vs. $\tilde{D}$ for various values of a_3 [Fig. 10].

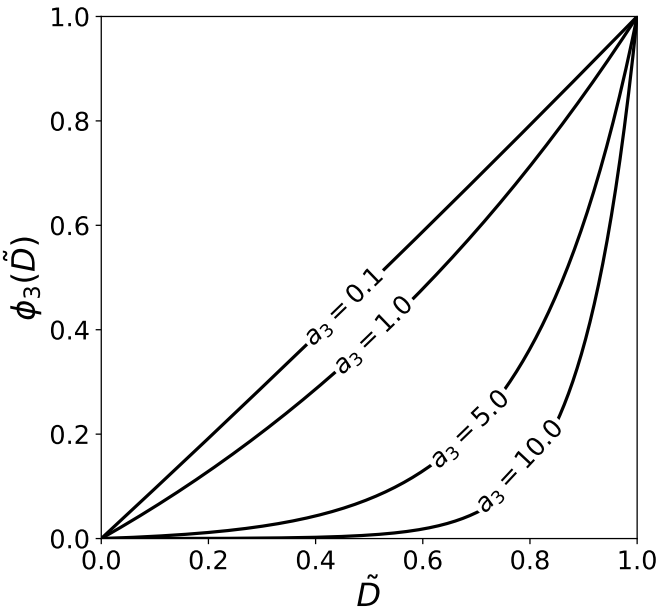


Figure 10: $\phi_3(\tilde{D})$ vs. $\tilde{D}$ for various values of a_3 [Eq. 36].

Since $\phi_3(1) = 1$, ν_3 is the maximum per-capita activation rate of the inactive stroma in response to chemotherapy.

Together, [Eq. 35] and [Eq. 34] form the first two terms of the active stroma equation,

$$\dot{x}_3 = \nu_3 \left(\frac{e^{a_3 \tilde{D}(t)} - 1}{e^{a_3} - 1} \right) (T - x_3) - \delta_3 \tilde{D}(t) x_3 + \{\text{Cancer Induced Activation}\}$$
$$- \{\text{Natural Inactivation}\}, \tag{37}$$

This approach captures how the strength of each process depends on how much of the stroma is already active. If $x_3 = 0$, then $\delta_3 \tilde{D}(t) x_3 = 0$ and if $x_3 = T$ then $\nu_3 \phi_3(\tilde{D}(t))(T - x_3) = 0$.

We would like to ensure that our approach successfully reproduces the schematic in [Fig. 9] and as such we will study the reduced equation,

$$\frac{1}{T}\frac{dx_3}{dt} = \frac{d\tilde{x}_3}{dt} = \nu_3 \phi_3 \left(\tilde{D}(t)\right)(1 - \tilde{x}_3) - \delta_3 \tilde{D}(t)\tilde{x}_3, \tag{38}$$

where,

$$\tilde{x}_3 = \frac{x_3}{T}.$$

This is the per-capita growth rate of the active stroma in response to chemotherapy, with the cancer induced activation and natural inactivation terms omitted. [Fig. 9] refers specifically to the per-capita growth rate when the active and inactive stroma are in equal proportion, thus we must examine [Eq. 38] evaluated at $\tilde{x}_3 = \frac{1}{2}$ for various different but fixed-in-time values of $\tilde{D}(t) = \tilde{D}$.

$$\left.\frac{d\tilde{x}_3}{dt}\right|_{\tilde{x}_3 = \frac{1}{2}} = \frac{\nu_3}{2}\phi_3(\tilde{D}) - \frac{\delta_3}{2}\tilde{D}. \tag{39}$$

[Eq. 39] matches the qualitative expectations outlined at the beginning of this section if:

1. $\left.\frac{d\tilde{x}_3}{dt}\right|_{\tilde{x}_3 = \frac{1}{2}} > 0$ when $\tilde{D} = 1$, and
2. There exists $\tilde{D}_{r3} \in (0, 1)$ such that $\left.\frac{d\tilde{x}_3}{dt}\right|_{\tilde{x}_3 = \frac{1}{2}} = 0$ if $\tilde{D} = \tilde{D}_{r3}$ ($\tilde{D}_{r3}$ corresponds to the critical intensity in [Fig. 9]),

both hold. In appendix A.2, we show that conditions (1) and (2) both hold if,

$$\frac{a_3}{e^{a_3} - 1} < \frac{\delta_3}{\nu_3} < 1. \tag{40}$$

With this, we can plot $\tilde{D}_{r3}$ against a_3 for various fixed ratios of $\frac{\delta_3}{\nu_3}$ [Fig. 11]. This figure highlights the flexibility of our modelling approach, since once the ratio $\frac{\delta_3}{\nu_3}$ is known, we can use a_3 to choose any desired critical chemotherapy intensity.

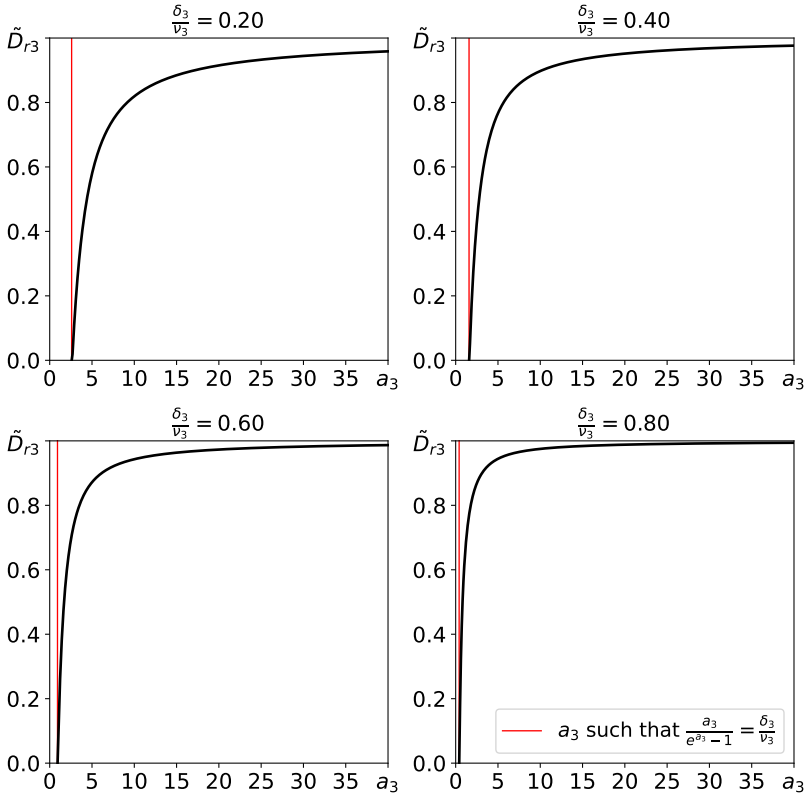


Figure 11: Plot of $\tilde{D}_{r3}$ vs a_3 for various fixed $\frac{\delta_3}{\nu_3}$. Red line indicates the value of a_3 at which $\frac{a_3}{e^{a_3}-1} = \frac{\delta_3}{\nu_3}$.

We can now produce some sample plots of [Eq. 39] and compare them to our schematic [Fig. 9]. We are only interested in the qualitative shape of these plots (when it is positive/negative or equal to zero), so for now, rather than specifying particular values for ν_3 and δ_3, we will examine [Eq. 39] for various different values of the ratio $\frac{\delta_3}{\nu_3}$. To do this, we introduce the time rescaling,

$$\tau = \frac{\nu_3}{2} t$$

and plot,

$$\left.\frac{d\tilde{x}_3}{d\tau}\right|_{\tilde{x}_3=\frac{1}{2}} = \phi_3(\tilde{D}) - \frac{\delta_3}{\nu_3}\tilde{D} \tag{41}$$

vs. $\tilde{D}$, see [Fig. 12].

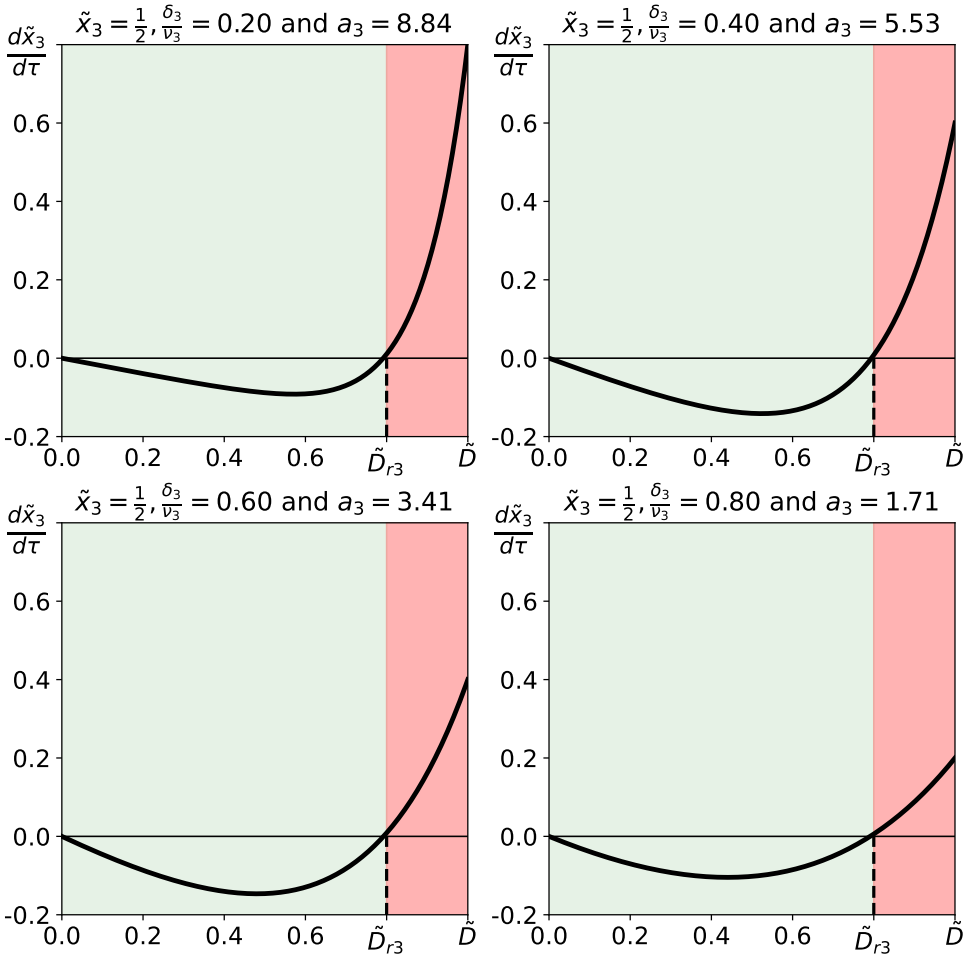


Figure 12: Plots of [Eq. 41] vs. $\tilde{D}$ for various fixed $\frac{\delta_3}{\nu_3}$. The region $\tilde{D} < \tilde{D}_{r3}$ is coloured green and indicates negative values of $\frac{d\tilde{x}_3}{d\tau}\big|_{\tilde{x}_3=\frac{1}{2}}$. The region $\tilde{D} > \tilde{D}_{r3}$ is coloured red and indicates positive values of $\frac{d\tilde{x}_3}{d\tau}\big|_{\tilde{x}_3=\frac{1}{2}}$. In each case, the values of a_3 was chosen such that $\tilde{D}_{r3} \approx 0.8$.

This shows that our modelling approach well matches the qualitative behaviour described at the beginning of this section.

All of the above analysis is for the case $\tilde{x}_3 = \frac{1}{2}$. If $\tilde{x}_3 < \frac{1}{2}$, more weight is given to the activation term and if $\tilde{x}_3 > \frac{1}{2}$, the death term gets more weight. We can visualise this behaviour by fixing $\frac{\delta_3}{\nu_3}$ and plotting,

$$\frac{d\tilde{x}_3}{d\tau} = 2\phi_3(\tilde{D})(1-\tilde{x}_3) - 2\frac{\delta_3}{\nu_3}\tilde{D}\tilde{x}_3 \tag{42}$$

vs. $\tilde{D}$ for various fixed values of $\tilde{x}_3$ [Fig. 13]. Here, we no longer set $\tilde{x}_3 = \frac{1}{2}$ but we again use the rescaled time τ to examine the qualitative shape of [Eq. 38] while just specifying the ratio $\frac{\delta_3}{\nu_3}$.

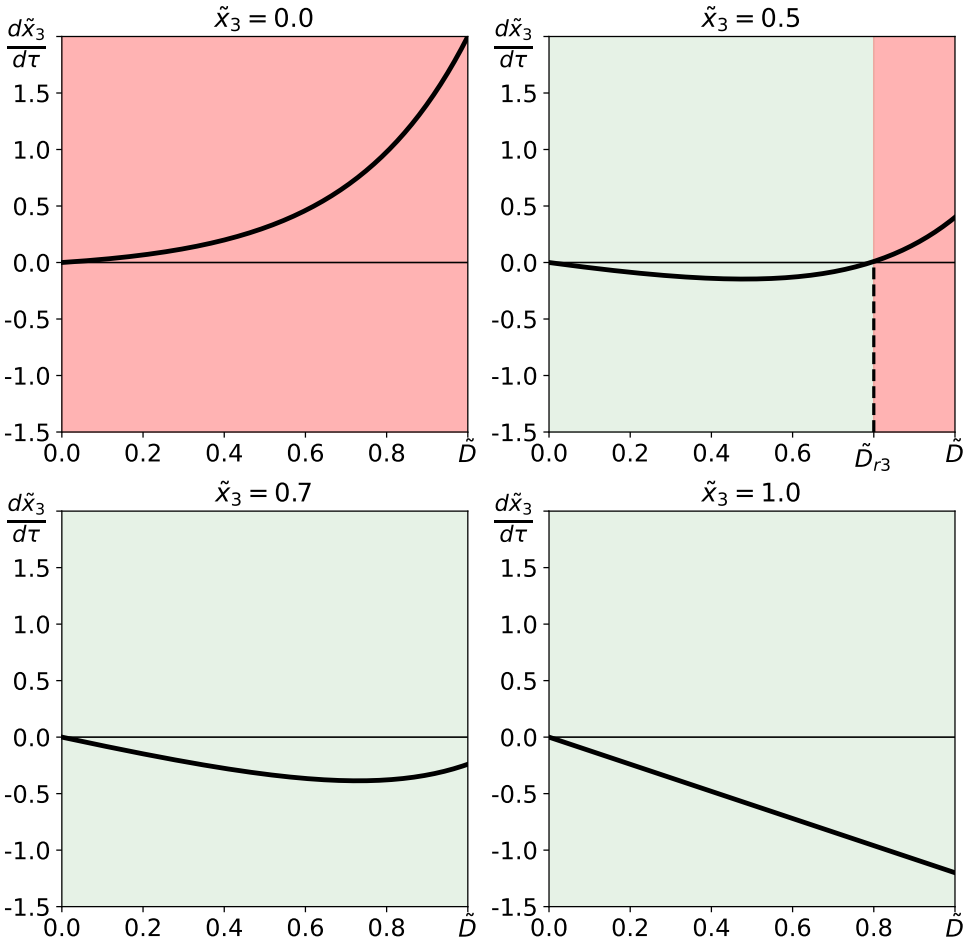


Figure 13: Plots of [Eq. 42] vs. $\tilde{D}$ for various fixed values of $\tilde{x}_3$. The region $\tilde{D} < \tilde{D}_{r3}$ is coloured green and indicates negative values of $\frac{d\tilde{x}_3}{d\tau}$. The region $\tilde{D} > \tilde{D}_{r3}$ is coloured red and indicates positive values of $\frac{d\tilde{x}_3}{d\tau}$. $\frac{\delta_3}{\nu_3} = 0.6$ and $a_3 = 3.41$ in each plot.

Finally, we also produce a heat map of [Eq. 42] over the whole $\tilde{D}$–$\tilde{x}_3$ plane [Fig. 14]. This allows us to observe for which combinations of $\tilde{D}$ and $\tilde{x}_3$, [Eq. 38] is positive, negative or equal to zero.

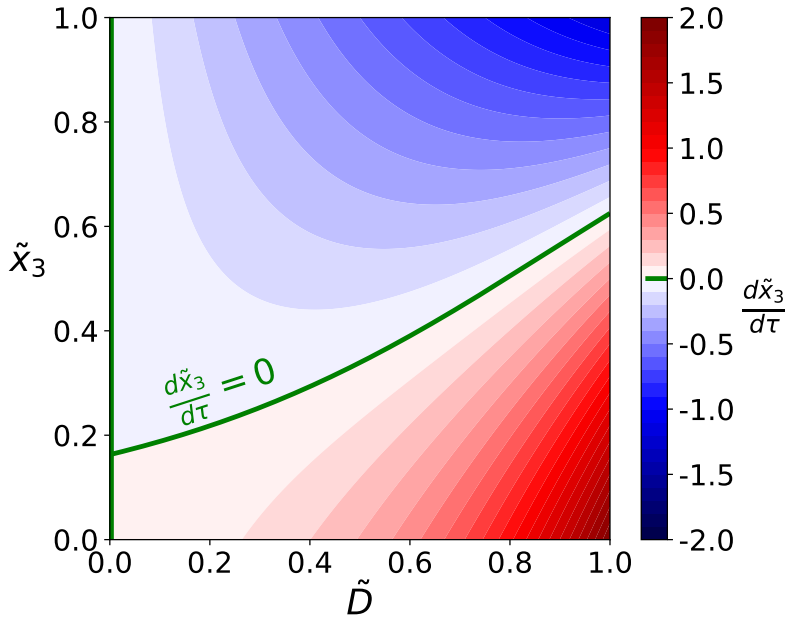


Figure 14: Heatmap of [Eq. 42] over the $\tilde{D}$–$\tilde{x}_3$ plane. The green lines represent the level curves where $\frac{d\tilde{x}_3}{d\tau} = 0$, i.e. the equilibrium position. Parameter values are $\frac{\delta_3}{\nu_3} = 0.6$ and $a_3 = 3.41$.

(14) & (15) Sensitive and resistant cancer-induced activation of inactive stroma. Cancer cells themselves can also trigger stromal cell activation. Cytokines and paracrine signalling molecules such as transforming growth factor beta (TGF-β) and platelet-derived growth factor (PDGF) released by cancer induce activation of fibroblasts into CAFs [34, 16, 65]. Paracrine cell signalling takes place over short distances, so we assume that a cancer cell must come into contact with an inactive fibroblast to induce the CAF phenotype. We follow the law of mass action and model cancer mediated activation of the stroma with the terms,

$$\rho_{31} x_1 (T - x_3)$$

and,

$$\rho_{32} x_2 (T - x_3)$$

for sensitive and resistant cancer respectively. With this our equation becomes,

$$\begin{aligned} \dot{x}_3 = &\{\text{Chemotherapy Induced Activation}\} - \{\text{Chemotherapy Induced Death}\} \\ &+ \rho_{31} x_1 (T - x_3) + \rho_{32} x_2 (T - x_3) - \{\text{Natural Inactivation}\}. \end{aligned} \tag{43}$$

(16) Slow inactivation of active stroma in the absence of stressors. Following successful cancer treatment where the cancer has entered full remission, we assume the stroma will slowly return to an inactive state after a long period

of time. We include a slow inactivation term,

$$-\epsilon x_3$$

where $\epsilon \ll \min(\rho_{31}, \rho_{32}, \nu_3)$. This is the final component of our equation,

$$\begin{aligned}\dot{x}_3 = &\{\text{Chemotherapy Induced Activation}\} - \{\text{Chemotherapy Induced Death}\} \\ &+\{\text{Cancer Induced Activation}\} - \epsilon x_3,\end{aligned} \tag{44}$$

and combined we obtain the complete active stroma equation as,

$$\begin{aligned}\dot{x}_3 = &\underbrace{\nu_3 \left(\frac{e^{a_3 \tilde{D}(t)} - 1}{e^{a_3} - 1} \right) (T - x_3)}_{\text{Chemotherapy Induced Activation}} - \underbrace{\delta_3 \tilde{D}(t) x_3}_{\text{Chemotherapy Induced Death}} \\ &+ \underbrace{\rho_{31} x_1 (T - x_3) + \rho_{32} x_2 (T - x_3)}_{\text{Cancer Induced Activation}} - \underbrace{\epsilon x_3}_{\text{Natural Inactivation}}\end{aligned} \tag{45}$$

The inactive stroma equation is then fixed by the condition $x_3(t) + x_4(t) = T \in \mathbb{R}$.

2.3.1 $\dot{x}_3$ and $\dot{x}_4$ System Sanity Check.

Similarly to what was done in Section 2.2.3, we will analyse the qualitative behaviour of [Eq. 45] for different but fixed in time values of $\tilde{D}(t) = \tilde{D}$, x_1 and x_2. Since x_1 and x_2 are fixed in time, we will define $C = x_1 + x_2$ to be the total amount of sensitive and resistant cancer combined. The aim of this analysis is to ensure that our model of the stroma behaves as we expect. Again, we will make use of some temporary variable rescalings and simplifying assumptions which will all be reintroduced prior to simulating the model.

The simplifying assumptions we will make are,

1. $\rho_{31} = \rho_{32} = \rho_{3C}$.

The variable rescalings we will use are,

1. $\tilde{x}_{1/2} = \frac{x_{1/2}}{C^*}$. Also, since x_1 and x_2 are fixed in time, we have that $\tilde{C} = \frac{C}{C^*} = \tilde{x}_1 + \tilde{x}_2$ is the total, rescaled amount of sensitive and resistant cancer combined.
2. $\tilde{x}_3 = \frac{x_3}{T}$.
3. $\tilde{t} = r_1 t$.

Again, see Section 3.1 for the full details.

With these rescalings and simplifications the $\frac{d\tilde{x}_3}{d\tilde{t}}$ equation becomes,

$$\frac{d\tilde{x}_3}{d\tilde{t}} = \tilde{\nu}_3 \left(\frac{e^{a_3\tilde{D}} - 1}{e^{a_3} - 1} \right) (1 - \tilde{x}_3) - \tilde{\delta}_3 \tilde{D}\tilde{x}_3 + \tilde{\rho}_{3C}\tilde{C}(1 - \tilde{x}_3) - \tilde{\epsilon}\tilde{x}_3, \tag{46}$$

where: $\tilde{\nu}_3 = \frac{\nu_3}{r_1}$, $\tilde{\delta}_3 = \frac{\delta_3}{r_1}$, $\tilde{\rho}_{3C} = \frac{\rho_{3C}C^*}{r_1}$ and $\tilde{\epsilon} = \frac{\epsilon}{r_1}$.

We can now solve for the only equilibrium solution of [Eq. 46], $\tilde{x}_3^e$, as follows,

$$\begin{aligned}
\dot{\tilde{x}}_3 &= 0 \\
\tilde{\rho}_{3C}\tilde{C} + \tilde{\nu}_3 \left(\frac{e^{a_3\tilde{D}} - 1}{e^{a_3} - 1} \right) &= \tilde{x}_3^e \left(\tilde{\rho}_{3C}\tilde{C} + \tilde{\nu}_3 \frac{e^{a_3\tilde{D}} - 1}{e^{a_3} - 1} + \tilde{\delta}_3\tilde{D} + \tilde{\epsilon} \right) \\
\tilde{x}_3^e &= \frac{\tilde{\rho}_{3C}\tilde{C} + \tilde{\nu}_3 \left(\frac{e^{a_3\tilde{D}} - 1}{e^{a_3} - 1} \right)}{\tilde{\rho}_{3C}\tilde{C} + \tilde{\nu}_3 \left(\frac{e^{a_3\tilde{D}} - 1}{e^{a_3} - 1} \right) + \tilde{\delta}_3\tilde{D} + \tilde{\epsilon}}
\end{aligned} \tag{47}$$

This equilibrium solution is always stable since,

$$\begin{aligned}
\frac{d}{d\tilde{x}_3} \left(\frac{d\tilde{x}_3}{d\tilde{t}} \right) &= \frac{d}{d\tilde{x}_3} \left(\tilde{\nu}_3 \left(\frac{e^{a_3\tilde{D}} - 1}{e^{a_3} - 1} \right) (1 - \tilde{x}_3) - \tilde{\delta}_3\tilde{D}\tilde{x}_3 + \tilde{\rho}_{3C}\tilde{C}(1 - \tilde{x}_3) - \tilde{\epsilon}\tilde{x}_3 \right) \\
&= -\tilde{\nu}_3 \left(\frac{e^{a_3\tilde{D}} - 1}{e^{a_3} - 1} \right) - \tilde{\delta}_3\tilde{D} - \tilde{\rho}_{3C}\tilde{C} - \tilde{\epsilon} \\
&= -\left(\tilde{\nu}_3 \left(\frac{e^{a_3\tilde{D}} - 1}{e^{a_3} - 1} \right) + \tilde{\delta}_3\tilde{D} + \tilde{\rho}_{3C}\tilde{C} + \tilde{\epsilon} \right) < 0.
\end{aligned}$$

Thus,

$$\frac{d}{d\tilde{x}_3} \left(\frac{d\tilde{x}_3}{d\tilde{t}} \right) \Bigg|_{\tilde{x}_3 = \tilde{x}_3^e} < 0$$

for any $\tilde{x}_3^e$.

We will first analyse the behaviour of the equilibrium position for the special cases,

1. $\tilde{D} = 0$

$$\tilde{x}_3^e|_{\tilde{D}=0} = \frac{\tilde{\rho}_{3C}\tilde{C}}{\tilde{\rho}_{3C}\tilde{C} + \tilde{\epsilon}} \tag{48}$$

2. $\tilde{C} = 0$

$$\tilde{x}_3^e|_{\tilde{C}=0} = \frac{\tilde{\nu}_3 \left(\frac{e^{a_3\tilde{D}} - 1}{e^{a_3} - 1} \right)}{\tilde{\nu}_3 \left(\frac{e^{a_3\tilde{D}} - 1}{e^{a_3} - 1} \right) + \tilde{\delta}_3\tilde{D} + \tilde{\epsilon}} \tag{49}$$

We can show that $\tilde{x}_3^e|_{\tilde{D}=0}$ and $\tilde{x}_3^e|_{\tilde{C}=0}$ are non-decreasing functions of $\tilde{C} \in [0, 1]$ and $\tilde{D} \in [0, 1]$ respectively, see appendix A.3. This means that if $\tilde{D} = 0$ is fixed, then as cancer size increases, the active stroma equilibrium also increases.

Similarly, if $\tilde{C} = 0$ is fixed, then as chemotherapy intensity increases, the active stroma equilibrium also increases. This agrees with what we expect since cancer growth can only stimulate stromal activation and applying chemotherapy to a healthy patient only agitates the stroma, and is of no benefit. To illustrate this we plot $\tilde{x}_3^e|_{\tilde{D}=0}$ and $\tilde{x}_3^e|_{\tilde{C}=0}$ vs. $\tilde{C}$ and $\tilde{D}$ respectively [Fig. 15]. For the plot of $\tilde{x}_3^e|_{\tilde{D}=0}$, we fix $\tilde{\epsilon}$ and present various different values of $\tilde{\rho}_{3C}$. For the plot of $\tilde{x}_3^e|_{\tilde{C}=0}$, we fix $\tilde{\delta}_3$, $\tilde{\epsilon}$ and a_3 and present various different values of $\tilde{\nu}_3$.

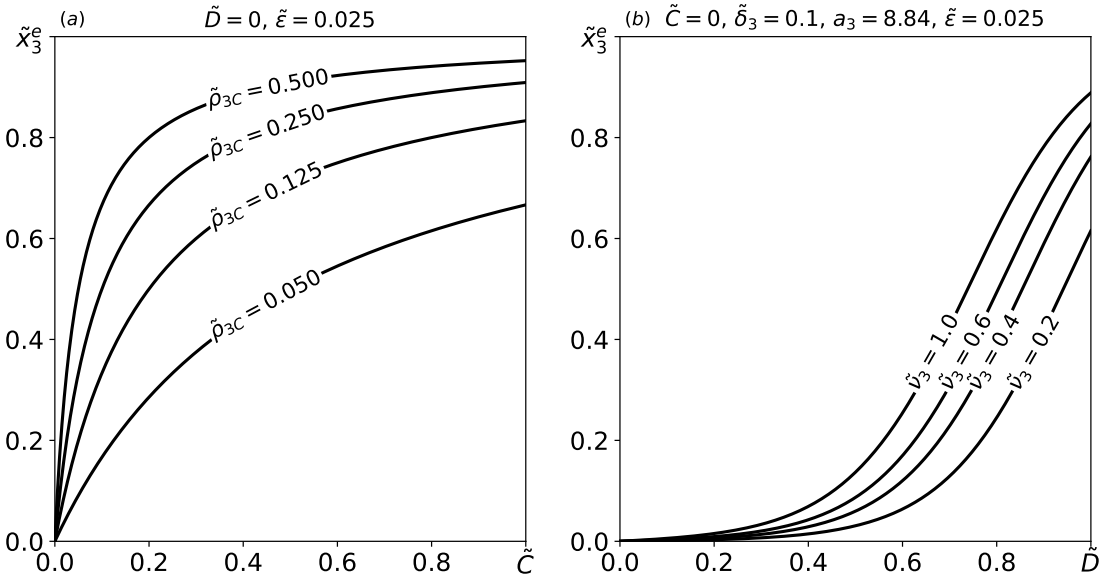


Figure 15: (a) Plots of $\tilde{x}_3^e$ vs. $\tilde{C}$ [Eq. 48] for various $\tilde{\rho}_{3C}$, with $\tilde{D} = 0$ and $\tilde{\epsilon} = 0.025$. (b) Plots of $\tilde{x}_3^e$ vs. $\tilde{D}$ [Eq. 49] for various $\tilde{\nu}_3$, with $\tilde{C} = 0$, $\tilde{\delta}_3 = 0.1$, $a_3 = 8.84$ and $\tilde{\epsilon} = 0.025$.

From [Fig. 15], we can see that $\tilde{x}_3^e|_{\tilde{D}=0}$ increases rapidly at first with increasing $\tilde{C}$, but then slows as $\tilde{C}$ approaches 1. The rapid increase occurs because $\tilde{\epsilon} \ll \tilde{\rho}_{3C}$. We have that $\tilde{x}_3^e|_{\tilde{D}=0} > \frac{1}{2}$ if $\tilde{C} > \frac{\tilde{\epsilon}}{\tilde{\rho}_{3C}}$ and so only small values of $\tilde{C}$ are required to obtain large values of $\tilde{x}_3^e$. As $\tilde{x}_3$ becomes large, $\tilde{\rho}_{3C}\tilde{C}(1 - \tilde{x}_3)$ becomes small and $\tilde{\epsilon}\tilde{x}_3$ becomes large, which explains why the graph tapers off.

$\tilde{x}_3^e|_{\tilde{C}=0}$ behaves differently. Initially as $\tilde{D}$ increases, $\tilde{x}_3^e|_{\tilde{C}=0}$ rises very slowly, only becoming large as $\tilde{D}$ approaches 1. We have that $\tilde{x}_3^e > \frac{1}{2}$ if $\tilde{\nu}_3\phi_3(\tilde{D}) - \tilde{\delta}_3\tilde{D} > \tilde{\epsilon}$, but chemotherapy induced stromal activation only dominates for high intensity chemotherapy, thus large values of $\tilde{D}$ are required to obtain large values $\tilde{x}_3^e$.

We can now produce a heatmap of $\frac{d\tilde{x}_3}{d\tilde{t}}$ in the $\tilde{D}$–$\tilde{x}_3$ plane, similar to [Fig. 14], which now includes all terms of the $\frac{d\tilde{x}_3}{d\tilde{t}}$ equation [Fig. 16]. Aside from including the complete equation, the set up for this figure also differs from [Fig. 14] in another way. We are now using the rescaled time $\tilde{t}$ instead of τ, and as such must specify particular values of ν_3 and δ_3 which we choose using [Fig. 15].

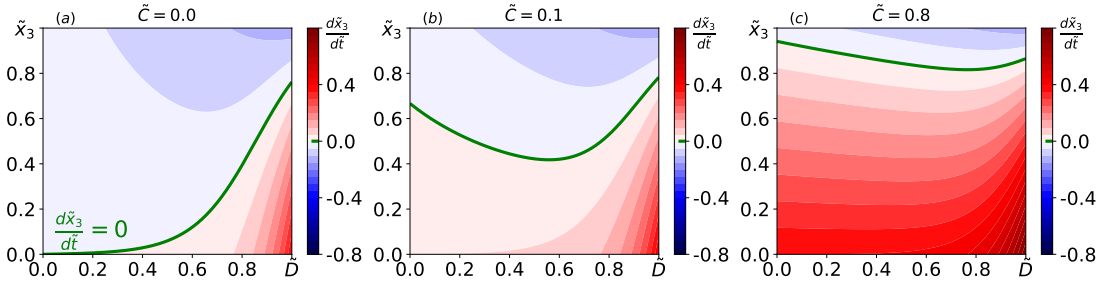


Figure 16: Heat maps of [Eq. 46], $\frac{d\tilde{x}_3}{d\tilde{t}}$, over the whole $\tilde{D}$–$\tilde{x}_3$ plane, with (a) $\tilde{C} = 0.0$, (b) $\tilde{C} = 0.1$ and (c) $\tilde{C} = 0.8$. Parameter values across all three plots are, $\tilde{\rho}_{3C} = 0.5$, $a_3 = 8.84$, $\tilde{\nu}_3 = 0.4$, $\tilde{\delta}_3 = 0.1$ and $\tilde{\epsilon} = 0.025$. The green line in each figure represents the level curve where $\dot{\tilde{x}}_3 = 0$, i.e. the equilibrium position $\tilde{x}_3^e$.

Next, we examine the behaviour of $\tilde{x}_3^e$ as we vary both $\tilde{D}$ and $\tilde{C}$. To do this we produce plots of $\tilde{x}_3^e$ vs. $\tilde{D}$ for various $\tilde{C}$ [Fig. 17(a)] as well as a heat map of $\tilde{x}_3^e$ in the $\tilde{D}$–$\tilde{C}$ plane [Fig. 17(b)]. We use the same set of parameter values for both figures as was used in [Fig. 16].

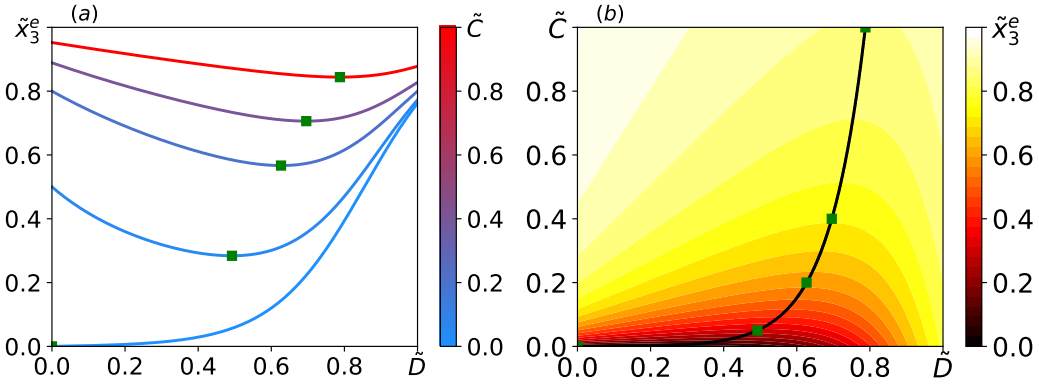


Figure 17: (a) Plots of $\tilde{x}_3^e$ vs. $\tilde{D}$ [Eq. 47] for $\tilde{C} \in [0.00, 0.05, 0.20, 0.40, 1.00]$. Green squares indicate the minimum value of $\tilde{x}_3^e$ for each $\tilde{C}$. (b) A heat map of $\tilde{x}_3^e$ [Eq. 47] in the $\tilde{D}$–$\tilde{C}$ plane. The black curve shows the locations of the minimum values of $\tilde{x}_3^e$ for each fixed $\tilde{C}$. The green squares correspond to the particular minima plotted in (a). Parameter values for both figures are $\tilde{\rho}_{3C} = 0.5$, $\tilde{\nu}_3 = 0.4$, $a_3 = 8.84$, $\tilde{\delta}_3 = 0.1$ and $\tilde{\epsilon} = 0.025$.

From [Fig. 17(a)], we see that by increasing $\tilde{C}$ the left tail of $x_3^e|_{\tilde{C}=0}$ rises rapidly and a dip appears in the curve. This shows that once cancer has developed, it can be advantageous to apply a certain intensity of chemotherapy in order to minimise the amount of active stroma. [Fig. 17(b)] showcases the behaviour of $\tilde{x}_3^e$ across the entire $\tilde{D}$–$\tilde{C}$ plane and the chemotherapy intensities which minimise $\tilde{x}_3^e$ given any fixed $\tilde{C}$.

This analysis verifies that our model of stromal activation behaves how we expect. However, this analysis is based on fixed in time $\tilde{C}(t)$ and $\tilde{D}(t)$, in reality cancer size will itself depend on both chemotherapy intensity and the active

stroma and as such the true behaviour of the system will be different.

2.4 Immune System Equation ($\dot{x}_5$)

To include the immune system in our model, we follow the work of Kuznetsov et al. [38]. Their model describes tumour-immune interaction within the TME. It captures important biological processes such as the innate immune system, the adaptive immune response to cancer and cancer-induced immune suppression [47, 51, 79, 87].

In order to combine this model with ours, it is necessary to consider how the immune system responds to chemotherapy. Chemotherapy is a foreign agent that damages cells, which triggers an immune response [89, 7, 62]. However, at high doses, chemotherapy becomes very toxic damaging the immune cells themselves and suppressing the immune system [89, 67].

In [Fig. 18] we present a qualitative schematic of how we understand the immune system to respond to chemotherapy intensity. When the intensity of chemotherapy is zero (absence of chemotherapy), the immune system strength is at normal levels. As the intensity increases, the immune system strength rises attaining a maximum at some optimal intensity. Beyond this point, the immune system strength weakens, falling below normal levels after some critical intensity is reached. At the maximum tolerated dose, the number of effective immune cells present in the tumour microenvironment is greatly diminished.

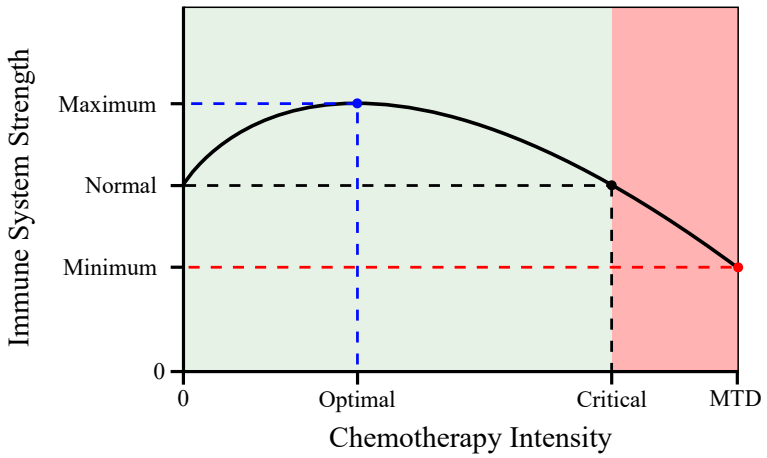


Figure 18: Schematic of immune response to chemotherapy.

While this is how the immune system responds to chemotherapy in general, there is variation in each individual's immune system. Such variation can arise from factors including sex, genetics, age, gut microbiota and lifestyle choices including smoking habits [9]. This results in patients whose immune systems

vary in their responsiveness to stimuli [33], in our case, to chemotherapy. As such we aim for flexibility, such that the model can describe two classes of patient, unresponsive and responsive.

The schematics in [Fig. 19] compare the immune responses of unresponsive and responsive patients to chemotherapy intensity. Immune stimulation of unresponsive patients may be weaker than responsive patients, leading to a lower maximum immune strength. This also leads to a lower critical chemotherapy intensity, meaning unresponsive patients are less able to withstand intense chemotherapy. The optimal and critical chemotherapy intensities can change depending on whether an individual has a responsive or unresponsive immune system.

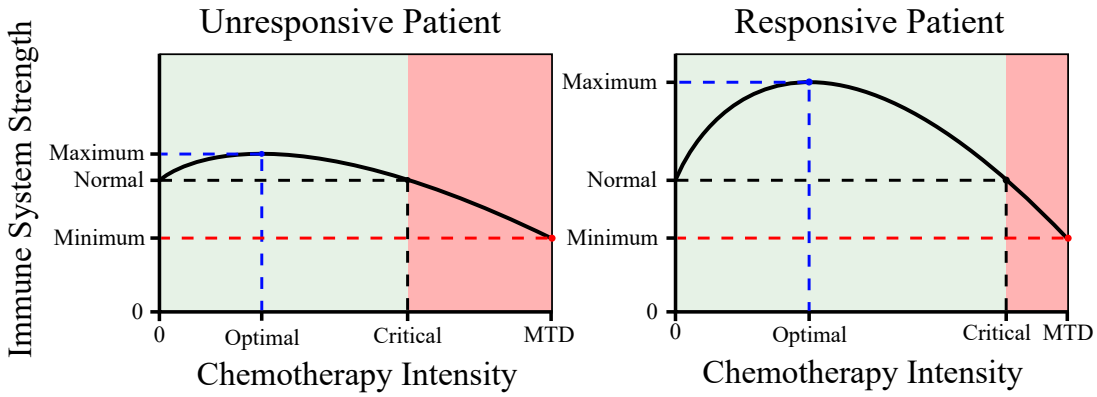


Figure 19: Schematics of unresponsive and responsive patient's immune responses to chemotherapy intensity.

With these considerations in mind we will re-derive the model from Kuznetsov et al. [38] with the addition of our own chemotherapy response term. The model will take the following form,

$$\begin{aligned}\dot{x}_5 =&\{\text{Cell Influx}\}\cdot\{\text{Chemotherapy Response}\}-\{\text{Natural Cell Death}\}\\&+\{\text{Cancer Induced Stimulation}\}-\{\text{Cancer Induced Supression}\}.\end{aligned}\tag{50}$$

(17) Constant source of immune cells.

Immune cells are produced in the bone marrow, mature at various different organs and are transported through blood and lymph vessels throughout the body. These cells are part of the innate immune system [51]. To model the innate immune system, we assume there is a constant influx of immune cells in the absence of stressors and include the term,

$$s$$

in the $\dot{x}_5$ equation. This forms the cell influx component of the immune system model,

$$\begin{aligned}\dot{x}_5 = s\cdot\{\text{Chemotherapy Response}\} - \{\text{Natural Cell Death}\} \\ +\{\text{Cancer Induced Stimulation}\} - \{\text{Cancer Induced Supression}\}.\end{aligned} \tag{51}$$

(18) Natural death of immune cells.

We assume that these immune cells have a natural life cycle and undergo cell death to maintain a stable immune system in the absence of stressors. We model this with the term,

$$-dx_5.$$

This, together with the influx term, the $\dot{x}_5$ equation becomes,

$$\begin{aligned}\dot{x}_5 = s\cdot\{\text{Chemotherapy Response}\} - dx_5 \\ +\{\text{Cancer Induced Stimulation}\} - \{\text{Cancer Induced Supression}\}.\end{aligned} \tag{52}$$

Thus, in the absence of any stressors, there is an equilibrium level of immune cells,

$$x^e_{5,0} = \frac{s}{d}.$$

In reality, this equilibrium only exists on relatively short time scales of a few years, as an individual's immune system strength can weaken with age. Additionally, the specific values of s and d may depend on the tissue into which the immune cells are entering. Consequently, $\frac{s}{d}$ will vary across different tissues and as such, the initial or equilibrium level of immune cells within a tumour microenvironment, prior to cancer development, will depend on the tissue in which the cancer originates. This equilibrium is then disrupted by the presence of cancer and the administration of chemotherapy.

This also provides a definition, in terms of the model parameters, for I_0, which was introduced in Sections 2.2.3 and 2.3.1 as the strength of the immune system under normal circumstances,

$$I_0 = x^e_{5,0} = \frac{s}{d}.$$

(19) & (20) Death vs. stimulation of the immune system in response to chemotherapy.

Intense chemotherapy is immunosuppressive, with many chemotherapeutic drugs having the capacity to impair and kill T-cells [7, 68, 89, 62].

On the other hand, low doses of chemotherapy were shown to be able to stimulate an immune response through direct immune cell activation and depletion of

immune suppressor cells [7, 62, 89, 27]. Chemotherapy can convert immunosuppressive type-M2 macrophages into anti-tumour type-M1 macrophages [7, 53, 27]. It also depletes other immune suppressor cells such as regulatory T-cells, which in turn encourages T-cell proliferation. Some types of chemotherapy, anthracyclines in particular, can cause immunogenic cell death which triggers a further adaptive immune response [7, 89, 53, 27].

We propose that, in the absence of cancer, the equilibrium position of the $\dot{x}_5$ equation as a function of $\tilde{D}(t)$ should be given by,

$$\frac{s}{d}\phi_{51}(\tilde{D}(t))$$

where,

$$\phi_{51}(\tilde{D}(t)) = \frac{e^{a_{51}b} + e^{-\eta a_{51}b}}{e^{-a_{51}(\tilde{D}(t)-b)} + e^{\eta a_{51}(\tilde{D}(t)-b)}} \tag{53}$$

and,

$$b = \tilde{D}_{\text{opt},5} + \frac{\ln(\eta)}{a_{51} + \eta a_{51}}. \tag{54}$$

See appendix A.4 for the derivation of $\tilde{D}_{\text{opt},5}$. ϕ_{51} is a shifted and asymmetric sech function that we have taken from [60]. When $\tilde{D}(t) = 0$, $\phi_{51} = 1$. Initially, as $\tilde{D}(t)$ increases, ϕ_{51} also increases. ϕ_{51} attains a maximum value, $\phi_{51,\max}$, at $\tilde{D}(t) = \tilde{D}_{\text{opt},5}$. As $\tilde{D}(t)$ increases above $\tilde{D}_{\text{opt},5}$, ϕ_{51} decreases, eventually falling below $\phi_{51} = 1$. We implicitly define $\tilde{D}(t) = \tilde{D}_{r5}$ as the non-zero chemotherapy intensity at which $\phi_{51} = 1$, i.e., the solution to,

$$\frac{e^{a_{51}b} + e^{-\eta a_{51}b}}{e^{-a_{51}(\tilde{D}(t)-b)} + e^{\eta a_{51}(\tilde{D}(t)-b)}} = 1.$$

Thus, $\phi_{51} \geq 1$ for $\tilde{D}(t) \in [0, \tilde{D}_{r5}]$ and $\phi_{51} < 1$ for $\tilde{D}(t) \in (\tilde{D}_{r5}, 1]$. Such an equilibrium aligns with the schematic shown in [Fig. 18] and reflects our expectations of the immune system's response to chemotherapy. This can be seen by examining the shape of $\phi_{51}(\tilde{D})$, plotted in [Fig. 20].

To derive such an equilibrium, we introduce a chemotherapy response term, $G(\tilde{D}(t))$, into the $\dot{x}_5$ equation as follows,

$$\dot{x}_5 = s - dx_5 + G(\tilde{D}(t)). \tag{55}$$

We then solve for the equilibrium solution, $x^e_{5,D}$, by setting $\dot{x}_5 = 0$ in [Eq. 55]. The resulting expression for $x^e_{5,D}$ is set equal to $\frac{s}{d}\phi_{51}(\tilde{D}(t))$, allowing us to solve for $G(\tilde{D}(t))$,

$$x^e_{5,D} = \frac{s + G(D)}{d} = \frac{s}{d}\phi_{51}(\tilde{D}(t)).$$

Solving for $G(\tilde{D}(t))$, we obtain,

$$G(\tilde{D}(t)) = s(\phi_{51}(\tilde{D}(t)) - 1),$$

Finally, substituting this back into [Eq. 55] yields,

$$\begin{aligned}\dot{x}_5 &= s - dx_5 + s(\phi_{51}(\tilde{D}(t)) - 1) \\ &= s\phi_{51}(\tilde{D}(t)) - dx_5\end{aligned}$$

Therefore, in the absence of cancer, the $\dot{x}_5$ equation becomes,

$$\begin{aligned}\dot{x}_5 = s\phi_{51}(\tilde{D}(t)) - dx_5 &+ \{\text{Cancer Induced Stimulation}\} \\ &- \{\text{Cancer Induced Supression}\}.\end{aligned} \tag{56}$$

This modelling approach ensures that for fixed values of $\tilde{D}(t) = \tilde{D}$, the equilibrium solution $x^e_{5,\mathrm{D}}$ is given by,

$$x^e_{5,\mathrm{D}} = \frac{s}{d}\phi_{51}(\tilde{D}).$$

This function of $\tilde{D}$ is a scaled version of $\phi_{51}(\tilde{D})$. From the plots in [Fig. 20], it is evident that the immune system's qualitative response to chemotherapy matches our expectations, as discussed earlier in Section 2.4, featuring both optimal ($\tilde{D}_{\mathrm{opt},5}$) and critical ($\tilde{D}_{r5}$) chemotherapy intensities in its response. [Fig. 20] also highlights the flexibility of the shape of $\phi_{51}(\tilde{D})$, allowing us to account for both responsive and unresponsive patients.

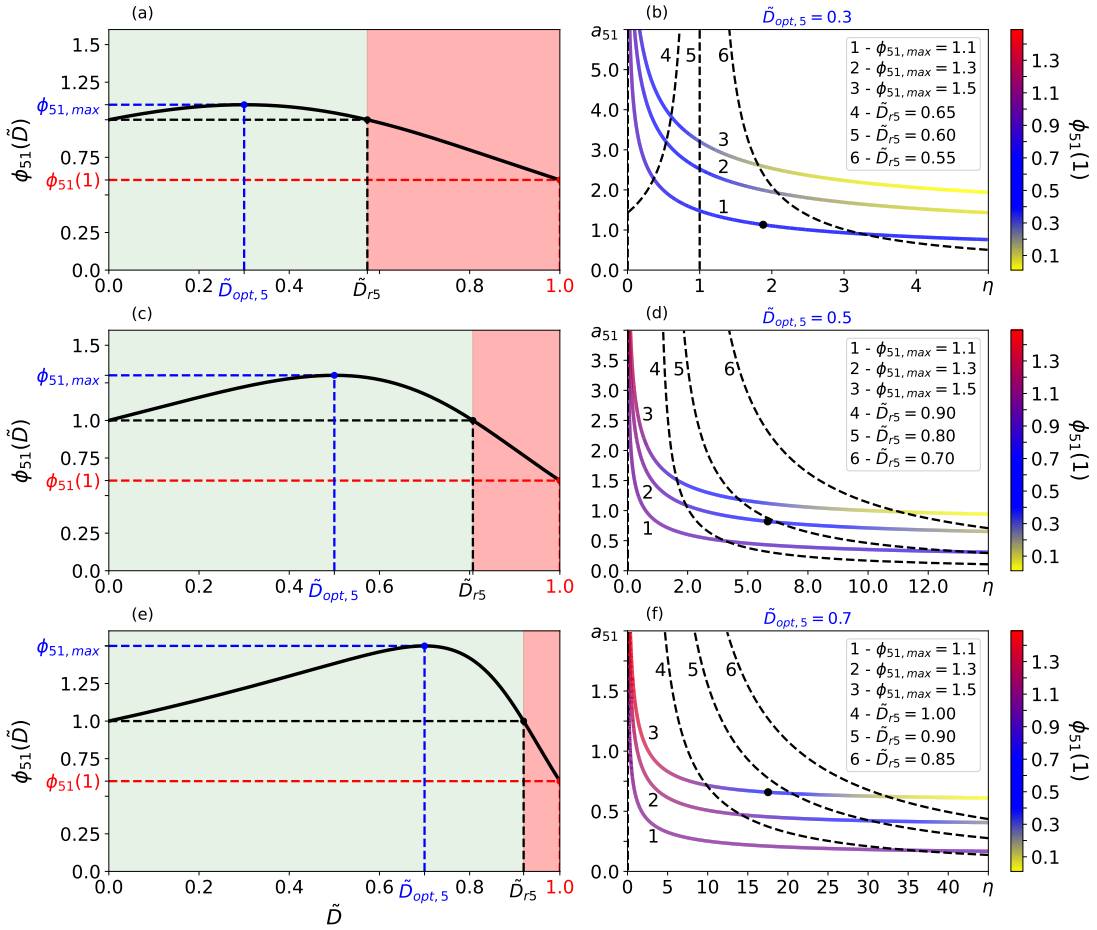


Figure 20: Left Column: Plots of $\phi_{51}(\tilde{D})$ for **(a)** $\tilde{D}_{\text{opt},5} = 0.3$, $a_{51} = 1.1313$ and $\eta = 1.88$, **(c)** $\tilde{D}_{\text{opt},5} = 0.5$, $a_{51} = 0.8206$ and $\eta = 5.83$ and **(e)** $\tilde{D}_{\text{opt},5} = 0.7$, $a_{51} = 0.6585$ and $\eta = 17.53$. Parameters were chosen such that $\phi_{51}(1) \approx 0.6$ and $\phi_{51,\max} = 1.1$, 1.3 and 1.5 in each of (a), (c) and (e) respectively. **Right Column:** Level curves of $\phi_{51,\max}$ (coloured) and $\tilde{D}_{r5}$ (dashed black) in the η–a_{51} plane. $\tilde{D}_{\text{opt},5} = 0.3$, 0.5 and 0.7 fixed in (b), (d) and (f) respectively. The colouring of the $\phi_{51,\max}$ level curves corresponds to the values of $\phi_{51}(1)$ at those parameter values. Red implies $\phi_{51}(1) > 0.7$, blue implies $0.7 > \phi_{51}(1) > 0.4$ and yellow implies $0.4 > \phi_{51}(1)$. Each level curve is numbered $1-6$ and the legend provides the constant values of $\phi_{51,max}$ (1-3) and $\tilde{D}_{r5}$ (4-6) along each curve. The black dots mark the parameters chosen to produce the corresponding figure on the left within each row.

(21) & (22) Cancer Induced Immune Stimulation and Suppression.

Cancer growth will also dictate immune system function. Macrophages at the tumour site respond to cancer by producing cytokines that recruit other immune cells such as neutrophils [2, p.1531], [51]. Additionally, dendritic cells respond to cancer cell induced damage and communicate with T and B cells to trigger an adaptive immune response [51, 47]. In this way, cancer growth stimulates an immune response which increases the number of immune cells.

On the other hand, cancer cells express immune checkpoint molecules on their surface. These molecules suppress the activity of immune cells such as T-cells

when they come into contact with the cancer cell. Additionally, repeated exposure of T-cells to cancer may lead to T-cell exhaustion whereby T-cell function is diminished [87, 38].

As such we assume that the immune system initially responds to small tumours, but then becomes overwhelmed as the tumour grows leading to immune supression. To model stimulation and suppression respectively, we let

$$C(t) = x_1(t) + x_2(t),$$

and include the terms,

$$\rho_{5C}\phi_{52}(C(t))x_5 \quad \text{and} \quad -\sigma_{5C}C(t)x_5,$$

where,

$$\phi_{52}(C(t)) = \frac{C(t)}{a_{52} + C(t)}$$

in the $\dot{x}_5$ equation. The functional response term, ϕ_{52}, is included to model limited immune cell accumulation, within the tumour microenvironment, as the tumour grows large. This is due to natural limits on the rates at which immune cells can travel to and permeate into the tumour [38].

With these terms the $\dot{x}_5$ equation becomes,

$$\begin{aligned}\dot{x}_5 =& \{\text{Cell Influx}\} \cdot \{\text{Chemotherapy Response}\} - \{\text{Natural Cell Death}\} \\ &+ \rho_{5C}\phi_{52}(C(t))x_5 - \sigma_{5C}C(t)x_5. \end{aligned} \tag{57}$$

We would like to ensure that there is always an initial increase in the immune system for small tumours, thus we must ensure the existence of a $C(t) > 0$ root of,

$$\rho_{5C}\phi_{52}(C(t))x_5 - \sigma_{5C}C(t)x_5 \tag{58}$$

The roots are given by,

$$C(t) = 0 \quad \text{and} \quad C(t) = \frac{\rho_{5C} - \sigma_{5C}a_{52}}{\sigma_{5C}}.$$

Thus, we impose,

$$\rho_{5C} > \sigma_{5C}a_{52}.$$

Once again, let $C(t) = C$ represent different but fixed-in-time values of $C(t)$. We would like to make it easier to fix the shape of the immune system response to cancer and we will do this by reparameterising the cancer terms of the $\dot{x}_5$ equation [Eq. 57]. Consider the per-capita growth rate of x_5 with $s = d = 0$, i.e.

just the cancer terms,

$$\left.\frac{\dot{x}_5}{x_5}\right|_{s,d=0} = \rho_{5C}\phi_{52}(C) - \sigma_{5C}C. \tag{59}$$

We will reparameterise this expression in terms of the new parameters C_r, C_{opt} and M, which are defined as follows: C_r is the non-zero C for which [Eq. 59] is zero, that is, its non-zero root. C_{opt} is the value of C at which [Eq. 59] attains a maximum. M is the value of [Eq. 59] evaluated at C_{opt}, that is, its maximum value. With this reparameterisation, we will be able to explicitly choose, using the model parameters, the optimal cancer size for immune stimulation and its magnitude, as well as the critical cancer size at which the immune system starts to become suppressed. Calculations for this reparameterisation are given in appendix A.5 and the transformation is given by,

$$\begin{aligned} C_r &= \frac{\rho_{5C}}{\sigma_{5C}} - a_{52} \\ C_{\text{opt}} &= -a_{52} + \sqrt{\frac{\rho_{5C}a_{52}}{\sigma_{5C}}} \\ M &= \left(\sqrt{\rho_{5C}} - \sqrt{\sigma_{5C}a_{52}}\right)^2 \end{aligned} \tag{60}$$

This transformation holds on the condition that,

$$\rho_{5C} > \sigma_{5C}a_{52}.$$

which we have already assumed to be true. The inverse transformation is given by,

$$\begin{aligned} a_{52} &= \frac{C_{\text{opt}}^2}{C_r - 2C_{\text{opt}}} \\ \rho_{5C} &= M\left(\frac{C_r - C_{\text{opt}}}{C_r - 2C_{\text{opt}}}\right)^2 \\ \sigma_{5C} &= \frac{M}{C_r - 2C_{\text{opt}}}, \end{aligned} \tag{61}$$

on the condition that,

$$C_{\text{opt}} < \frac{C_r}{2}.$$

This is equivalent to the condition, $\rho_{5C} > \sigma_{5C}a_{52}$.

Under this change of parameters, [Eq. 59] becomes,

$$\left.\frac{\dot{x}_5}{x_5}\right|_{s,d=0} = MC\left(\frac{C_r - C}{C_{\text{opt}}^2 + C\left(C_r - 2C_{\text{opt}}\right)}\right) \tag{62}$$

To produce a sensible plot of this expression we will rescale some of the model variables as follows,

1. $\tilde{C} = \frac{C}{C^*}$.

2. $\tilde{t} = r_1 t$.

Note that rescaling x_5 would have no effect on the right hand side of [Eq. 62]. With this, [Eq. 62] becomes,

$$\left(\frac{1}{x_5}\frac{dx_5}{d\tilde{t}}\right)\Big|_{s,d=0} = \tilde{M}\tilde{C}\left(\frac{\tilde{C}_r - \tilde{C}}{\tilde{C}_{\text{opt}}^2 + \tilde{C}\left(\tilde{C}_r - 2\tilde{C}_{\text{opt}}\right)}\right) \tag{63}$$

where,

$$\tilde{M} = \frac{M}{r_1} \quad , \quad \tilde{C}_r = \frac{C_r}{C^*} \quad \text{and} \quad \tilde{C}_{\text{opt}} = \frac{C_{\text{opt}}}{C^*}. \tag{64}$$

are the rescaled values of M, C_r and C_{opt} respectively. We can now plot [Eq. 63] for a sample choice of $\tilde{M}$, $\tilde{C}_r$ and $\tilde{C}_{\text{opt}}$ [Fig. 21].

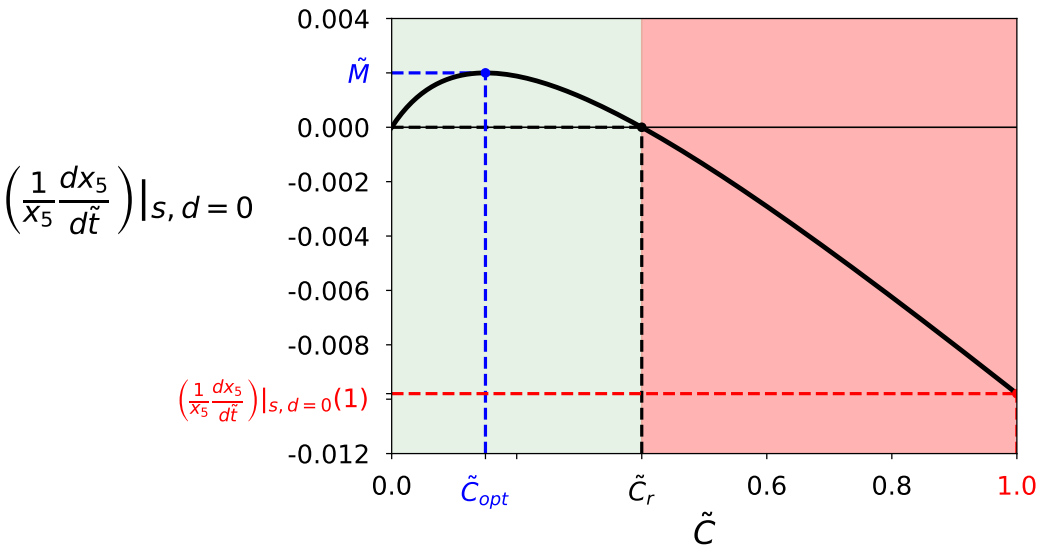


Figure 21: Plot of [Eq. 63]. The dashed blue line highlights the relationship between the parameters $\tilde{C}_{\text{opt}}$ and $\tilde{M}$. The dashed black line highlights that the non-zero root of [Eq. 63] occurs at $\tilde{C}_r$. Dashed red line highlights that [Eq. 63] is negative by the time cancer reaches the lethal threshold. $\tilde{C}_r = 0.4$, $\tilde{C}_{\text{opt}} = 0.15$ and $\tilde{M} = 0.002$.

Combining all of the derived terms, we obtain the complete $\dot{x}_5$ equation in

terms of the original parameters as follows,

$$\dot{x}_5 = \underbrace{s}_{\text{Cell Influx}} \cdot \underbrace{\phi_{51}(\tilde{D}(t))}_{\text{Chemotherapy Response}} - \underbrace{dx_5}_{\text{Natural Cell Death}} + \underbrace{\rho_{5C}\left(\frac{x_1+x_2}{a_{52}+x_1+x_2}\right)x_5}_{\text{Cancer Induced Stimulation}} - \underbrace{\sigma_{5C}(x_1+x_2)x_5}_{\text{Cancer Induced Supression}} . \tag{65}$$

The complete equation after the reparameterisation is given by,

$$\dot{x}_5 = \underbrace{s}_{\text{Cell Influx}} \cdot \underbrace{\phi_{51}(\tilde{D}(t))}_{\text{Chemotherapy Response}} - \underbrace{dx_5}_{\text{Natural Cell Death}} + \underbrace{M\,(x_1+x_2)\left(\frac{C_r-(x_1+x_2)}{C_{\text{opt}}^2+(x_1+x_2)\,(C_r-2C_{\text{opt}})}\right)x_5}_{\text{Cancer Induced Stimulation/Supression}} . \tag{66}$$

We will switch between these two equivalent formulations depending on which is more convenient for a given objective.

2.4.1 $\dot{x}_5$ Sanity Check.

As was done with the previous equations in Sections 2.2.3 and 2.3.1, we will now analyse the qualitative behaviour of the $\dot{x}_5$ equation assuming different but fixed in time values of $\tilde{D}(t) = \tilde{D}$, x_1 and x_2. This will allow us to verify that our model of the immune system behaves sensibly. For the purposes of this analysis we will again work with the below variable rescalings,

1. $\tilde{x}_{1/2} = \frac{x_{1/2}}{C^*}$.
2. $\tilde{x}_5 = \frac{x_5}{I_0} = \frac{dx_5}{s}$.
3. $\tilde{t} = r_1 t$.

See Section 3.1 for details.

With these rescalings the $\frac{d\tilde{x}_5}{d\tilde{t}}$ equation becomes,

$$\frac{d\tilde{x}_5}{d\tilde{t}} = \tilde{d}\phi_{51}(\tilde{D}) - \tilde{d}\tilde{x}_5 + \tilde{\rho}_{5C}\left(\frac{\tilde{C}}{\tilde{a}_{52}+\tilde{C}}\right)\tilde{x}_5 - \tilde{\sigma}_{5C}\tilde{C}\tilde{x}_5. \tag{67}$$

where: $\tilde{d} = \frac{d}{r_1}$, $\tilde{\rho}_{5C} = \frac{\rho_{5C}}{r_1}$, $\tilde{a}_{52} = \frac{a_{52}}{C^*}$ and $\tilde{\sigma}_{5C} = \frac{\sigma_{5C}C^*}{r_1}$.

In terms of the parameters $\tilde{M}$, $\tilde{C}_r$ and $\tilde{C}_{\text{opt}}$, the $\frac{d\tilde{x}_5}{d\tilde{t}}$ equation becomes,

$$\frac{d\tilde{x}_5}{d\tilde{t}} = \tilde{d}\phi_{51}(\tilde{D}) - \tilde{d}\tilde{x}_5 + \tilde{M}\tilde{C}\left(\frac{\tilde{C}_r-\tilde{C}}{\tilde{C}_{\text{opt}}^2+\tilde{C}\left(\tilde{C}_r-2\tilde{C}_{\text{opt}}\right)}\right)\tilde{x}_5. \tag{68}$$

We can solve for the equilibrium solution, $\tilde{x}_5^e$, of [Eq. 67] as follows,

$$\begin{aligned}
\frac{d\tilde{x}_5}{d\tilde{t}} &= 0 \\
-\tilde{d}\phi_{51}(\tilde{D}) &= \tilde{x}_5^e \left(-\tilde{d} + \tilde{\rho}_{5C} \left(\frac{\tilde{C}}{\tilde{a}_{52} + \tilde{C}} \right) - \tilde{\sigma}_{5C} \tilde{C} \right) \\
\tilde{x}_5^e &= \frac{\tilde{d}\phi_{51}(\tilde{D})}{\tilde{d} - \tilde{\rho}_{5C} \left(\frac{\tilde{C}}{\tilde{a}_{52} + \tilde{C}} \right) + \tilde{\sigma}_{5C} \tilde{C}}
\end{aligned} \tag{69}$$

We can solve for the stability of this equilibrium by computing the sign of,

$$\frac{d}{d\tilde{x}_5} \frac{d\tilde{x}_5}{d\tilde{t}},$$

evaluated at $\tilde{x}_5^e$.

$$\begin{aligned}
\frac{d}{d\tilde{x}_5} \frac{d\tilde{x}_5}{d\tilde{t}} &= \frac{d}{d\tilde{x}_5} \left(\tilde{d}\phi_{51}(\tilde{D}) - \tilde{d}\tilde{x}_5 + \tilde{\rho}_{5C} \left(\frac{\tilde{C}}{\tilde{a}_{52} + \tilde{C}} \right) \tilde{x}_5 - \tilde{\sigma}_{5C} \tilde{C} \tilde{x}_5 \right) \\
&= - \left(\tilde{d} - \tilde{\rho}_{5C} \left(\frac{\tilde{C}}{\tilde{a}_{52} + \tilde{C}} \right) + \tilde{\sigma}_{5C} \tilde{C} \right),
\end{aligned} \tag{70}$$

which is the negation of the denominator of $\tilde{x}_5^e$. Thus, since $\tilde{d}\phi_{51}(\tilde{D}) > 0$, we have that $\tilde{x}_5^e$ is stable if it is positive and unstable if it is negative. This begs the question, when is $\tilde{x}_5^e > 0$, i.e. when is the equilibrium solution physical.

In appendix A.6 we show that this equilibrium solution is positive, and is thus stable, for all $\tilde{C} > 0$ if,

$$\tilde{d} > \tilde{M} = \left(\sqrt{\tilde{\rho}_{5C}} - \sqrt{\tilde{\sigma}_{5C} \tilde{a}_{52}} \right)^2. \tag{71}$$

There are two other possible cases,

1. $\tilde{d} = \tilde{M}$.
2. $\tilde{d} < \tilde{M}$.

(1) if $\tilde{d} = \tilde{M}$, then there is a single value of $\tilde{C} > 0$ for which,

$$\left(\tilde{d} - \tilde{\rho}_{5C} \frac{\tilde{C}}{\tilde{a}_{52} + \tilde{C}} + \tilde{\sigma}_{5C} \tilde{C} \right) = 0. \tag{72}$$

This value of $\tilde{C}$ is,

$$\hat{\tilde{C}} = \frac{-\left(\frac{\tilde{d} - (\tilde{\rho}_{5C} - \tilde{\sigma}_{5C} \tilde{a}_{52})}{\tilde{\sigma}_{5C}} \right)}{2}$$

Detailed calculations are given in appendix A.6. In this case, and for this particular value of $\tilde{C}$, the $\frac{d\tilde{x}_5}{d\tilde{t}}$ equation reduces to

$$\frac{d\tilde{x}_5}{d\tilde{t}} = \tilde{d}\phi_{51}(\tilde{D})$$

and experiences unbounded linear growth in time. However, recall that we have assumed here that $\tilde{C}$ remains fixed in time, in reality as the immune system becomes large, it will kill cancer pushing $\tilde{C}$ away from this problematic value $\hat{\tilde{C}}$.

(2) if $\tilde{d} < \tilde{M}$, then there are two values of $\tilde{C} > 0$ for which,

$$\left(\tilde{d} - \tilde{\rho}_{5C}\frac{\tilde{C}}{\tilde{a}_{52} + \tilde{C}} + \tilde{\sigma}_{5C}\tilde{C}\right) = 0.$$

These values of $\tilde{C}$ are,

$$\tilde{C}_{2,1} = \frac{-\left(\frac{\tilde{d}-(\tilde{\rho}_{5C}-\tilde{\sigma}_{5C}\tilde{a}_{52})}{\tilde{\sigma}_{5C}}\right) \pm \sqrt{\left(\frac{\tilde{d}-(\tilde{\rho}_{5C}-\tilde{\sigma}_{5C}\tilde{a}_{52})}{\tilde{\sigma}_{5C}}\right)^2 - \frac{4\tilde{d}\tilde{a}_{52}}{\tilde{\sigma}_{5C}}}}{2}$$

where $\tilde{C}_2$ corresponds to the positive square root. Again, see appendix A.6 for details. Thus, in the case $\tilde{d} < \tilde{M}$ and for $\tilde{C} = \tilde{C}_1$ or $\tilde{C} = \tilde{C}_2$, the $\frac{d\tilde{x}_5}{d\tilde{t}}$ equation reduces to

$$\frac{d\tilde{x}_5}{d\tilde{t}} = \tilde{d}\phi_{51}(\tilde{D}),$$

which again results in unbounded linear growth of the immune system in time. To describe the behaviour of $\tilde{x}_5^e$ away from $\tilde{C}_1$ and $\tilde{C}_2$, we will divide $\tilde{C}$ into three separate intervals: $[0, \tilde{C}_1)$, $(\tilde{C}_1, \tilde{C}_2)$ and $(\tilde{C}_2, \infty)$ and classify the stability of $\tilde{x}_5^e$ within each. Calculations are given in appendix A.7.

1. $[0, \tilde{C}_1)$: $\tilde{x}_5^e > 0$ and is a stable equilibrium.
2. $(\tilde{C}_1, \tilde{C}_2)$: $\tilde{x}_5^e < 0$ and is an unstable equilibrium.
3. $(\tilde{C}_2, \infty)$: $\tilde{x}_5^e > 0$ and is a stable equilibrium.

Hence for $\tilde{C} \in [\tilde{C}_1, \tilde{C}_2]$ the immune system experiences unbounded growth. The growth is linear in time if $\tilde{C} = \tilde{C}_1$ or $\tilde{C} = \tilde{C}_2$, and the growth is exponential in time if $\tilde{C} \in (\tilde{C}_1, \tilde{C}_2)$. In reality, for $\tilde{C}$ not fixed in time, as the immune system becomes large it will kill cancer and force $\tilde{C}$ out of the problematic region $[\tilde{C}_1, \tilde{C}_2]$. See [Fig. 22] for plots of $\tilde{x}_5^e$ vs. $\tilde{C}$ and $\tilde{M}$, for parameter values which elicit this behaviour.

Given [Eq. 69] with $\tilde{d} > \tilde{M}$, we can plot the immune system equilibrium position as a function of $\tilde{D}$ for various fixed $\tilde{C}$ and vice versa [Fig. 23].

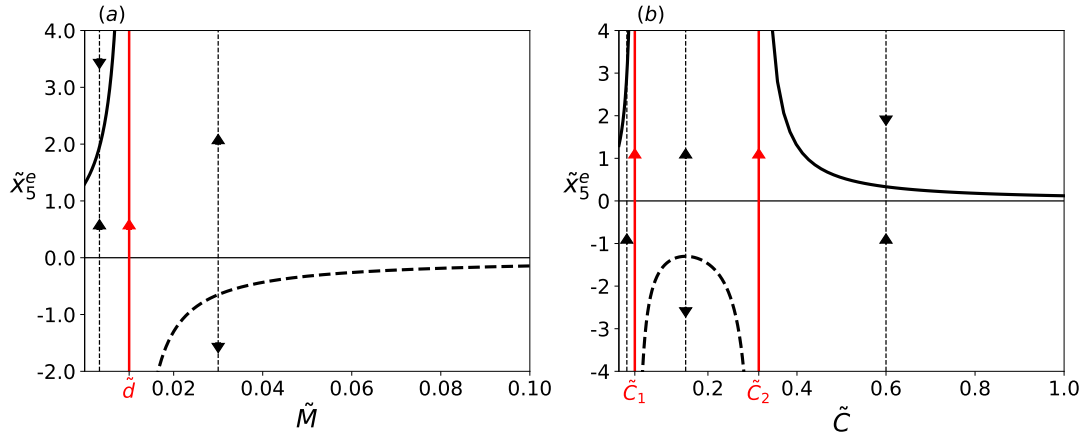


Figure 22: Plots of stable and unstable branches of $\tilde{x}_5^e$ vs. $\tilde{M}$ and $\tilde{C}$ [Eq. 69]. The solid black lines represents stable equilibrium branches, and the dashed black lines represent unstable equilibrium branches. Vertical, dashed black lines with arrows indicate the direction of the flow of $\tilde{x}_5$. Vertical red lines indicate the points at which $\tilde{x}_5$ grows linearly in time and the flow direction at these points. **(a)** Plot of $\tilde{x}_5^e$ vs. $\tilde{M}$ [Eq. 69]. For this plot we fixed $\tilde{C} = \tilde{C}_{\text{opt}}$. **(b)** Plot of $\tilde{x}_5^e$ vs. $\tilde{C}$ [Eq. 69]. For this plot we fixed $\tilde{M} = 0.02$. Our parameter choices obtain that $\tilde{C}_1 = 0.036$ and $\tilde{C}_2 = 0.314$. In both (a) and (b) the parameter values chosen were: $\tilde{C}_r = 0.4$, $\tilde{C}_{\text{opt}} = 0.15$, $\tilde{D} = 0.5$, $\tilde{d} = 0.01$, $a_{51} = 0.8206$, $\eta = 5.83$ and $\tilde{D}_{\text{opt},5} = 0.5$.

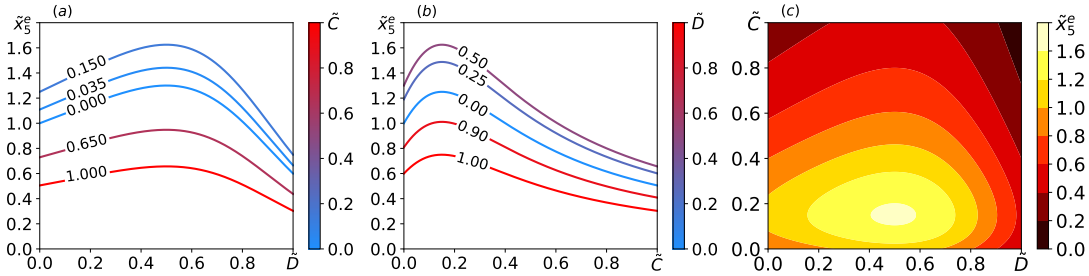


Figure 23: **(a)** Plots of $\tilde{x}_5^e$ vs. $\tilde{D}$ [Eq. 69] for various fixed $\tilde{C}$. Line colour corresponds to which value of $\tilde{C}$ the line was plotted for. Blue indicates small cancer and red indicates large cancer. **(b)** Plots of $\tilde{x}_5^e$ vs. $\tilde{C}$ [Eq. 69] for various fixed $\tilde{D}$. Line colour corresponds to which value of $\tilde{D}$ the line was plotted for. Blue indicates low intensity chemotherapy and red indicates high intensity chemotherapy. **(c)** Heatmap of $\tilde{x}_5^e$ [Eq. 69] in the $\tilde{D}$–$\tilde{C}$ plane. Parameter values used to produce all plots were: $\tilde{d} = 0.01$, $a_{51} = 0.8206$, $\eta = 5.83$, $\tilde{D}_{\text{opt},5} = 0.5$, $\tilde{C}_{\text{opt}} = 0.15$, $\tilde{C}_r = 0.4$ and $\tilde{M} = 0.002$.

All of this analysis is based on values of $\tilde{C}$ and $\tilde{D}$ that have been fixed in time. How closely this analysis resembles the true dynamics of the system will depend on the relative time-scales for $\tilde{x}_5$, $\tilde{C}(\tilde{t})$ and $\tilde{D}(\tilde{t})$.

2.4.2 $\dot{x}_5$ and $\dot{x}_1$ with No Treatment System Sanity Check.

The last system sanity check we will carry out will be to analyse the interaction between the immune system and cancer in the absence of treatment for fixed in time values of the active stroma. For this, we will once again use the variable

rescalings and simplifying assumptions introduced previously, see Section 3.1. In this treatment free scenario, i.e. $\tilde{D}(t) = 0$, we have that resistance cannot develop, therefore we can set $\tilde{x}_2 = 0$. This gives us the following system of equations to analyse,

$$\frac{d\tilde{x}_1}{d\tilde{t}} = \left(1 + \tilde{\rho}_{C3}\frac{\tilde{A}\,(1+a_C)}{\tilde{A}+a_C} - \tilde{\gamma}_T\right)\tilde{x}_1 - \tilde{\gamma}\tilde{x}_1^2 - \tilde{\sigma}_{15}\tilde{x}_5 e^{-\tilde{\kappa}_5\tilde{A}}\tilde{x}_1 \tag{73}$$

$$\frac{d\tilde{x}_5}{d\tilde{t}} = \tilde{d} - \tilde{d}\tilde{x}_5 + \tilde{\rho}_{5C}\left(\frac{\tilde{x}_1}{\tilde{a}_{52}+\tilde{x}_1}\right)\tilde{x}_5 - \tilde{\sigma}_{5C}\tilde{x}_1\tilde{x}_5. \tag{74}$$

For this sanity check, the goal will be to determine whether this system can model the process of cancer immunoediting discussed in Section 1.2.4. To model this process we must have an 'extinction threshold' in phase space such that sufficiently small cancer populations are unable to grow to carrying capacity due to the immune system.

As a starting point, we will remove the coupling terms from the immune system equation. With these terms removed, the immune system has an equilibrium point at its normal strength $\tilde{x}_5 = 1$, and is neither stimulated nor suppressed by cancer. We do this for two reasons:

1. We can choose parameter values that reasonably describe cancer growth when the immune is fixed at its normal strength.

2. We can highlight the absence of the extinction threshold without these terms, proving they are necessary.

Further, since we are primarily interested in behaviour during the early stages of cancer growth when the stroma is inactive, we will fix $\tilde{A} = 0$. With this, we have the system,

$$\frac{d\tilde{x}_1}{d\tilde{t}} = (1 - \tilde{\gamma}_T)\,\tilde{x}_1 - \tilde{\gamma}\tilde{x}_1^2 - \tilde{\sigma}_{15}\tilde{x}_5\tilde{x}_1 \tag{75}$$

$$\frac{d\tilde{x}_5}{d\tilde{t}} = \tilde{d} - \tilde{d}\tilde{x}_5 \tag{76}$$

The immune system equation has an equilibrium point at it's normal strength, $\tilde{x}_5 = 1$. To obtain the equilibrium points of this 2D system, we can set $\tilde{x}_5 = 1$ in [Eq. 75] and solve,

$$\frac{d\tilde{x}_1}{d\tilde{t}} = (1 - \tilde{\gamma}_T)\,\tilde{x}_1 - \tilde{\gamma}\tilde{x}_1^2 - \tilde{\sigma}_{15}\tilde{x}_1 = 0. \tag{77}$$

[Eq. 77] is a logistic equation which we discussed in Section 2.2.3. The system has an extinction equilibrium,

$\boldsymbol{e_0}$:

$$(\tilde{x}_1, \tilde{x}_5) = (0, 1),$$

and a carrying capacity given by,

$\boldsymbol{e_3}$:

$$(\tilde{x}_1, \tilde{x}_5) = \left(\frac{(1 - \tilde{\gamma}_T - \tilde{\sigma}_{15})}{\tilde{\gamma}}, 1 \right). \tag{78}$$

We reserve the names e_1 and e_2 for other equilibrium points of the complete system defined by [Eq. 73] and [Eq. 74], which we will discuss later in this section. If we assume the immune system is in equilibrium at its normal strength, then it remains so and is unable to respond to cancer. We therefore expect that in such a case cancer will grow to the lethal threshold. To achieve this, we must choose parameters such that the carrying capacity exceeds the lethal threshold, $\tilde{x}_1 = 1$. This gives us the following condition,

$$0 < \tilde{\sigma}_{15} < 1 - \tilde{\gamma}_T - \tilde{\gamma}. \tag{79}$$

We will choose $\tilde{\sigma}_{15} = 0.5$, $\tilde{\gamma}_T = 0.3$ and $\tilde{\gamma} = \frac{1}{6}$, which meets condition [Eq. 79] and places the cancer carrying capacity at $\tilde{x}_1 = 1.2$. See [Fig. 24] for a phase portrait of the system defined by [Eq. 75] and [Eq. 76], for these parameter choices. We choose $\tilde{d} = 0.23$ throughout this section since Kuznetsov et al. [38] estimate $r_1 = 0.18$ and $d = 0.0412$ for analogous parameters in their model.

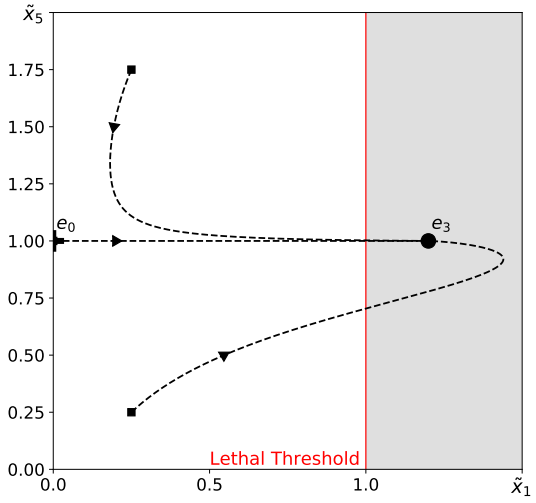


Figure 24: Phase portrait for the simplified system, [Eq. 75] and [Eq. 76]. Solid black circles are stable nodes and black plus signs are unstable saddle points. Dashed black lines are sample trajectories through phase space. Parameter values used were: $\tilde{d} = 0.23$, $\tilde{\sigma}_{15} = 0.5$, $\tilde{\gamma}_T = 0.3$ and $\tilde{\gamma} = \frac{1}{6}$. The vertical red line marks the lethal size of the cancer population $\tilde{x}_1 = 1$ and the gray region covers cancer population sizes above this threshold. There are three sample trajectories with initial conditions marked by black squares: $(\tilde{x}_1, \tilde{x}_5) = (10^{-9}, 1)$, $(0.25, 0.25)$ and $(0.25, 1.75)$.

In [Fig. 24] we observe that all trajectories converge to the cancer carrying capacity e_3, which exceeds the lethal threshold. We also observe non-monotonicity in the evolution of the cancer variable. For the trajectory with the initial condition $(\tilde{x}_1, \tilde{x}_5) = (0.25, 1.75)$, the immune system is initially strong. This causes a decrease in the cancer population at first, before it grows towards the carrying capacity. For the trajectory with the initial condition $(\tilde{x}_1, \tilde{x}_5) = (0.25, 0.25)$, the immune system is initially weak. This causes the cancer population to overshoot the carrying capacity before being reduced back down once the immune systems strength increases.

We will now re-introduce the immune stimulation and immune suppression terms,

$$\tilde{\rho}_{5C}\left(\frac{\tilde{x}_1}{\tilde{a}_{52}+\tilde{x}_1}\right)\tilde{x}_5 \quad \text{and} \quad -\tilde{\sigma}_{5C}\tilde{x}_1\tilde{x}_5,$$

separately for small values of $\tilde{\rho}_{5C}$ and $\tilde{\sigma}_{5C}$ to see how these terms perturb the phase portrait in [Fig. 24]. See [Fig. 25 (a)] for the perturbed system including the immune stimulation term, and [Fig. 25 (b)] for the perturbed system including the immune suppression term. In each case and throughout this section we use $\tilde{a}_{52} = 2.25 \times 10^{-5}$ since we can obtain an extinction threshold in the full system with this value, which we will later see.

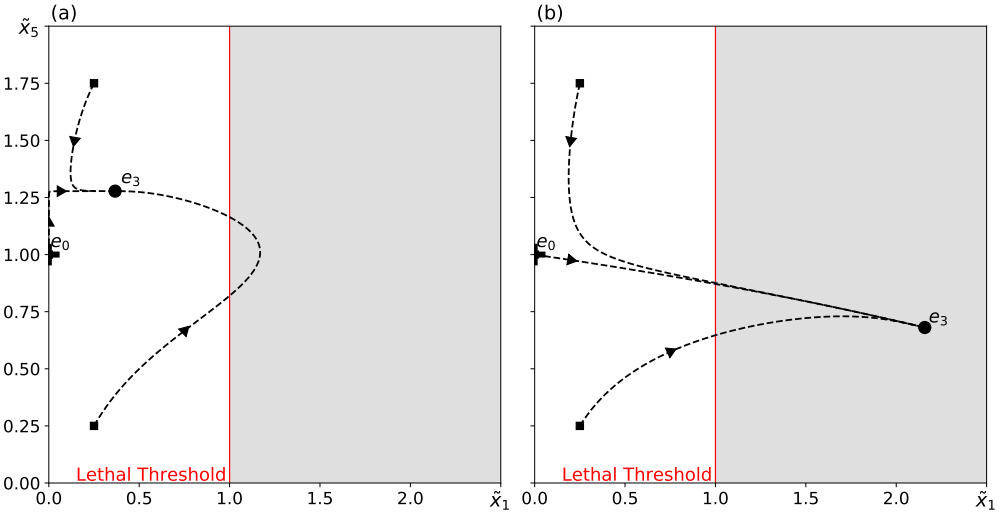


Figure 25: Phase portrait for the simplified system, [Eq. 75] and [Eq. 76], including (a) the immune stimulation term with $\tilde{\rho}_{5C} = 0.05$ and $\tilde{a}_{52} = 2.25 \times 10^{-5}$ and (b) the immune suppression term with $\tilde{\sigma}_{5C} = 0.05$. Solid black circles are stable nodes and black plus signs are unstable saddle points. Dashed black lines are sample trajectories through phase space. Other parameter values used were: $\tilde{d} = 0.23$, $\tilde{\sigma}_{15} = 0.5$, $\tilde{\gamma}_T = 0.3$ and $\tilde{\gamma} = \frac{1}{6}$. The vertical red line marks the lethal size of the cancer population $\tilde{x}_1 = 1$ and the gray region covers cancer population sizes above this threshold. There are three sample trajectories with initial conditions marked by black squares: $(\tilde{x}_1, \tilde{x}_5) = (10^{-9}, 1)$, $(0.25, 0.25)$ and $(0.25, 1.75)$.

Including the immune stimulation term lowers the carrying capacity in terms of the cancer cell population size, and including the immune suppression term increases it. In neither case do we observe the formation of an extinction threshold. However, by combining these two terms together in the right way, we can introduce an extinction threshold into the system. To see this we will return to the full system defined by [Eq. 73] and [Eq. 74] and solve for the equilibrium solutions.

We can easily see that the full system also has a trivial equilibrium solution that corresponds to a cancer free scenario,

e_0 :

$$(\tilde{x}_1^{e_0}, \tilde{x}_5^{e_0}) = (0, 1). \tag{80}$$

Here there is no cancer cell population and since the immune system is not exposed to any stressors it is in equilibrium at the normal immune-strength, $\tilde{x}_5 = 1$ or $x_5 = I_0$. We can obtain the stability of this equilibrium point by evaluating the Jacobian matrix of the system at this point,

$$\begin{aligned} \boldsymbol{J} &= \begin{pmatrix} \left(1 + \tilde{\rho}_{C3}\frac{\tilde{A}(1+a_C)}{\tilde{A}+a_C} - \tilde{\gamma}_T\right) - 2\tilde{\gamma}\tilde{x}_1 - \tilde{\sigma}_{15}\tilde{x}_5 e^{-\tilde{\kappa}_5\tilde{A}} & -\tilde{\sigma}_{15}e^{-\tilde{\kappa}_5\tilde{A}}\tilde{x}_1 \\ \tilde{\rho}_{5C}\frac{\tilde{a}_{52}}{(\tilde{a}_{52}+\tilde{x}_1)^2}\tilde{x}_5 - \tilde{\sigma}_{5C}\tilde{x}_5 & -\tilde{d} + \tilde{\rho}_{5C}\frac{\tilde{x}_1}{\tilde{a}_{52}+\tilde{x}_1} - \tilde{\sigma}_{5C}\tilde{x}_1 \end{pmatrix} \\ \boldsymbol{J}\Big|_{\left(\tilde{x}_1^{e_0}, \tilde{x}_5^{e_0}\right)} &= \begin{pmatrix} \left(1 + \tilde{\rho}_{C3}\frac{\tilde{A}(1+a_C)}{\tilde{A}+a_C} - \tilde{\gamma}_T\right) - \tilde{\sigma}_{15}e^{-\tilde{\kappa}_5\tilde{A}} & 0 \\ \frac{\tilde{\rho}_{5C}}{\tilde{a}_{52}} - \tilde{\sigma}_{5C} & -\tilde{d} \end{pmatrix} \end{aligned} \tag{81}$$

Then, since $\tilde{d} > 0$, we have that this equilibrium is a stable node if,

$$\left(1 + \tilde{\rho}_{C3}\frac{\tilde{A}\,(1+a_C)}{\tilde{A}+a_C} - \tilde{\gamma}_T\right) < \tilde{\sigma}_{15}e^{-\tilde{\kappa}_5\tilde{A}} \tag{82}$$

and unstable saddle if,

$$\left(1 + \tilde{\rho}_{C3}\frac{\tilde{A}\,(1+a_C)}{\tilde{A}+a_C} - \tilde{\gamma}_T\right) > \tilde{\sigma}_{15}e^{-\tilde{\kappa}_5\tilde{A}}. \tag{83}$$

Notice that the left hand side of the inequality [Eq. 83] is an increasing function of $\tilde{A}$, and the right hand side is a decreasing function of $\tilde{A}$. This means that this inequality will hold for any $\tilde{A} > 0$ if it holds for $\tilde{A} = 0$, and by setting $\tilde{A} = 0$ we obtain,

$$1 - \tilde{\gamma}_T > \tilde{\sigma}_{15}.$$

But this must hold since we have already assumed condition [Eq. 79] to be true which says,

$$1 - \tilde{\gamma}_T - \tilde{\gamma} > \tilde{\sigma}_{15}$$

which is a stronger assumption. Therefore we can say with certainty that e_0 will always be an unstable saddle. The stable manifold of e_0 is along the $\tilde{x}_5$ axis, since if we set $\tilde{x}_1 = 0$ in the complete system, we are left with,

$$\frac{d\tilde{x}_5}{d\tilde{t}} = d - d\tilde{x}_5,$$

which describes stabilisation of the immune system to e_0 over time. This also highlights an important fact that the $\tilde{x}_5$ axis is invariant in this system.

Setting $\frac{d\tilde{x}_5}{d\tilde{t}} = 0$ and solving for $\tilde{x}_5$ using [Eq. 74], we obtain,

$$\begin{aligned} 0 &= \tilde{d} - \tilde{d}\tilde{x}_5 + \tilde{\rho}_{5C}\left(\frac{\tilde{x}_1}{\tilde{a}_{52}+\tilde{x}_1}\right)\tilde{x}_5 - \tilde{\sigma}_{5C}\tilde{x}_1\tilde{x}_5 \\ \tilde{d} &= \tilde{d}\tilde{x}_5 - \tilde{\rho}_{5C}\left(\frac{\tilde{x}_1}{\tilde{a}_{52}+\tilde{x}_1}\right)\tilde{x}_5 + \tilde{\sigma}_{5C}\tilde{x}_1\tilde{x}_5 \\ \tilde{x}_5 &= \frac{\tilde{d}}{\tilde{d} - \tilde{\rho}_{5C}\left(\frac{\tilde{x}_1}{\tilde{a}_{52}+\tilde{x}_1}\right) + \tilde{\sigma}_{5C}\tilde{x}_1}. \end{aligned} \tag{84}$$

We can substitute this back into [Eq. 73], setting $\frac{d\tilde{x}_1}{d\tilde{t}} = 0$ and assuming $\tilde{x}_1 \neq 0$, to obtain additional equilibrium points of the system. Doing this, see appendix A.8, we obtain the following,

$$\psi_3\tilde{x}_1^3 + \psi_2\tilde{x}_1^2 + \psi_1\tilde{x}_1 + \psi_0 = 0, \tag{85}$$

where,

$$\begin{aligned} \psi_3 &= -\tilde{\gamma}\tilde{\sigma}_{5C} \\ \psi_2 &= \left(1 + \tilde{\rho}_{C3}\frac{\tilde{A}\,(1+a_C)}{\tilde{A}+a_C} - \tilde{\gamma}_T\right)\tilde{\sigma}_{5C} - \tilde{\gamma}\left(\tilde{d} - \tilde{\rho}_{5C} + \tilde{a}_{52}\tilde{\sigma}_{5C}\right) \\ \psi_1 &= \left(1 + \tilde{\rho}_{C3}\frac{\tilde{A}\,(1+a_C)}{\tilde{A}+a_C} - \tilde{\gamma}_T\right)\left(\tilde{d} - \tilde{\rho}_{5C} + \tilde{a}_{52}\tilde{\sigma}_{5C}\right) - \tilde{a}_{52}\tilde{d}\left(\tilde{\gamma} + \tilde{\sigma}_{15}e^{-\tilde{\kappa}_5\tilde{A}}\right) \\ \psi_0 &= \tilde{a}_{52}\tilde{d}\left[\left(1 + \tilde{\rho}_{C3}\frac{\tilde{A}\,(1+a_C)}{\tilde{A}+a_C} - \tilde{\gamma}_T\right) - \tilde{\sigma}_{15}e^{-\tilde{\kappa}_5\tilde{A}}\right] \end{aligned}$$

This cubic polynomial in $\tilde{x}_1$ may have up to three real and positive solutions depending on the values of ψ_3, ψ_2, ψ_1 and ψ_0. If we assume the previously derived condition $\tilde{d} > \tilde{M}$ [Eq. 71] holds, then [Eq. 84] is positive given $\tilde{x}_1 > 0$. This means that each of the $\tilde{x}_1 > 0$ solutions of the above cubic equation, are the $\tilde{x}_1$ components of physical equilibrium solutions ($\tilde{x}_1 > 0$ and $\tilde{x}_5 > 0$) of the system. There cannot exist any equilibrium solution such that $\tilde{x}_1 > 0$ and $\tilde{x}_5 < 0$.

One can determine the number of physical equilibrium solutions that are

possible for a given combination of the signs of ψ_3, ψ_2, ψ_1 and ψ_0 using Descartes' rule of signs, see table 1 in appendix A.8. Given that [Eq. 83] holds, and using table 1, we can deduce two possible cases.

1. There exists two physical equilibrium solutions in the system including the cancer extinction equilibrium e_0.

2. There exists four phyiscal equilibrium solutions in the system including the cancer extinction equilibrium e_0.

We will demonstrate that the existence of four physical equilibrium points in case 2 above allows for the formation of an extinction threshold. Due to the algebraic complexity of [Eq. 85], we will show this numerically by producing a phase portrait of the system for a choice of parameters that obtain the extinction threshold [Fig. 26 (a) & (b)]. We have once again set $\tilde{A} = 0$ for simplicity, since we are focused on behaviour in the early stages of cancer growth.

From these plots we can see that there are four equilibrium points:

1. An unstable saddle e_0 which is the cancer extinction equilibrium.

2. A stable node e_3 which is the cancer carrying capacity

3. A stable node that we call e_1.

4. An unstable saddle point that we call e_2.

The stable manifold of e_2 separates the basins of attraction of e_1 and e_3 shaded in gray and white respectively. This manifold forms the extinction threshold, as it is a boundary in phase space such that very small cancer populations on the order of of $\tilde{x}_1 \approx 10^{-4}$ or less, cannot grow to carrying capacity. Instead such populations converge to e_1, see the sample trajectory in blue. New cancerous cells regularly form in the body and the immune system remains constantly stimulated in the fight to remove these cells. e_1 can be seen as the long-term average of these constantly competing populations.

The shape of this threshold is delicate and can become very different, or be lost entirely, if the model parameters are varied. We previously determined,

$$0 < \tilde{\sigma}_{15} < 1 - \tilde{\gamma}_T - \tilde{\gamma},$$

to be the reasonable range for $\tilde{\sigma}_{15}$. In [Fig. 26 (c) & (d)] we have reduced the value of $\tilde{\sigma}_{15}$, compared to what was used in [Fig. 26 (a) & (b)], while keeping it in the sensible range. The stable manifold of e_2 then forms a heteroclinic connection with e_0. This implies that for sub-normal immune system strength, any cancer

population no matter how small, will grow towards the carrying capacity, again see the sample trajectory in blue. In [Fig. 26 (e) & (f)], we have further reduced $\tilde{\sigma}_{15}$. Here we can see that the basins of attraction of e_1 and e_3 are significantly different to those in [Fig. 26 (a) & (b)]. Now, regardless of immune system strength, very small cancer populations are capable of what Kuznetsov et al [38] term 'sneaking through,' whereby they sneak past the immune systems defenses and grow to carrying capacity.

When allowed to vary, the active stroma will effectively lower $\tilde{\sigma}_{15}$ while increasing the cancer growth rate. This could cause the extinction threshold to change shape in this way, which might serve as one explanation as to how cancer can develop despite the immune systems best efforts to prevent it.

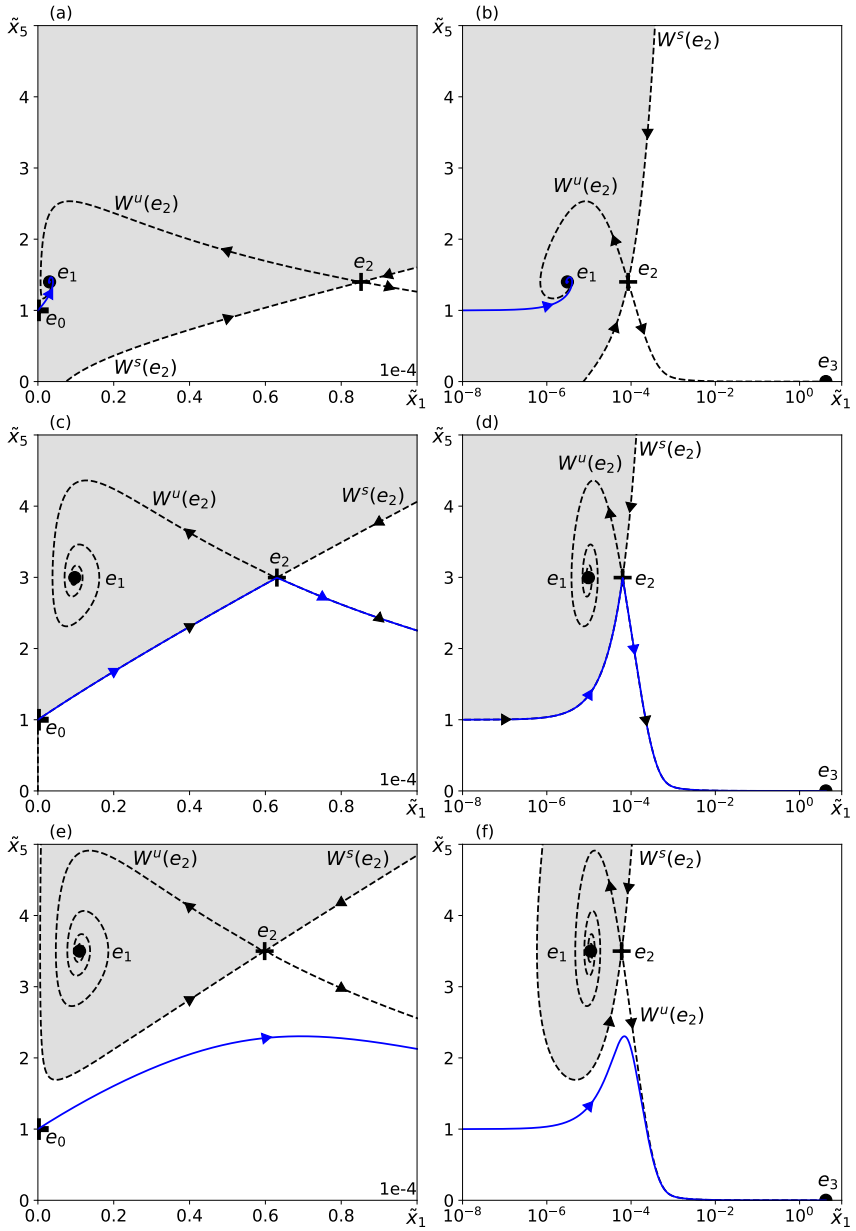


Figure 26: Phase portraits of the $\frac{d\tilde{x}_1}{dt}$ and $\frac{d\tilde{x}_5}{dt}$ system without treatment for (a) & (b): $\tilde{\sigma}_{15} = 0.5$, (c) & (d): $\tilde{\sigma}_{15} = 0.233613$ and (e) & (f): $\tilde{\sigma}_{15} = 0.2$. In each figure $\tilde{A} = 0$, and all other parameters are fixed as follows: $\tilde{\gamma}_T = 0.3$, $\tilde{\gamma} = \frac{1}{6}$, $\tilde{d} = 0.23$, $\tilde{M} = 0.225$ ($\tilde{\rho}_{5C} = 0.689$), $\tilde{C}_r = 10^{-4}$ ($\tilde{a}_{52} = 2.25\,\mathrm{x}\,10^{-5}$) and $\tilde{C}_{\mathrm{opt}} = 3\,\mathrm{x}\,10^{-5}$ ($\tilde{\sigma}_{5C} = 5.625\,\mathrm{x}\,10^{3}$). Figures in the left column are plotted with a linear scale of the $\tilde{x}_1$ axis that ranges from 0 to 10^{-4}. Figures in the right column are plotted with a log-scale of the $\tilde{x}_1$ axis that ranges from 10^{-8} to 10. Solid black dots represent stable nodes and black plus signs represent unstable saddle points. The dashed black lines are the stable, $W^s(e_2)$, and unstable, $W^u(e_2)$, manifolds of e_2. The solid blue line is a sample trajectory given the initial condition $(\tilde{x}_1, \tilde{x}_5) = (10^{-8}, 1)$ in each figure. The basins of attraction of e_1 and e_3 are shaded in grey and white respectively.

This extinction threshold can be lost entirely through a saddle node bifurcation of e_1 with e_2. This results in a transition from case 1 to case 2 above. This bifurcation can be brought about by varying the parameter $\tilde{\rho}_{5C}$, see [Fig. 27] for

the bifurcation diagram.

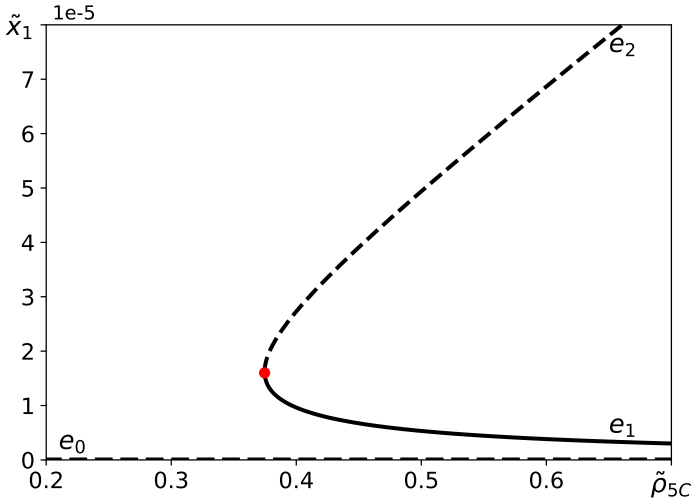


Figure 27: Bifurcation diagram showcasing the saddle-node bifurcation that occurs between e_1 and e_2 as $\tilde{\rho}_{5C}$ is varied. The $\tilde{x}_1$ component of each equilibrium is plotted versus $\tilde{\rho}_{5C}$. Solid black lines represent the stable branches of the equilibrium points, and the dashed black lines represent the unstable branches of the equilibrium points. The red dot marks the bifurcation point at $\tilde{\rho}_{5C} \approx 0.375$. Parameter values used to generate this plot were: $\tilde{A} = 0$, $\tilde{\gamma} = \frac{1}{6}$, $\tilde{\gamma}_T = 0.3$, $\tilde{\sigma}_{15} = 0.5$, $\tilde{d} = 0.23$, $\tilde{a}_{52} = 2.25 \,\mathrm{x}\, 10^{-5}$, $\tilde{\sigma}_{5C} = 5.625 \,\mathrm{x}\, 10^3$.

Remark. *Obtaining a sufficiently small extinction threshold required us to choose a much larger value of $\tilde{\sigma}_{5C}$ relative to $\tilde{\sigma}_{15}$.*

Doing this makes the assumption that cancer cells have a major advantage in the competition with immune cells, with the implication being that once the cancer population size exceeds the extinction threshold, i.e. once it enters the 'escape' stage of it's growth, it strongly suppresses the immune system. This causes the tumour-antagonising immune cell population within the TME to die out in the early stages of cancer development. This can be seen by observing the steepness of the unstable manifold of e_2 in the phase portrait [Fig. 26 (b)]. The immune system subsequently has very little effect on the cancer population during the remainder of its growth.

A reasonable biological argument can be made to support this assumption. As cancer cells divide, they become less immunogenic, enabling them to escape immune surveillance and impair immune function. This occurs through the loss of antigen expression and activation of immune suppression pathways. Cancer cells recruit T-regulatory cells into the tumour microenvironment, inhibiting T-cell activity. Additionally, cancer cells can directly 'delete' T-cells through apoptosis [83]. Prolonged exposure to cancer antigens also leads to T-cell exhaustion and dysfunction, while the cytotoxic function of natural killer cells is also inhibited [41].

While this indicates that the cancer cell population is well able to win the fight against the immune cell population, we could not find direct quantitative evidence to support the assumption that cancer should have such a strong advantage in this competition. This provides an opportunity for future study, one could modify the model terms, or take the harvesting approach mentioned in Section 2.2.1, in order to try and obtain a sufficiently small extinction threshold without giving cancer such a strong advantage.

3 Complete Model Equations

Now that we have derived each equation, we can state the complete model as follows,

$$\begin{aligned}
\dot{x}_1 =& \left(r_1 - \lambda\tilde{D}(t)e^{-\kappa_D x_3} + \rho_{13}\frac{x_3(1+a_1)}{x_3+a_1T}\right)x_1 - x_1\big[\gamma_{11}x_1 + \gamma_{12}x_2 + \gamma_{1T}T\big] \\
& - \delta_1\tilde{D}(t)e^{-\kappa_D x_3}x_1 - \sigma_{15}x_5e^{-\kappa_5 x_3}x_1 \qquad (86)\\
\dot{x}_2 =& \lambda\tilde{D}(t)e^{-\kappa_D x_3}x_1 + \left(r_2 + \rho_{23}\frac{x_3(1+a_2)}{x_3+a_2T}\right)x_2 - x_2\big[\gamma_{21}x_1 + \gamma_{22}x_2 + \gamma_{2T}T\big] \\
& - \delta_2\tilde{D}(t)e^{-\kappa_D x_3}x_2 - \sigma_{25}x_5e^{-\kappa_5 x_3}x_2 \qquad (87)\\
\dot{x}_3 =& \nu_3\left(\frac{e^{a_3\tilde{D}(t)}-1}{e^{a_3}-1}\right)(T-x_3) - \delta_3\tilde{D}(t)x_3 + \rho_{31}x_1(T-x_3) \\
& + \rho_{32}x_2(T-x_3) - \epsilon x_3 \qquad (88)\\
x_4 =& T - x_3 \qquad (89)\\
\dot{x}_5 =& s\phi_{51}(\tilde{D}(t)) - dx_5 + \rho_{5C}\left(\frac{x_1+x_2}{a_{52}+x_1+x_2}\right)x_5 - \sigma_{5C}(x_1+x_2)x_5. \qquad (90)
\end{aligned}$$

This is the complete model prior to any simplifying assumptions and with the only rescaling arising from the normalised chemotherapy intensity $\tilde{D}(t)$. The complete system in terms of the non-normalised $D(t)$ is provided in Appendix B. In the next sub-section we will simplify and non-dimensionalise this system of equations.

3.1 Simplifying Assumptions and Non-Dimensionalisation

In this section we will systematically introduce the simplifying assumptions and variable rescalings that were temporarily used during the model derivation, most often during the system sanity checks.

The complete set of simplifying assumptions that we will use, and their interpretations, are as follows,

1. $\rho_{13} = \rho_{23} = \rho_{C3}$.
   This assumes that the maximum growth promotion of cancer cells due to the active stroma is independent of whether the cells are sensitive or resistant to chemotherapy, and only depends on their relative population sizes. We replace 1 and 2 in the subscripts of ρ_{13} and ρ_{23} with C to indicate that these parameters now apply more generally to all cancer types. We use similar notation changes for other parameters in the remaining simplifying assumptions.

2. $a_1 = a_2 = a_C$.
   This assumption is related to the previous assumption about the growth promotion of cancer by the active stroma. Here, we assume that the shape of the response of cancer to the active stroma is independent of whether the cells are sensitive or resistant to chemotherapy.

3. $\gamma_{ij} = \gamma_{iT} = \gamma$ for all $i, j \in \{1, 2\}$.
   This assumes that the impact of resource and space competition on cells is independent of cell type, and depends only on their relative population sizes.

4. $\rho_{31} = \rho_{32} = \rho_{3C}$.
   This assumes that the activation rate of the stroma due to cancer is independent of whether the cancer cells are sensitive or resistant to chemotherapy, and depends only on their relative population sizes.

5. $r_2 = r_1$.
   This assumes that the intrinsic per-capita growth rate for small cancer populations (i.e. such that $x_i x_j \approx 0$ for all $i, j \in \{1, 2, 3, 4, 5\}$) is independent of whether the cancer cells are sensitive or resistant to chemotherapy.

Next, we will fully non-dimensionalise the model by introducing the complete set of variable rescalings as follows,

1. $\tilde{x}_{1/2} = \frac{x_{1/2}}{C^*}$.
   Here C^* denotes the lethal tumour burden, i.e. if $x_1 + x_2 \geq C^*$ we assume that the patient has died.

2. $\tilde{x}_{3/4} = \frac{x_{3/4}}{T}$.
   Here T denotes the total, and fixed in time, amount of active and inactive stroma combined, $x_3(t) + x_4(t) = T \in \mathbb{R}$.

3. $\tilde{x}_5 = \frac{x_5}{I_0} = \left(\frac{d}{s}\right) x_5$.
   Here we rescale by $I_0 = \frac{s}{d}$ which we assume is a fixed ratio. I_0 denotes the equilibrium level of the immune system under normal circumstances, i.e. no cancer or chemotherapy.

4. $\tilde{t} = r_1 t$.
   r_1 is the intrinsic per-capita growth rate of a "small" population (i.e. $x_i x_j \approx 0$ for all $i, j \in \{1, 2, 3, 4, 5\}$) of sensitive cancer cells and this rescaling allows us to choose other parameter values relative to this rate.

With this, we can write the fully simplified and non-dimensionalised model as follows,

$$\begin{aligned}
\frac{d\tilde{x}_1}{d\tilde{t}} =& \left(1 - \tilde{\lambda}\tilde{D}\left(\frac{\tilde{t}}{r_1}\right)e^{-\tilde{\kappa}_D\tilde{x}_3} + \tilde{\rho}_{C3}\frac{\tilde{x}_3(1+a_C)}{\tilde{x}_3+a_C}\right)\tilde{x}_1 - \tilde{\gamma}\tilde{x}_1\left[\tilde{x}_1+\tilde{x}_2\right] - \tilde{\gamma}_T\tilde{x}_1 \\
& - \tilde{\delta}_1\tilde{D}\left(\frac{\tilde{t}}{r_1}\right)e^{-\tilde{\kappa}_D\tilde{x}_3}\tilde{x}_1 - \tilde{\sigma}_{15}\tilde{x}_5 e^{-\tilde{\kappa}_5\tilde{x}_3}\tilde{x}_1 \qquad (91)\\
\frac{d\tilde{x}_2}{d\tilde{t}} =& \tilde{\lambda}\tilde{D}\left(\frac{\tilde{t}}{r_1}\right)e^{-\tilde{\kappa}_D\tilde{x}_3}\tilde{x}_1 + \left(1 + \tilde{\rho}_{C3}\frac{\tilde{x}_3(1+a_C)}{\tilde{x}_3+a_C}\right)\tilde{x}_2 - \tilde{\gamma}\tilde{x}_2\left[\tilde{x}_1+\tilde{x}_2\right] - \tilde{\gamma}_T\tilde{x}_2 \\
& - \tilde{\delta}_2\tilde{D}\left(\frac{\tilde{t}}{r_1}\right)e^{-\tilde{\kappa}_D\tilde{x}_3}\tilde{x}_2 - \tilde{\sigma}_{25}\tilde{x}_5 e^{-\tilde{\kappa}_5\tilde{x}_3}\tilde{x}_2 \qquad (92)\\
\frac{d\tilde{x}_3}{d\tilde{t}} =& \tilde{\nu}_3\left(\frac{e^{a_3\tilde{D}\left(\frac{\tilde{t}}{r_1}\right)}-1}{e^{a_3}-1}\right)(1-\tilde{x}_3) - \tilde{\delta}_3\tilde{D}\left(\frac{\tilde{t}}{r_1}\right)\tilde{x}_3 \\
& + \tilde{\rho}_{3C}\left(\tilde{x}_1+\tilde{x}_2\right)(1-\tilde{x}_3) - \tilde{\epsilon}\tilde{x}_3 \qquad (93)\\
\tilde{x}_4 =& 1 - \tilde{x}_3 \qquad (94)\\
\frac{d\tilde{x}_5}{d\tilde{t}} =& \tilde{d}\phi_{51}\left(\tilde{D}\left(\frac{\tilde{t}}{r_1}\right)\right) - \tilde{d}\tilde{x}_5 + \tilde{\rho}_{5C}\left(\frac{\tilde{x}_1+\tilde{x}_2}{\tilde{a}_{52}+\tilde{x}_1+\tilde{x}_2}\right)\tilde{x}_5 - \tilde{\sigma}_{5C}(\tilde{x}_1+\tilde{x}_2)\tilde{x}_5. \qquad (95)
\end{aligned}$$

Where: $\tilde{\lambda} = \frac{\lambda}{r_1}$, $\tilde{\kappa}_D = \kappa_D T$, $\tilde{\rho}_{C3} = \frac{\rho_{C3}}{r_1}$, $\tilde{\gamma} = \frac{\gamma C^*}{r_1}$, $\tilde{\gamma}_T = \frac{\gamma T}{r_1}$, $\tilde{\delta}_1 = \frac{\delta_1}{r_1}$, $\tilde{\sigma}_{15} = \frac{\sigma_{15} I_0}{r_1} = \frac{\sigma_{15} s}{r_1 d}$, $\tilde{\kappa}_5 = \kappa_5 T$, $\tilde{\delta}_2 = \frac{\delta_2}{r_1}$, $\tilde{\sigma}_{25} = \frac{\sigma_{25} I_0}{r_1} = \frac{\sigma_{25} s}{r_1 d}$, $\tilde{\nu}_3 = \frac{\nu_3}{r_1}$, $\tilde{\delta}_3 = \frac{\delta_3}{r_1}$, $\tilde{\rho}_{3C} = \frac{\rho_{3C} C^*}{r_1}$, $\tilde{\epsilon} = \frac{\epsilon}{r_1}$, $\tilde{d} = \frac{d}{r_1}$, $\tilde{\rho}_{5C} = \frac{\rho_{5C}}{r_1}$, $\tilde{a}_{52} = \frac{a_{52}}{C^*}$ and $\tilde{\sigma}_{5C} = \frac{\sigma_{5C} C^*}{r_1}$

From this point forward we will work with the fully simplified and non-dimensionalised equations above and all simulations in Sections 4 and 5 are carried out using these equations.

4 Model Simulations Without Treatment:

In the following sections, we will simulate various versions of our model, beginning with simplified versions where specific components are removed. We will then progress to the full model, both with and without treatment.

Since we are carrying out a qualitative study of our model and we do not focus on a particular type of cancer, we will not estimate precise parameter values. Where possible, we will reference the literature to obtain reasonable values at the correct orders of magnitude. When quantitative data is unavailable, our approach will be to test out hypothetical values that represent different biological scenarios. We will simulate our model under these different conditions and compare the qualitative behaviours predicted in each scenario. Future work could carry out a quantitative case-study of our model applied to a particular type of cancer and this would involve more precise parameter estimation.

4.1 Reduced Model A: Cancer Growth without the Stroma, the Immune System or Treatment.

As a starting point, we will simulate a reduced version of our model that omits the effects of the stroma and the immune system, solely modelling untreated cancer growth. To do this, we set $\tilde{x}_3 = \tilde{x}_4 = \tilde{x}_5 = \tilde{D}\left(\frac{\tilde{t}}{r_1}\right) = 0$, which results in a simple logistic growth model,

$$\frac{d\tilde{x}_1}{d\tilde{t}} = \tilde{x}_1 - \tilde{\gamma}\tilde{x}_1^2. \tag{96}$$

This model has an extinction equilibrium at $\tilde{x}_1 = 0$ and a carrying capacity equilibrium at $\tilde{x}_1 = \tilde{K} = \frac{1}{\tilde{\gamma}}$. The cancer carrying capacity, $\tilde{K}$, should be larger than the lethal threshold [19], and we can use the sole parameter of this model $\tilde{\gamma}$, to determine how much larger it is. [Fig. 28] showcases simulations of the model given by [Eq. 96] for various values of $\tilde{\gamma}$ and consequently $\tilde{K}$.

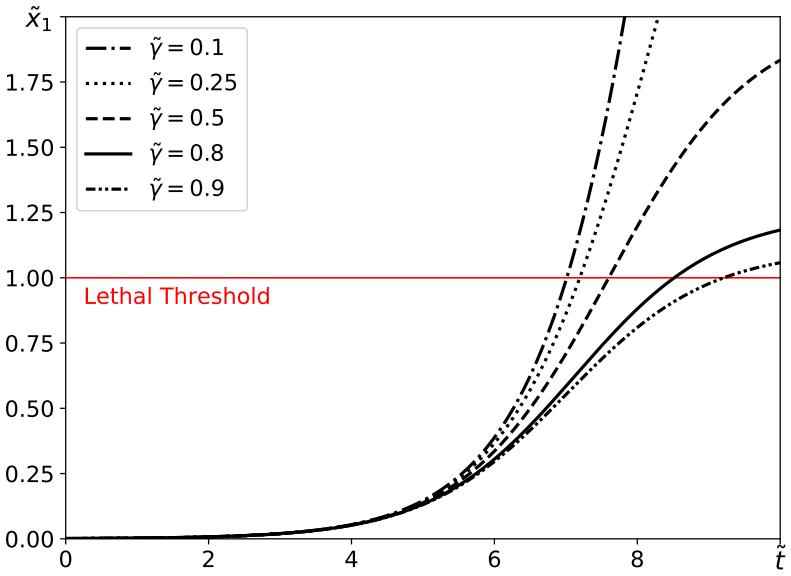


Figure 28: Simulation of our cancer growth model omitting the effects of the stroma and the immune system [Eq. 96], for various values of $\tilde{\gamma} \in \{0.1, 0.25, 0.5, 0.8, 0.9\}$. The initial cancer size used in each case was $\tilde{x}_{1,0} = 10^{-3}$.

The important qualitative choice with this model is whether the lethal threshold should lie above or below the inflection point of the logistic growth curve. If it is below, only exponential growth of the cancer population is observed prior to patient death. If it is above, a deceleration in cancer growth is observed prior to patient death. Martin et al. [49] and Viossat and Noble [84] opt for the former, estimating the cancer carrying capacity to be ten and four times greater than the lethal threshold, respectively. A choice of $\tilde{\gamma} = 0.1$ or $\tilde{\gamma} = 0.25$ would agree with these estimates. On the other hand, Spratt et al. [76] opt for the latter and estimate that after reaching the inflection point in its growth, the cancer population doubles in size approximately one more time before reaching the lethal size. For the logistic model this means that the lethal size would be equal to the carrying capacity, since the inflection point occurs at half the size of the carrying capacity. Additionally, Vaghi et al. [81] present murine lung and breast cancer growth data that also indicate a slowdown in cancer growth before reaching the lethal threshold. Choices of $\tilde{\gamma} = 0.8$ or $\tilde{\gamma} = 0.9$, align better with these findings. The correct choice will depend on the particular type of cancer being modelled.

One limitation of the logistic model is that any cancer cell population, regardless of the initial size, will grow towards carrying capacity. This drawback is addressed by including the other components of our model.

4.2 Reduced Model B: Cancer Growth without the Immune System or Treatment.

Next, we will simulate untreated cancer growth in the presence of the stroma, but not the immune system. To do this we set $\tilde{x}_5 = \tilde{D}\left(\frac{\tilde{t}}{r_1}\right) = 0$ which results in the following system of equations,

$$\begin{aligned}\frac{d\tilde{x}_1}{d\tilde{t}} &= \left(1 + \tilde{\rho}_{C3}\frac{\tilde{x}_3\left(1+a_C\right)}{\tilde{x}_3 + a_C}\right)\tilde{x}_1 - \tilde{\gamma}\tilde{x}_1^2 - \tilde{\gamma}_T\tilde{x}_1 \\ \frac{d\tilde{x}_3}{d\tilde{t}} &= \tilde{\rho}_{3C}\tilde{x}_1\left(1-\tilde{x}_3\right) - \tilde{\epsilon}\tilde{x}_3. \end{aligned} \tag{97}$$

This model has six parameters, compared to the model in Section 4.1, which had just one parameter.

$\tilde{\gamma}$: From Section 4.1, we observed how larger values of $\tilde{\gamma}$ result in lower cancer carrying capacities which are closer to the lethal threshold and smaller values resulted in larger carrying capacities. We have opted to use a large value of $\tilde{\gamma}$ for the remainder of our simulations, however, we are limited in our choice of $\tilde{\gamma}$ by assumptions made in section 2.4.2. There, we assumed $\tilde{\sigma}_{15} = 0.5$ and we assumed the relationship in [Eq. 79] holds. This gives us the following reasonable range for $\tilde{\gamma}$,

$$0 < \tilde{\gamma} < 1 - \tilde{\gamma}_T - \tilde{\sigma}_{15} = 0.5 - \tilde{\gamma}_T. \tag{98}$$

Later in this section we will show that an upper estimate for $\tilde{\gamma}_T$ is given by $\tilde{\gamma}_T = 0.22\gamma$, and therefore [Eq. 98] becomes,

$$0 < \tilde{\gamma} < 0.4. \tag{99}$$

We hence choose a reasonably high value within this range and set $\tilde{\gamma} = 0.35$.

$\tilde{\gamma}_T$: We will next obtain possible values for $\tilde{\gamma}_T$. Since,

$$\tilde{\gamma}_T = \frac{T}{C^*}\tilde{\gamma},$$

and given $\tilde{\gamma} = 0.35$, the value of $\tilde{\gamma}_T$ can be derived based on the ratio $\frac{T}{C^*}$, which will vary by cancer type. Certain cancers, such as pancreatic and breast cancer, can have more substantial stromal components than others [14, 46], resulting in larger values of $\frac{T}{C^*}$.

In BRAF-mutated melanoma, estimated by Picco et al. [64], the cancer carrying capacity is approximately $5000mm^3$ with a stromal size of around $60mm^3$, which gives $T \approx 0.01K$ where K is the carrying capacity. Then, if we assume

$K \approx 1.25C^*$, we find $T \approx 0.01K = 0.0125C^*$ which yields,

$$\tilde{\gamma}_T \approx 0.0125\tilde{\gamma} \approx 0.005.$$

Similarly, Moorman et al. [54] observed stromal compartments making up 30% to 80% of the breast cancer microenvironent, with their data primarily coming from stage I and II breast cancer tumours. We will assume that at these stages, primary tumours are about $20mm$ in diameter [29]. A primary breast cancer tumour exceeding $50mm$ is considered large [75]. These tumours can grow to over $90mm$ at which point they are likely to have metastasised [29]. We will thus take $90mm$ to be the lethal tumour size in this case. Our model assumes the size of the stroma is constant, therefore we expect the 30%-80% stromal proportion range to reduce to 6.6%-17.8% as the cancer population increases bringing the tumour to its lethal size. This allows us to compute a possible reasonable range for $\tilde{\gamma}_T$ in breast cancer,

$$\tilde{\gamma}_T \in \left\{ \frac{6.6}{93.4}\tilde{\gamma}, \frac{17.8}{82.2}\tilde{\gamma} \right\} \approx \{0.07\tilde{\gamma}, 0.22\tilde{\gamma}\} \approx \{0.02, 0.08\}.$$

We round to two decimal place above since these are only ball-park estimates of what might constitute reasonable values.

$\tilde{\boldsymbol{\rho}}_{\boldsymbol{C3}}$: Returning to work by Picco et al. [64], we can obtain an estimate of $\tilde{\rho}_{C3}$ for BRAF-mutated melanoma. They posit that the active stroma boosts the growth rate of the drug resistant cancer cells by 90% and thus we have,

$$\tilde{\rho}_{C3} = 0.9.$$

Orimo et al. [59] estimate that the presence of CAFs in breast cancer can cause between a 1.6- to a 2.8-fold increase in the growth rate of breast cancer. This indicates that an estimate of,

$$\tilde{\rho}_{C3} = 1.2,$$

representing a 2.2-fold increase in the growth rate, could be considered typical for breast cancer.

$\tilde{\boldsymbol{\epsilon}}$: Earlier, in Section 2.3, we assumed $\tilde{\epsilon} \ll \tilde{\rho}_{3C}$ and hence we set,

$$\tilde{\epsilon} = 0.01,$$

such that it is almost two orders of magnitude smaller than the low estimate of $\tilde{\rho}_{C3} = 0.9$.

a_C : Recall that the parameter a_C decides the relationship between stro-

mal activation and the growth promotion of cancer. In particular, it determines whether the growth promotion increases linearly with stromal activation, or whether cancer becomes near maximally boosted at low levels of stromal activation. It is difficult to ascertain quantitative information about this relationship and therefore we opt to use a value that is between these two extremes,

$$a_C = 0.2,$$

see [Fig. 6].

$\tilde{\boldsymbol{\rho}}_{\boldsymbol{3C}}$ **:** Finally, we are left with the parameter, $\tilde{\rho}_{3C}$, which controls the rate of stromal activation in response to cancer. This varies greatly across different types of cancer [25]. We will adopt a similar approach to Flach et al. [25] by presenting two scenarios: an aggressive cancer that rapidly activates the stroma,

$$\tilde{\rho}_{3C} = 3,$$

and a less aggressive cancer that is less capable of activating the stroma,

$$\tilde{\rho}_{3C} = 0.3.$$

Based on the above considerations for possible parameter values, we will present four different types of tumour microenvironments.

1. Low stromal volume and weak cancer promotion ($\tilde{\gamma}_T = 0.005$, $\tilde{\rho}_{C3} = 0.9$) with less aggressive cancer ($\tilde{\rho}_{3C} = 0.3$) [Fig. 29 (a)].

2. Low stromal volume and strong cancer promotion ($\tilde{\gamma}_T = 0.005$, $\tilde{\rho}_{C3} = 1.2$) with more aggressive cancer ($\tilde{\rho}_{3C} = 3$) [Fig. 29 (b)].

3. High stromal volume and weak cancer promotion ($\tilde{\gamma}_T = 0.08$, $\tilde{\rho}_{C3} = 0.9$) with less aggressive cancer ($\tilde{\rho}_{3C} = 0.3$) [Fig. 29 (c)].

4. High stromal volume and strong cancer promotion ($\tilde{\gamma}_T = 0.08$, $\tilde{\rho}_{C3} = 1.2$) with more aggressive cancer ($\tilde{\rho}_{3C} = 3$) [Fig. 29 (d)].

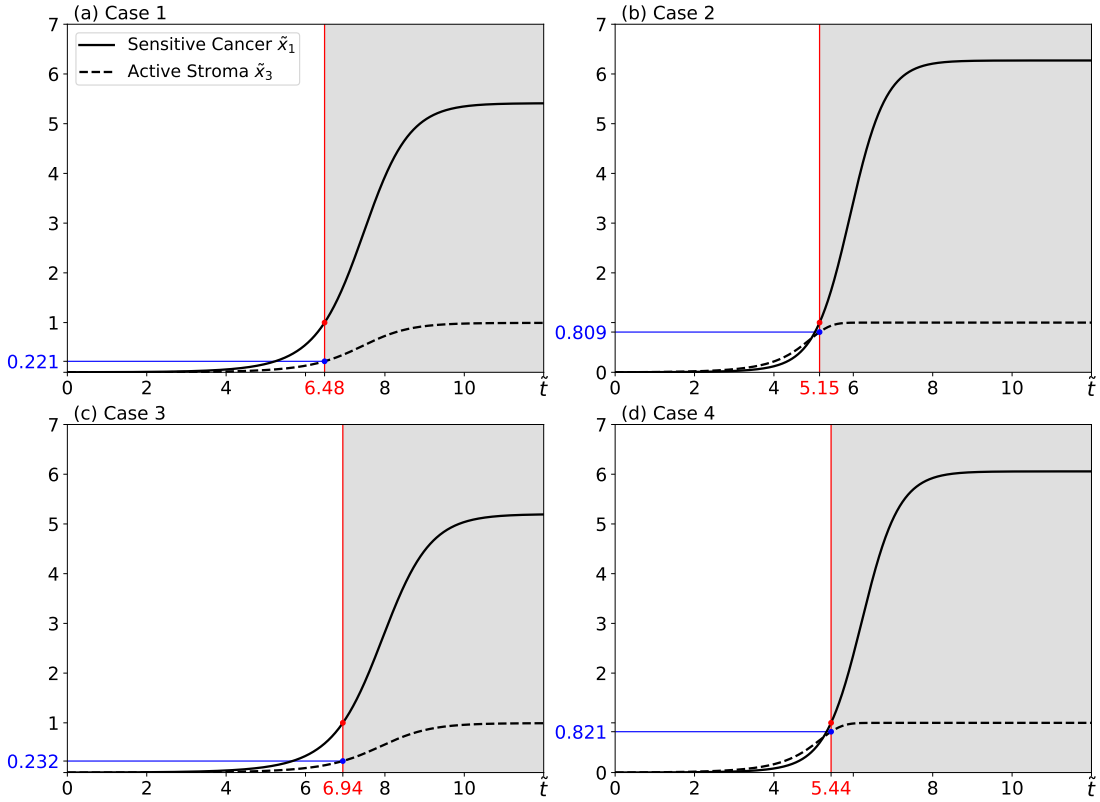


Figure 29: Simulations of sensitive cancer growth and stromal activation in the absence of the immune system and treatment [Eq. 97]. In each plot, the initial conditions used were $(\tilde{x}_{1,0} = 10^{-3}, \tilde{x}_{3,0} = 0)$. Other parameter values common across each plot were: $\tilde{\gamma} = 0.35$, $a_C = 0.2$ and $\tilde{\epsilon} = 0.01$. The parameter values that vary across each of the plots were: (a) $\tilde{\gamma}_T = 0.005$, $\tilde{\rho}_{C3} = 0.9$ and $\tilde{\rho}_{3C} = 0.3$, (b) $\tilde{\gamma}_T = 0.005$, $\tilde{\rho}_{C3} = 1.2$ and $\tilde{\rho}_{3C} = 3$, (c) $\tilde{\gamma}_T = 0.08$, $\tilde{\rho}_{C3} = 0.9$ and $\tilde{\rho}_{3C} = 0.3$ and finally (d) $\tilde{\gamma}_T = 0.08$, $\tilde{\rho}_{C3} = 1.2$ and $\tilde{\rho}_{3C} = 3$. The vertical red line indicates the time at which the cancer population reaches the lethal size and any growth in the shaded region takes place after this time. The blue line indicates the extent of stromal activation by the time the cancer population reaches the lethal threshold.

We observe variation in the cancer patient survival times across each of the cases in [Fig. 29], which highlights the stroma's critical role in cancer development.

Comparing case 1 with case 3 and case 2 with case 4 reveals an interesting observation. Tumours with larger stromal compartments might result in longer survival times. Initially, a substantial amount of stroma can inhibit tumour growth by forming a physical barrier [12]. However, as the tumour expands, the resultant stress creates a hypoxic environment that favours tumour growth [78]. This, along with the stromal activation, eventually results in aggressive tumour growth. This effect is captured in our model through the spatial competition between the stroma and the cancer cells. This observation does assume that both the large volume stroma and the small volume stroma are equally capable of the promoting cancer growth, i.e. $\tilde{\rho}_{3C}$ is the same in each case. This assumption

is in line with previous assumptions discussed in Section 2.2.1, whereby cancer cells are only able to process a limited amount of growth promoting molecules in a given amount of time. Therefore, even if the stromal volume increases, the growth promotion may remain the same.

Cases 2 and 3 represent extreme growth conditions with case 2 illustrating cancer growth in optimal environmental conditions and case 3 illustrating cancer growth in the least optimal environmental conditions. Case 1 and 4 represent more typical scenarios. Parameter values for Case 4 align with what we expect for breast cancer growth: a dense and aggressive stromal compartment. The extent of the stromal activation in this case aligns with Kalluri and Zeisberg's observations that about 80% of the stroma becomes active during breast cancer growth [35].

In the sections to follow we will integrate patient immune response and treatment, exploring further types of TMEs through additional simulations.

4.3 Complete Model: Cancer Growth without Treatment.

Finally we arrive at the complete tumour microenvironment model without treatment. Here we only make the assumption that $\tilde{D}\left(\frac{\tilde{t}}{r_1}\right) = 0$ which leaves us with the following system of equations,

$$\begin{aligned}
\frac{d\tilde{x}_1}{d\tilde{t}} &= \left(1 + \tilde{\rho}_{C3}\frac{\tilde{x}_3\left(1+a_C\right)}{\tilde{x}_3 + a_C}\right)\tilde{x}_1 - \tilde{\gamma}\tilde{x}_1^2 - \tilde{\gamma}_T\tilde{x}_1 - \tilde{\sigma}_{15}\tilde{x}_5 e^{-\tilde{\kappa}_5\tilde{x}_3}\tilde{x}_1 \\
\frac{d\tilde{x}_3}{d\tilde{t}} &= \tilde{\rho}_{3C}\tilde{x}_1\left(1-\tilde{x}_3\right) - \tilde{\epsilon}\tilde{x}_3. \\
\frac{d\tilde{x}_5}{d\tilde{t}} &= \tilde{d} - \tilde{d}\tilde{x}_5 + \tilde{\rho}_{5C}\left(\frac{\tilde{x_1}}{\tilde{a}_{52}+\tilde{x}_1}\right)\tilde{x}_5 - \tilde{\sigma}_{5C}\tilde{x}_1\tilde{x}_5
\end{aligned} \tag{100}$$

Inclusion of the immune system has introduced six new parameters that we must find potential values for.

$\boldsymbol{\tilde{d}}$ **:** Kuznetsov et al. [38] estimate that $d \approx 0.23 r_1$, for analogous parameters in their model, and hence we will use,

$$\tilde{d} = 0.23.$$

$\boldsymbol{\tilde{\kappa}_5}$ **:** We will base our estimate of the parameter $\tilde{\kappa}_5$ on results obtained by Lakins et al. [39] who conducted experiments to directly observe the reduced cytotoxic capacity of T-cells in the presence of CAFs. Their experiments indicate that in the presence of normal fibroblasts, around 20% of melanoma cancer cells survive co-culture with T-cells, whereas in the presence of CAFs around 35% of the melanoma cancer cells survive. Similar protection was observed for lung

cancer cells as well. This indicates that the active stroma might reduce the ability of the immune system to kill cancer cells by roughly 20%. Based on this we estimate,

$$\tilde{\kappa}_5 = 0.22,$$

since then, when $\tilde{x}_3 = 1$, we have that,

$$\tilde{\sigma}_{15} e^{-\tilde{\kappa}_5} \approx 0.8\tilde{\sigma}_{15}.$$

$\tilde{\sigma}_{15}$, $\tilde{\rho}_{5C}$, $\tilde{a}_{52}$, and $\tilde{\sigma}_{5C}$: The remaining parameters are chosen in line with those used in Section 2.4.2 and as such we set, $\tilde{\sigma}_{15} = 0.5$, $\tilde{\rho}_{5C} = 0.689$, $\tilde{a}_{52} = 2.25 \,\mathrm{x}\, 10^{-5}$ and $\tilde{\sigma}_{5C} = 5.625 \,\mathrm{x}\, 10^{3}$. Through experimentation, these values were found to permit the existence of a reasonably small extinction threshold in the cancer population. Despite the fact that some of our other parameters in this section, such as $\tilde{\gamma}$ and $\tilde{\gamma}_T$, vary from those used in Section 2.4.2, these parameter values still generate qualitatively equivalent behaviour to that discussed in Section 2.4.2.

With this, we are now in a position to simulate the complete tumour microenvironment model in the absence of treatment. In addition to the parameter values chosen above we will, for the purposes of this simulation, choose the other parameter values of the model in line with those from case 4 in Section 4.2. Therefore we will set $\tilde{\gamma}_T = 0.08$, $\tilde{\rho}_{C3} = 1.2$ and $\tilde{\rho}_{3C} = 3$. The time series plots from the simulations are provided in [Fig. 30].

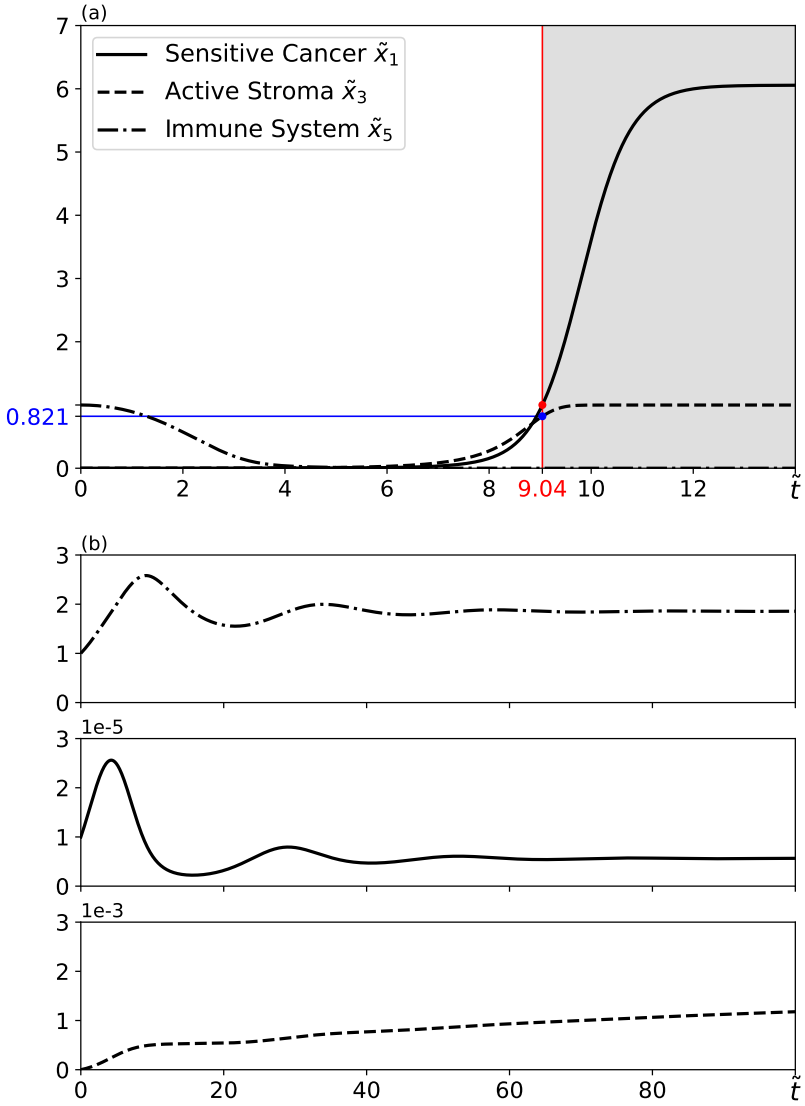


Figure 30: Simulation of the complete tumour microenvironment model in the absence of treatment. (a) We use the initial conditions $(\tilde{x}_{1,0} = 10^{-4}, \tilde{x}_{3,0} = 0, \tilde{x}_{5,0} = 1)$. The vertical red line indicates the time at which the cancer population reaches the lethal size and any growth in the shaded region takes place after this time. The blue line indicates the extent of stromal activation by the time the cancer population reaches the lethal threshold. (b) We use the initial conditions $(\tilde{x}_{1,0} = 10^{-5}, \tilde{x}_{3,0} = 0, \tilde{x}_{5,0} = 1)$. The top panel showcases the time series for the immune cell population, the middle panel showcases the time series for the cancer cell population and the bottom panel showcases the time series for the active stroma variable. Parameter values for both (a) and (b) were fixed as follows: $\tilde{\rho}_{C3} = 1.2$, $\tilde{a}_C = 0.2$, $\tilde{\gamma} = 0.35$, $\tilde{\gamma}_T = 0.08$, $\tilde{\sigma}_{15} = 0.5$, $\tilde{\kappa}_5 = 0.22$, $\tilde{\rho}_{3C} = 3$, $\tilde{\epsilon} = 0.01$, $\tilde{d} = 0.23$, $\tilde{\rho}_{5C} = 0.689$, $\tilde{a}_{52} = 2.25 \times 10^{-5}$ and $\tilde{\sigma}_{5C} = 5.625 \times 10^3$

In contrast to [Fig. 29 (d)], [Fig. 30 (a)] shows that, initially, there is a functioning immune cell population within the tumour microenvironment. Since we initialise the cancer cell population above the extinction threshold, this immune cell population is overrun by the cancer cell population and dies out by $\tilde{t} = 4$, after which the cancer cell population grows to carrying capacity uninhibited. The

cancer cell population must spend time overcomming the patient's immune defenses which delays the time until the cancer cell population becomes detectable. This in turn leads to an increase in the patient survival time compared to that in [Fig. 29 (d)], however this extension of life occurs when the cancer is still too small to be detected so it is not something that one would observe in a clinical setting. Once the cancer attains a detectable size, perhaps $\tilde{x}_1 = 0.01$, the growth is quite similar to that seen in [Fig. 29].

In [Fig. 30 (b)] we initialise the cancer cell populations below the extinction threshold. In this case, we plot each population on a separate panel because they evolve on very different scales. We observe an initial spike in the immune system, stopping the growth of the cancer cell population and causing it to decay. This is followed by damped oscillations as both populations settle down to an equilibrium level. During this time, a small percentage of the stroma becomes active.

5 Model Simulations With Treatment:

Our next objective will be to simulate the complete tumour microenvironment model with treatment. In this case we assume that all of the model variables are free to vary in time and that chemotherapy intensity is not fixed at zero. This results in following complete system of equations,

$$\begin{aligned}
\frac{d\tilde{x}_1}{d\tilde{t}} =& \left(1 - \tilde{\lambda}\tilde{D}\left(\frac{\tilde{t}}{r_1}\right)e^{-\tilde{\kappa}_D\tilde{x}_3} + \tilde{\rho}_{C3}\frac{\tilde{x}_3(1+a_C)}{\tilde{x}_3+a_C}\right)\tilde{x}_1 - \tilde{\gamma}\tilde{x}_1\big[\tilde{x}_1+\tilde{x}_2\big] - \tilde{\gamma}_T\tilde{x}_1 \\
& - \tilde{\delta}_1\tilde{D}\left(\frac{\tilde{t}}{r_1}\right)e^{-\tilde{\kappa}_D\tilde{x}_3}\tilde{x}_1 - \tilde{\sigma}_{15}\tilde{x}_5 e^{-\tilde{\kappa}_5\tilde{x}_3}\tilde{x}_1 \\
\frac{d\tilde{x}_2}{d\tilde{t}} =& \tilde{\lambda}\tilde{D}\left(\frac{\tilde{t}}{r_1}\right)e^{-\tilde{\kappa}_D\tilde{x}_3}\tilde{x}_1 + \left(1 + \tilde{\rho}_{C3}\frac{\tilde{x}_3(1+a_C)}{\tilde{x}_3+a_C}\right)\tilde{x}_2 - \tilde{\gamma}\tilde{x}_2\big[\tilde{x}_1+\tilde{x}_2\big] - \tilde{\gamma}_T\tilde{x}_2 \\
& - \tilde{\delta}_2\tilde{D}\left(\frac{\tilde{t}}{r_1}\right)e^{-\tilde{\kappa}_D\tilde{x}_3}\tilde{x}_2 - \tilde{\sigma}_{25}\tilde{x}_5 e^{-\tilde{\kappa}_5\tilde{x}_3}\tilde{x}_2 \\
\frac{d\tilde{x}_3}{d\tilde{t}} =& \tilde{\nu}_3\left(\frac{e^{a_3\tilde{D}\left(\frac{\tilde{t}}{r_1}\right)}-1}{e^{a_3}-1}\right)(1-\tilde{x}_3) - \tilde{\delta}_3\tilde{D}\left(\frac{\tilde{t}}{r_1}\right)\tilde{x}_3 \\
& + \tilde{\rho}_{3C}\left(\tilde{x}_1+\tilde{x}_2\right)(1-\tilde{x}_3) - \tilde{\epsilon}\tilde{x}_3 \\
\tilde{x}_4 =& 1 - \tilde{x}_3 \\
\frac{d\tilde{x}_5}{d\tilde{t}} =& \tilde{d}\phi_{51}\left(\tilde{D}\left(\frac{\tilde{t}}{r_1}\right)\right) - \tilde{d}\tilde{x}_5 + \tilde{\rho}_{5C}\left(\frac{\tilde{x}_1+\tilde{x}_2}{\tilde{a}_{52}+\tilde{x}_1+\tilde{x}_2}\right)\tilde{x}_5 - \tilde{\sigma}_{5C}(\tilde{x}_1+\tilde{x}_2)\tilde{x}_5.
\end{aligned}$$

This model has eleven additional parameters to assign values to compared to the complete model without treatment from Section 4.3.

$\tilde{\boldsymbol{\lambda}}$: Kozłowska et al. [36] developed a stochastic and multitype branching process to model the response of ovarian cancer to chemotherapy. Their model includes three parameters of importance to us: $b = 0.667\frac{1}{\text{day}}$ and $d = 0.661\frac{1}{\text{day}}$, which represent the intrinsic per-capita birth and death rates of ovarian cancer cells respectively, and $u = 1.6\times10^{-5}\frac{1}{\text{cell division}}$ which represents the probability, per cell division, that a resistant cell is produced. Hence, the intrinsic per-capita growth rate, denoted r_1 in our model, is given by $b-d = 0.006$, and the per-capita birth rate of resistant cells, denoted λ in our model, is given by $bu = 1.0672\,\text{x}\,10^{-5}$. Therefore,

$$\tilde{\lambda} = \frac{\lambda}{r_1} = \frac{1.0672\,\text{x}\,10^{-5}}{0.006} \approx 2\,\text{x}\,10^{-3}.$$

serves as an approximation for $\tilde{\lambda}$.

$\tilde{\boldsymbol{\kappa}}_{\boldsymbol{D}}$: Next we turn to work by Yang et al. [88] who conducted experiments to quantify the extent of CAF-mediated chemoresistance. They observed that the number of human gastric cancer cells surviving high dose chemotherapy treatment roughly doubled when in the presence of CAFs compared to normal fibroblasts.

This motivates the estimate,

$$\tilde{\kappa}_D = 0.7,$$

since then, when $\tilde{x}_3 = 1$, we have that,

$$\tilde{D}\left(\frac{\tilde{t}}{r_1}\right) e^{-\tilde{\kappa}_D} \approx 0.5\tilde{D}\left(\frac{\tilde{t}}{r_1}\right).$$

$\tilde{\delta}_1$ and $\tilde{\delta}_2$: We will discuss the values of $\tilde{\delta}_1$ and $\tilde{\delta}_2$ in Section 5.2, after we have defined explicit forms of $\tilde{D}\left(\frac{\tilde{t}}{r_1}\right)$ for different treatment regimens, see Section 5.1.

$\tilde{\sigma}_{25}$: It is difficult to obtain quantitative estimates of the reduction in immune sensitivity of chemo-resistant cancer compared to chemo-sensitive cancer. We will therefore use this as an opportunity to test a particular value that may result in some interesting dynamics. This parameter may not have a large effect on the dynamics once cancer has become large due to the heavily immune suppressive environment, however, it may have an effect during the emergence of resistant cancer following treatment. Suppose that chemotherapy eradicates the chemo-sensitive population and that the immune system restores to it's normal strength, then if $\tilde{\sigma}_{25}$ is small enough, the extinction threshold for the resistant population may take on the shape shown in [Fig. 26 (e)]. This may result in the resistant population growing to carrying capacity, despite initially being extremely small following treatment. To allow for and to investigate this potential behaviour, we will assume that chemo-resistant cells are half as sensitive to the immune system as chemo-sensitive cells and set,

$$\tilde{\sigma}_{25} = 0.5\tilde{\sigma}_{15} = 0.25.$$

Such an estimation ensures the shape of the extinction threshold for resistant cancer is as shown in [Fig. 26 (e)] given that we use parameter values as estimated in the treatment free simulations.

$\tilde{\delta}_3$, $\tilde{\nu}_3$ and a_3 : In line with what we did in Section 4.2, we will consider two qualitatively different cases for the stromal response to chemotherapy. We will consider a less responsive case,

$$\tilde{\delta}_3 = 0.1 \quad , \quad \tilde{\nu}_3 = 0.4 \quad \text{and} \quad a_3 = 8.84,$$

as well as a more responsive case,

$$\tilde{\delta}_3 = 1 \quad , \quad \tilde{\nu}_3 = 4 \quad \text{and} \quad a_3 = 8.84,$$

The parameter values of the former case align with the work done producing [Fig.

17] in Section 2.3.1. The parameter values from the latter case maintain the same ratio $\frac{\tilde{\delta}_3}{\tilde{\nu}_3}$ and the same value of a_3 as the former case and therefore $\tilde{D}_{\mathrm{r}3} \approx 0.8$ in both cases. This is chosen in line with the assumption that stromal activation due to chemotherapy is most prominent near MTD dosages [13]. The difference between these cases is simply that the magnitude of the response, in both the positive and negative direction, is more extreme in the latter case compared to the former case, i.e. the stroma is more responsive.

$\tilde{D}_{\mathrm{opt},5}$: Based on the results of a mathematical model by D.S. Park et al. [61], we might expect the optimal range of chemotherapy intensities for eliciting an immune response to be between $\tilde{D} = 0.4$ and $\tilde{D} = 0.5$. Based on this, we choose to set,

$$\tilde{D}_{\mathrm{opt},5} = 0.5,$$

as this choice is within the optimal range and also allows us to use [Fig. 20 (d)] to aid with the determination of η and a_{51}.

η and a_{51} : As discussed in Section 2.4, the choice of η and a_{51} will vary depending on whether the patient has a responsive or unresponsive immune system. Y.H. Park et al. [62] studied the chemotherapy induced immune responses of breast cancer patients undergoing neo-adjuvant chemotherapy. They observed a roughly 1.5-fold increase in the median density of tumour-infiltrating lymphocytes in the patients that later responded well, and they observed little to no increase in the patients that later had poorer outcomes. $\phi_{51,\max}$ determines the maximum scaling of the immune cell influx in response to chemotherapy and therefore we might expect $\phi_{51,\max} = 1.5$ for a responsive patient and $\phi_{51,\max} = 1.1$ for an unresponsive patient. We will assume that chemotherapy becomes immune suppressive for intensities above $\tilde{D}_{\mathrm{r}5} = 0.7$ allowing us to use [Fig. 20 (d)] to estimate,

$$\eta = 11 \quad \text{and} \quad a_{51} = 1,$$

for patients with responsive immune systems. These values are chosen based on the rough location of the intersection of lines 3 and 6 in [Fig. 20 (d)]. Similarly, we can estimate,

$$\eta = 34 \quad \text{and} \quad a_{51} = 0.3,$$

for a patient with an unresponsive immune system. These values are based on the rough location of the intersection of lines 1 and 6 which, while not visible in [Fig. 20 (d)], can be easily calculated.

5.1 Treatment Regimens and Pharmacokinetics

For the simulations in this section, we will consider two different treatment regimens: a maximum-tolerated dose (MTD) regimen and a low-dose metronomic (LDM) regimen. We will define a specific form of $\tilde{D}\left(\frac{\tilde{t}}{r_1}\right)$ for each case, $\tilde{D}_{\text{MTD}}\left(\frac{\tilde{t}}{r_1}\right)$ and $\tilde{D}_{\text{LDM}}\left(\frac{\tilde{t}}{r_1}\right)$ respectively. To do this we must first understand what typical courses of MTD and LDM chemotherapy involve, as well as how the body affects the drug once it is administered, i.e. the pharmacokinetics of the drug.

According to Cancer Research UK [80], a typical course of chemotherapy may last between 3-6 months, consisting of 2, 3 or 4 week long cycles with breaks in between. The cycles involve repeated administration of the drug followed by breaks so that the body can recover. Maiti [43] outlines that conventional MTD chemotherapy involves administration of the drug at it's maximum tolerated dose every one, two or three weeks, wheras LDM chemotherapy involves more frequent and continuous administration of the drug at lower doses, either weekly, every other day or daily. Such doses are usually between 1/10th and 1/3rd of the maximum tolerated dose. After administration, chemotherapeutic drugs are broken down by the body over time and this can be modelled as an exponential decay in the blood concentration of the drug [26, 48]. Conventional MTD therapy is then characterised by rise-and-fall cycles of the drug's blood concentration over time, and LDM chemotherapy is characterised by a sustained, low blood concentration of the drug over time [43].

Based on the above considerations we will model a three-month course of chemotherapy treatment. The MTD treatment will involve administration of the drug at the maximum tolerated dose once per week for three weeks followed by a week long break. This will then be repeated three times to complete the three-month course. The LDM treatment will involve daily, uninterrupted administration of the drug at 30% of the maximum tolerated dose for the entirety of the three month period.

To explicitly define $\tilde{D}_{\text{MTD}}\left(\frac{\tilde{t}}{r_1}\right)$ and $\tilde{D}_{\text{LDM}}\left(\frac{\tilde{t}}{r_1}\right)$ we will need to know the duration of non-dimensional time that corresponds to a week. To do this, we will fix the non-treatment related parameters in line with those used in Section 4.3. The simulation provided in [Fig. 30 (a)] is then representative of what occurs when treatment is not applied. We can use this simulation, along with estimates of the life-expectancy of patients with untreated cancer, to determine the length of a week in non-dimensional time. Johnstone et al. [32] indicate that the median survival time, measured from symptom onset, for untreated breast cancer is between 2.3 and 2.7 years. We will assume that it takes 2.5 years for

the cancer population to grow from a symptomatic size, approximately $\tilde{x}_1 = 0.1$, to the lethal size $\tilde{x}_1 = 1$. In [Fig. 30 (a)], $\tilde{x}_1 = 0.1$ at $\tilde{t} \approx 7.732$ and $\tilde{x}_1 = 1$ at $\tilde{t} \approx 9.044$, and hence we will assume that 2.5 years corresponds to 1.312 units of non-dimensional time. Given that there are 130 weeks in 2.5 years, we have that 1 week corresponds to approximately 0.01 non-dimensional time units.

With this we are now ready to explicitly define $\tilde{D}_{\text{MTD}}\left(\frac{\tilde{t}}{r_1}\right)$ and $\tilde{D}_{\text{LDM}}\left(\frac{\tilde{t}}{r_1}\right)$. Each of these functions will describe a three month course of their respective therapy regimens. Given an initial treatment administration time $\tilde{t}_0$, we let $\tilde{t}_{w,i}$ for $i \in \{0, 1, 2, ..., 12\}$ represent the time i-weeks after $\tilde{t}_0$, and we let $\tilde{t}_{d,i}$ for $i \in \{0, 1, 2, ..., 84\}$ represent the time i-days after $\tilde{t}_0$. For example, $\tilde{t}_{w,3} = \tilde{t}_0 + 3 \,\text{x}\, 0.01$ and $\tilde{t}_{d,3} = \tilde{t}_0 + 3 \,\text{x}\, \frac{0.01}{7}$. We then define,

$$\tilde{D}_{\text{MTD}}\left(\frac{\tilde{t}}{r_1}\right) = \begin{cases} 0, & \text{if } \tilde{t} < \tilde{t}_{w,0} = \tilde{t}_0. \\ e^{\omega\left(\tilde{t}_{w,i} - \tilde{t}\right)}, & \text{if } \tilde{t}_{w,i} \leq \tilde{t} < \tilde{t}_{w,i+1} \text{ and } (i+1) \text{ modulo } 4 \neq 0, \\ & \text{for } i \in \{0, 1, 2, ..., 11\}. \\ 0, & \text{if } \tilde{t}_{w,i} \leq \tilde{t} < \tilde{t}_{w,i+1} \text{ and } (i+1) \text{ modulo } 4 = 0, \\ & \text{for } i \in \{0, 1, 2, ..., 11\}, \text{ the treatment holidays.} \\ 0, & \text{if } \tilde{t} \geq \tilde{t}_{w,12}. \end{cases} \tag{101}$$

and,

$$\tilde{D}_{\text{LDM}}\left(\frac{\tilde{t}}{r_1}\right) = \begin{cases} 0, & \text{if } \tilde{t} < \tilde{t}_{d,0} = \tilde{t}_0. \\ 0.3e^{\omega\left(\tilde{t}_{d,i} - \tilde{t}\right)}, & \text{if } \tilde{t}_{d,i} \leq \tilde{t} < \tilde{t}_{d,i+1} \text{ for } i \in \{0, 1, 2, ..., 83\}. \\ 0, & \text{if } \tilde{t} \geq \tilde{t}_{d,84}. \end{cases} \tag{102}$$

We set $\omega = 500$ such that almost all of the drug has decayed a week after an MTD administration. In [Fig. 31 (a)] we plot the first month of the MTD treatment regimen and in [Fig. 31 (b)] we plot the first month of the LDM treatment regimen.

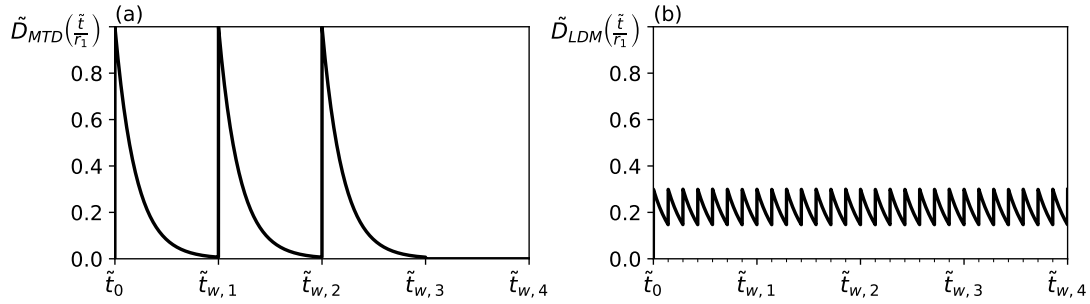


Figure 31: (a) Time series for $\tilde{D}_{\text{MTD}}$ during the first month of the three-month long treatment course. The maximum tolerated dose is administered at the start of each week for three weeks and a break is taken during the fourth week. The drug concertration decays to near zero over the course of each week. (b) Time series for $\tilde{D}_{\text{LDM}}$ during the first month of the three-month long treatment course. Every day, a 30% maximum dose is administered and no break is taken. The drug does not have time to fully decay, so a low concentration is maintained continuously overtime.

5.2 Simulations

We will run four simulations covering different types of patient responses to treatment and different treatment regimens.

1. A patient with a responsive stroma and an unresponsive immune system, undergoing MTD treatment ($\tilde{\delta}_3 = 1$, $\tilde{\nu}_3 = 4$, $\tilde{\eta} = 34$ and $a_{51} = 0.3$ with $\tilde{D} = \tilde{D}_{\text{MTD}}$) [Fig. 32 (a)].

2. A patient with a responsive stroma and an unresponsive immune system, undergoing LDM treatment ($\tilde{\delta}_3 = 1$, $\tilde{\nu}_3 = 4$, $\tilde{\eta} = 34$ and $a_{51} = 0.3$ with $\tilde{D} = \tilde{D}_{\text{LDM}}$) [Fig. 32 (b)].

3. A patient with an unresponsive stroma and a responsive immune system, undergoing MTD treatment ($\tilde{\delta}_3 = 0.1$, $\tilde{\nu}_3 = 0.4$, $\tilde{\eta} = 11$ and $a_{51} = 1$ with $\tilde{D} = \tilde{D}_{\text{MTD}}$) [Fig. 32 (c)].

4. A patient with an unresponsive stroma and a responsive immune system, undergoing LDM treatment ($\tilde{\delta}_3 = 0.1$, $\tilde{\nu}_3 = 0.4$, $\tilde{\eta} = 11$ and $a_{51} = 1$ with $\tilde{D} = \tilde{D}_{\text{LDM}}$) [Fig. 32 (d)].

In each case, we first initiate the treatment when the cancer becomes symptomatic, $\tilde{x}_1 = 0.1$. If the cancer then returns at a later point in time, we attempt the same treatment one more time, again initiating the follow-up treatment when the cancer becomes symptomatic $\tilde{x}_1 + \tilde{x}_2 = 0.1$.

Now that we have defined our treatment regimes and simulation scenarios, we will fix the values of $\tilde{\delta}_1$ and $\tilde{\delta}_2$. We will follow work by Martin et al. [48], who also model the effects of cancer chemotherapy. They study the effects of

three different strength drugs. The strength of each drug is determined by the fractional cell kill that occurs during the first week after an MTD administration of the drug. They consider a strong drug with a fractional cell kill of 90% after the first week, a moderate drug with a fractional cell kill of 50% after the first week and a weak drug with a fractional cell kill of just 10% after the first week. For our simulations, we will model a moderate to strong drug that kills approximately 75% of the cancer population after the first week. We obtain our estimate of $\tilde{\delta}_1$ through experimentation, with parameters fixed in line with case 1 above. We found that setting $\tilde{\delta}_1 = 800$ reduces the cancer population in case 1 by approximately 75% after the first week. We will assume that the resistant cancer has a ten-fold reduction in susceptibility to the drug and thus we will fix $\tilde{\delta}_2 = 80$. See [Fig. 32] for the results of the simulations.

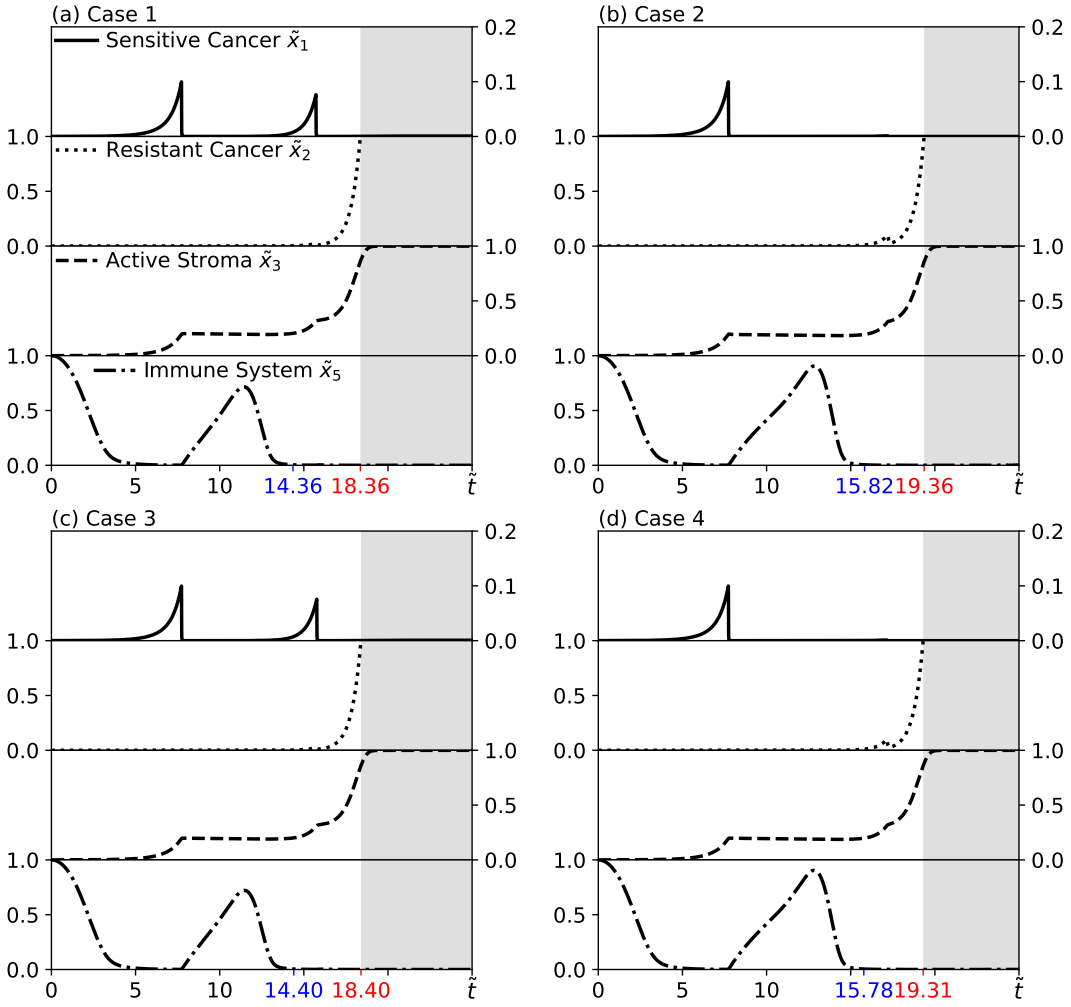


Figure 32: Simulations of the complete model with treatment for (a) case 1, (b) case 2, (c) case 3 and (d) case 4. Initial conditions in each simulation were $\tilde{x}_{1,0} = 10^{-4}$, $\tilde{x}_{2,0} = 0$, $\tilde{x}_{3,0} = 0$ and $\tilde{x}_{5,0} = 1$. The solid line represents $\tilde{x}_1$, the dotted line represents $\tilde{x}_2$, the dashed line represents $\tilde{x}_3$ and the dashed and dotted line represents $\tilde{x}_5$. The grey regions indicates the time after the cancer population has reached the lethal size. The blue time indicates the time at which the total cancer population becomes detectable upon relapse, $\tilde{x}_1 + \tilde{x}_2 = 0.01$. The red time indicates the time of patient death.

In case 1 [Fig. 32 (a)] treatment is first applied at $\tilde{t} = 7.73$ and the course is complete three months later at $\tilde{t} = 7.85$. Following treatment, the cancer population has been reduced far below the detection threshold of $\tilde{x}_1 = 0.01$. However, the cancer becomes detectable again at $\tilde{t} = 14.36$, almost 13 years later. During this time, the local immune-strength within the tumour microenvironment never fully recovered and thus the very small post-treatment cancer population was able to re-grow to a detectable size. The second treatment is initiated at $\tilde{t} = 15.72$ and is suspended after three months at $\tilde{t} = 15.84$. While this follow up seems successful initially, a small resistant population is present, and within just two weeks of the suspension of the follow-up treatment, at $\tilde{t} = 15.854$, there is a detectable cancer population almost entirely made up of resistant cells. Without

any new treatment this population grows to the lethal threshold. See [Fig. 33 (a) and (b)] for close up views of the evolution of the cancer variables during the treatment windows for case 1.

Comparing the outcome of MTD treatment in case 1 [Fig. 32 (a)] with LDM treatment in case 2 [Fig. 32 (b)] we observe a few differences but the outcome is still negative for the patient. This treatment is much more effective at killing the sensitive cancer population, and the immune system experiences better recovery-post treatment. However the patient still experiences a relapse at $\tilde{t} = 15.82$. This is 2.8 year improvement over the MTD case, but this time the recurring population is already almost completely resistant, and the follow-up treatment fails to reduce the cancer population below the detection threshold at all. See [Fig. 33 (c) and (d)] for close up views of the evolution of the cancer variables during the treatment windows for case 2.

Comparing case 1 [Fig. 32 (a)] with case 3 [Fig. 32 (c)] we see very little change. The patient in case 3 fares slightly better than the patient in case 1, surviving an extra month. Similarly, there is very little change comparing case 2 [Fig. 32 (b)] with case 4 [Fig. 32 (d)], however in this case, the patient with the responsive stroma and unresponsive immune system fares better, again surviving about an extra month. Given our approach to modelling chemotherapy, and given the parameters we have choosen, the stroma does not evolve quickly enough over the relatively short timescale on which treatment is applied, and therefore it does not respond strongly to the treatment. When treatment is being applied, cancer has already strongly suppressed the immune system and as such it also does not experience a noticeable response to the therapy. Future quantitative work, taking more care to estimate accurate parameter values and accurately modelling the pharmacokinetics of a particular drug, may find that these variables respond more significantly resulting in more variable treatment outcomes.

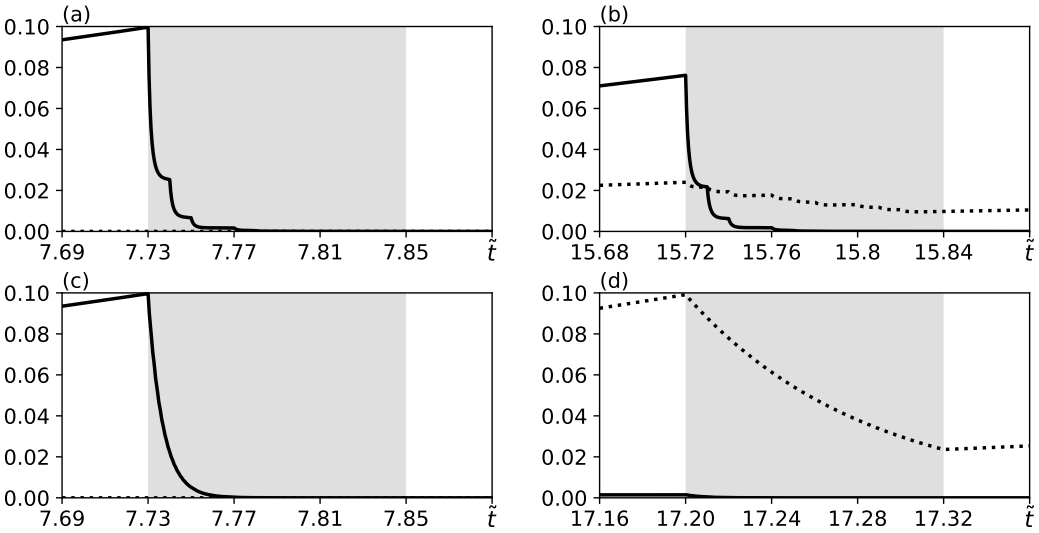


Figure 33: Close ups of the treatment windows for (a) and (b): case 1, and (c) and (d): case 2. The solid line represents chemo-sensitive cancer and the dotted line represents chemo-resistant cancer. In (a), it can be observed that our choice of $\tilde{\delta}_1 = 800$ results in a fractional cell kill of approximately 75% after the first week of MTD treatment. Comparing (a) and (c) highlights how the LDM treatment is more effective than the MTD treatment at reducing the sensitive cancer population.

We carried out an additional simulation to test what happens if the chemo-resistant cancer population is equally susceptible to the immune system as the chemo-sensitive cancer population. For this we set the parameters as they were in case 4 with the only change being that we set $\tilde{\sigma}_{25} = \tilde{\sigma}_{15} = 0.5$. The outcome of this simulation is provided in [Fig. 34].

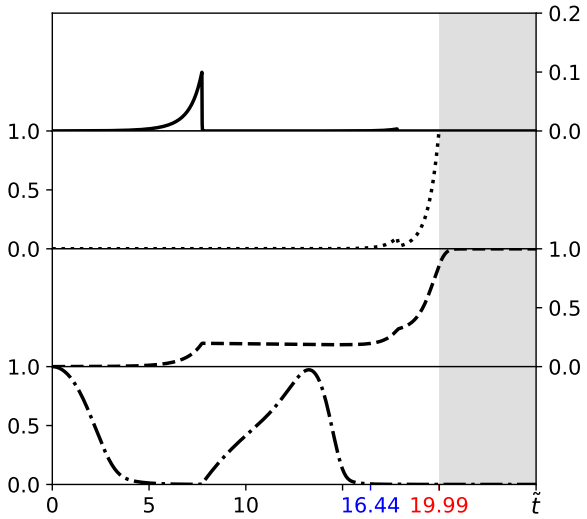


Figure 34: Simulation of case 4 with $\tilde{\sigma}_{25} = 0.5$. Line styles and figure annotations have the same interpretations as in [Fig. 32].

Comparing this simulation with [Fig. 32 (d)], we see that relapse does still occur albeit over a year later. There are two possible explanations: either the

immune system does not recover in time to trap the resistant cancer population below an extinction threshold, or, the immune system is prevented from sufficiently killing the cancer due to the now activated stroma. Future work with more accurate quantitative estimates may observe a different outcome. Future work could also incorporate immunotherapy into the model to investigate whether giving the immune system a therapeutic boost following chemotherapy might allow the cancer population to be restrained.

Finally, we aimed to determine whether setting $\tilde{\lambda} = 0$ in our model could prevent relapse, i.e. whether relapse still occurs given that resistance cannot develop. To test, this we ran two final simulations: one with $\tilde{\lambda} = 2 \times 10^{-3}$ as usual and one with $\tilde{\lambda} = 0$. All other parameters used for these simulations were the same as those used in [Fig. 32 (b)]. In both cases we applied a single, six-month course of LDM treatment, initiated when $\tilde{x}_1 = 0.1$ for the first time, without any subsequent follow-up treatment. The results of the simulations are shown in [Fig. 35].

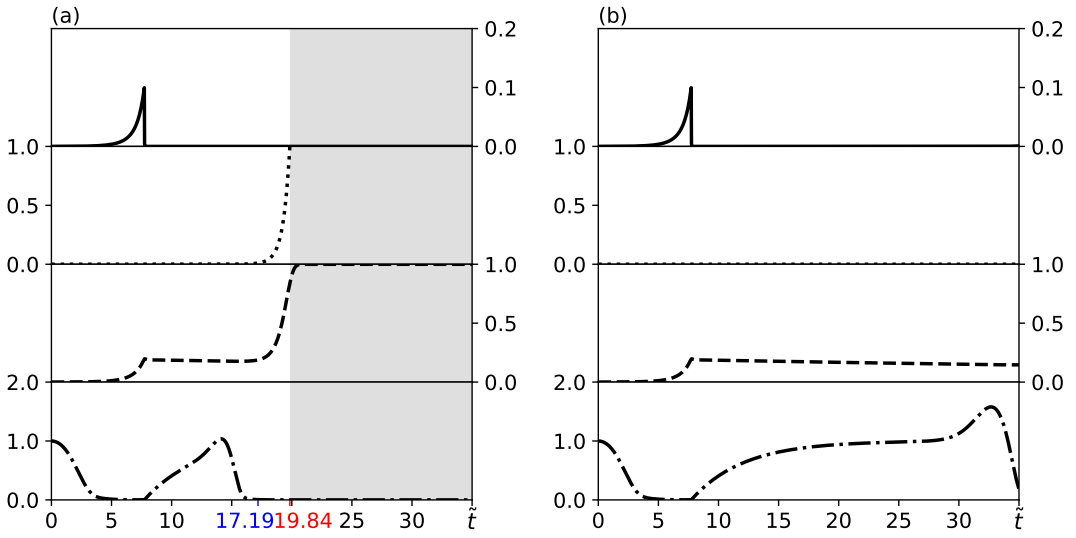


Figure 35: Simulations with a single, six-month long course of LDM treatment for (a) $\tilde{\lambda} = 2 \times 10^{-3}$ and (b) $\tilde{\lambda} = 0$. All other parameters were chosen in line with [Fig. 32 (b)] and line styles and figure annotations have the same interpretations as those in [Fig. 32].

In [Fig. 35 (a)] the LDM treatment course is initiated at $\tilde{t} = 7.73$ and is suspended six months later at $\tilde{t} = 7.97$. This treatment is initially successful; however, at $\tilde{t} = 17.19$, a resistant cancer population becomes detectable, leading to relapse. The patient ultimately dies at $\tilde{t} = 19.84$. In contrast, in [Fig. 35 (b)], the only difference is that $\tilde{\lambda} = 0$, preventing resistance from developing. In this case, up until after $\tilde{t} = 35$, there is no detectable cancer population following the initial treatment. Relapse eventually occurs, inferred from the decaying immune

cell population near $\tilde{t} = 35$, but it does not happen until over 50 years after the suspension of the initial treatment. By this point, most patients would likely have died of other causes, or, if they were young when first diagnosed, they would now be quite old. Therefore, for all practical purposes, we can assume that relapse does not occur in a clinically relevant time frame in this case.

While our model predicts that relapse can be prevented in a clinically relevant time frame, it does not predict complete prevention of relapse. This is likely due to the slow recovery of the immune cell population and the extremely slow normalization of the stroma following cancer removal. The small amount of stroma that remains active is likely sufficient to prevent the immune system from fully regaining control over the cancer, eventually leading to relapse. Future work with more accurate parameter estimates may find that relapse can be entirely prevented if the stroma and immune system recover at faster rates.

6 Conclusions and Results:

The primary aim of this research was to develop a mathematical model that captures the critical tripartite interaction between cancer cells, immune cells and the stroma. Our goal was to create a general model that could be parameterised to various carcinomas. By incorporating chemotherapy and addressing both reversible and irreversible drug resistance, we aimed to pave the way for future research into optimal treatment strategies that counteract the tumour-promoting influences of the TME. These objectives were motivated by the limitations of existing models which often do not integrate these critical tripartite interactions.

The main outcome of our research is the successful development of this comprehensive model. Our model effectively reproduces important qualitative behaviours, such as cancer immunoediting and the dual roles of the stroma in promoting and restraining tumour growth. Additionally, the model provides predictions of variable patient outcomes across different treatment modalities and levels of stromal aggression.

Our model consolidates the techniques and concepts from a variety of existing models into a unified framework. It serves as a valuable tool for exploring the complex interactions within the TME and can be integrated with micro-scale models as described by Byrne et al. [11]. It also provides a foundation for quantitative validation against specific cancer types and can subsequently guide experimental research and contribute to the development of optimal treatment strategies.

Despite the promising qualitative predictions, the model has several limitations. Parameter estimates were coarse and sometimes hypothetical, derived from diverse cancer types. While this was adequate for studying the qualitative behaviour of hypothetical TMEs that consisted of varying degrees of stromal aggression and immune strength, accurate quantitative validation will require more precise parameter estimation. Additionally, to incorporate cancer immunoediting, we assumed a strong advantage for cancer cells over the immune population in the TME, limiting the model's flexibility in representing varying degrees of cancer-induced immune suppression. It also assumes the log-kill hypothesis, which may not hold in all cases and our approach to chemotherapy pharmacokinetics was also significantly simplified. Furthermore, using ODEs to model the TME may have overlooked significant spatial effects.

The development of our model has opened several avenues for future research. One potential direction is to explore alternative growth models for the cancer cell population, such as the generalised logistic growth or the Gompertz growth models. Additionally, investigating alternative modelling approaches to immune-

induced death, like the harvesting approach discussed in Section 2.2.1, could also be valuable. The harvesting approach provides a straightforward way to include the extinction threshold in the cancer population and could enhance flexibility in modelling cancer-induced immune suppression. Future work carrying out quantitative validation of the model is essential but challenging due to the numerous parameters and processes involved; this validation is crucial for its application in clinical scenarios. Furthermore, techniques from optimal control theory could help identify optimal chemotherapy treatments schedules and dosages. Another extension could involve incorporating immunotherapy into the model. This would allow an investigation into whether administering immunotherapy after chemotherapy could help the immune system recover enough to prevent the outgrowth of chemotherapy-resistant cancer cell populations.

While there are limitations to address, our model provides a promising new framework for understanding the complexity of the TME. It can be integrated with other models and help to identify treatment startegies that overcome drug resistance by targeting tumour-promoting functions of the TME. With further refinement and validation, it has the potential to become a valuable tool for both research and clinical applications, advancing cancer treatment through a more comprehensive understanding of TME dynamics.

A Calculations

A.1 Calculations for the Sanity Check of the $\frac{d\tilde{x}_1}{d\tilde{t}}$ and $\frac{d\tilde{x}_2}{d\tilde{t}}$ Equations.

A.1.1 Solving for the equilibrium points.

We set the equations equal to zero and solve for $\tilde{x}_1$ and $\tilde{x}_2$.

$$\begin{aligned}\frac{d\tilde{x}_1}{d\tilde{t}} =& \left(1 - \tilde{\lambda}\tilde{D}e^{-\tilde{\kappa}_D\tilde{A}} + \tilde{\rho}_{C3}\frac{\tilde{A}(1+a_C)}{\tilde{A}+a_C}\right)\tilde{x}_1 - \tilde{\gamma}\tilde{x}_1\left[\tilde{x}_1+\tilde{x}_2\right] - \tilde{\gamma}_T\tilde{x}_1 \\ &- \tilde{\delta}_1\tilde{D}e^{-\tilde{\kappa}_D\tilde{A}}\tilde{x}_1 - \tilde{\sigma}_{15}\tilde{I}e^{-\tilde{\kappa}_5\tilde{A}}\tilde{x}_1 = 0 \qquad (103)\\ \frac{d\tilde{x}_2}{d\tilde{t}} =& \tilde{\lambda}\tilde{D}e^{-\tilde{\kappa}_D\tilde{A}}\tilde{x}_1 + \left(\tilde{r}_2 + \tilde{\rho}_{C3}\frac{\tilde{A}(1+a_C)}{\tilde{A}+a_C}\right)\tilde{x}_2 - \tilde{\gamma}\tilde{x}_2\left[\tilde{x}_1+\tilde{x}_2\right] + \tilde{\gamma}_T\tilde{x}_2 \\ &- \tilde{\delta}_2\tilde{D}e^{-\tilde{\kappa}_D\tilde{A}}\tilde{x}_2 - \tilde{\sigma}_{25}\tilde{I}e^{-\tilde{\kappa}_5\tilde{A}}\tilde{x}_2 = 0 \qquad (104)\end{aligned}$$

Clearly, setting $\tilde{x}_1 = 0$ and $\tilde{x}_2 = 0$ satisfies [Eq. 103] and [Eq. 104] and thus we have found our first equilibrium point,

$$\boldsymbol{e_0}: \qquad (\tilde{x}_1^{e_0}, \tilde{x}_2^{e_0}) = (0,0).$$

Next setting $\tilde{x}_1 = 0$ satisfies [Eq. 103], and we are left with the equation,

$$\begin{aligned}\frac{d\tilde{x}_2}{d\tilde{t}} =& \left(\tilde{r}_2 + \tilde{\rho}_{C3}\frac{\tilde{A}(1+a_C)}{\tilde{A}+a_C}\right)\tilde{x}_2 - \tilde{\gamma}\tilde{x}_2^2 + \tilde{\gamma}_T\tilde{x}_2 - \tilde{\delta}_2\tilde{D}e^{-\tilde{\kappa}_D\tilde{A}}\tilde{x}_2 \\ &- \tilde{\sigma}_{25}\tilde{I}e^{-\tilde{\kappa}_5\tilde{A}}\tilde{x}_2 = 0\end{aligned}$$

which we can use to solve for $\tilde{x}_2 \neq 0$ as follows,

$$\begin{aligned}0 =& \left(\tilde{r}_2 + \tilde{\rho}_{C3}\frac{\tilde{A}(1+a_C)}{\tilde{A}+a_C}\right) - \tilde{\gamma}\tilde{x}_2 + \tilde{\gamma}_T - \tilde{\delta}_2\tilde{D}e^{-\tilde{\kappa}_D\tilde{A}} \\ &- \tilde{\sigma}_{25}\tilde{I}e^{-\tilde{\kappa}_5\tilde{A}} \\ \tilde{\gamma}\tilde{x}_2 =& \tilde{r}_2 + \tilde{\rho}_{C3}\frac{\tilde{A}(1+a_C)}{\tilde{A}+a_C} + \tilde{\gamma}_T - \tilde{\delta}_2\tilde{D}e^{-\tilde{\kappa}_D\tilde{A}} - \tilde{\sigma}_{25}\tilde{I}e^{-\tilde{\kappa}_5\tilde{A}},\end{aligned}$$

then, defining,

$$\zeta_2 = \tilde{r}_2 + \tilde{\rho}_{C3}\frac{\tilde{A}(1+a_C)}{\tilde{A}+a_C} + \tilde{\gamma}_T - \tilde{\delta}_2\tilde{D}e^{-\tilde{\kappa}_D\tilde{A}} - \tilde{\sigma}_{25}\tilde{I}e^{-\tilde{\kappa}_5\tilde{A}}, \qquad (105)$$

we have,

$$\tilde{x}_2 = \frac{\zeta_2}{\tilde{\gamma}}. \tag{106}$$

Thus, we have found our second equilibrium point,

$$\boldsymbol{e_1}: \qquad (\tilde{x}_1^{e_1}, \tilde{x}_2^{e_1}) = (0, \frac{\zeta_2}{\tilde{\gamma}}).$$

Finally assuming both $\tilde{x}_1 \neq 0$ and $\tilde{x}_2 \neq 0$ and setting,

$$\zeta_1 = 1 - \tilde{\lambda}\tilde{D}e^{-\tilde{\kappa}_D\tilde{A}} + \tilde{\rho}_{C3}\frac{\tilde{A}(1+a_C)}{\tilde{A}+a_C} - \tilde{\gamma}_T - \tilde{\delta}_1\tilde{D}e^{-\tilde{\kappa}_D\tilde{A}} - \tilde{\sigma}_{15}\tilde{I}e^{-\tilde{\kappa}_5\tilde{A}},$$

we obtain the following from [Eq. 103],

$$\begin{aligned} 0 &= \zeta_1 - \tilde{\gamma}\left(\tilde{x}_1 + \tilde{x}_2\right). \\ \tilde{x}_1 + \tilde{x}_2 &= \frac{\zeta_1}{\tilde{\gamma}} \\ \tilde{x}_1 &= \frac{\zeta_1}{\tilde{\gamma}} - \tilde{x}_2. \end{aligned} \tag{107}$$

Plugging this into [Eq. 104] obtains,

$$0 = \tilde{\lambda}\tilde{D}e^{-\tilde{\kappa}_D\tilde{A}}\left(\frac{\zeta_1}{\tilde{\gamma}} - \tilde{x}_2\right) + \zeta_2\tilde{x}_2 - \zeta_1\tilde{x}_2$$

and then assuming,

$$0 \neq \zeta_1 + \tilde{\lambda}\tilde{D}e^{-\tilde{\kappa}_D\tilde{A}} - \zeta_2$$

we obtain,

$$\tilde{x}_2 = \frac{\zeta_1}{\tilde{\gamma}}\left(\frac{\tilde{\lambda}\tilde{D}e^{-\tilde{\kappa}_D\tilde{A}}}{\zeta_1 + \tilde{\lambda}\tilde{D}e^{-\tilde{\kappa}_D\tilde{A}} - \zeta_2}\right).$$

Plugging this into [Eq. 107] obtains,

$$\tilde{x}_1 = \frac{\zeta_1}{\tilde{\gamma}}\left(\frac{\zeta_1 - \zeta_2}{\zeta_1 + \tilde{\lambda}\tilde{D}e^{-\tilde{\kappa}_D\tilde{A}} - \zeta_2}\right). \tag{108}$$

Thus, we have found our third and final equilibrium point,

$$\boldsymbol{e_2}: \qquad (\tilde{x}_1^{e_2}, \tilde{x}_2^{e_2}) = \left(\frac{\zeta_1}{\tilde{\gamma}}\left(\frac{\zeta_1 - \zeta_2}{\zeta_1 + \tilde{\lambda}\tilde{D}e^{-\tilde{\kappa}_D\tilde{A}} - \zeta_2}\right), \frac{\zeta_1}{\tilde{\gamma}}\left(\frac{\tilde{\lambda}\tilde{D}e^{-\tilde{\kappa}_D\tilde{A}}}{\zeta_1 + \tilde{\lambda}\tilde{D}e^{-\tilde{\kappa}_D\tilde{A}} - \zeta_2}\right)\right)$$

A.1.2 Computing the eigenvalues and eigenvectors corresponding to e_0, e_1 and e_2.

The Jacobian matrix of our system in terms of ζ_1 and ζ_2 is,

$$\begin{aligned}\boldsymbol{J} &= \begin{pmatrix} \frac{\delta}{\delta\tilde{x}_1}\left(\frac{d\tilde{x}_1}{dt}\right) & \frac{\delta}{\delta\tilde{x}_2}\left(\frac{d\tilde{x}_1}{dt}\right) \\ \frac{\delta}{\delta\tilde{x}_1}\left(\frac{d\tilde{x}_2}{dt}\right) & \frac{\delta}{\delta\tilde{x}_2}\left(\frac{d\tilde{x}_2}{dt}\right) \end{pmatrix} \\ &= \begin{pmatrix} \zeta_1 - 2\tilde{\gamma}\tilde{x}_1 - \tilde{\gamma}\tilde{x}_2 & -\tilde{\gamma}\tilde{x}_1 \\ \tilde{\lambda}\tilde{D}e^{-\tilde{\kappa}_D\tilde{A}} - \tilde{\gamma}\tilde{x}_2 & \zeta_2 - 2\tilde{\gamma}\tilde{x}_2 - \tilde{\gamma}\tilde{x}_1 \end{pmatrix} \end{aligned} \tag{109}$$

1. $\boldsymbol{e_0}$ **:**

The Jacobian matrix evaluated at e_0 is given by,

$$\boldsymbol{J}\Big|_{\left(\tilde{x}_1^{e_0},\tilde{x}_2^{e_0}\right)} = \begin{pmatrix} \zeta_1 & 0 \\ \tilde{\lambda}\tilde{D}e^{-\tilde{\kappa}_D\tilde{A}} & \zeta_2 \end{pmatrix},$$

which is a lower triangular matrix and thus the eigenvalues are just the diagonal entries,

$$L_1^{e_0} = \zeta_1 \quad \text{and} \quad L_2^{e_0} = \zeta_2.$$

We can now obtain the eigenvectors by solving,

$$\left(\boldsymbol{J}\Big|_{\left(\tilde{x}_1^{e_0},\tilde{x}_2^{e_0}\right)} - L_{1,2}^{e_0}\boldsymbol{I}\right)\boldsymbol{v_{1,2}}^{e_0},$$

where $\boldsymbol{I}$ is the identity matrix and $\boldsymbol{v_{1,2}^{e_0}}$ are the eigenvectors corresponding to $L_1^{e_0}$ and $L_2^{e_0}$ respectively.

1. $\boldsymbol{L_1^{e_0}}$ **:**

$$\begin{pmatrix} \zeta_1 - \zeta_1 & 0 \\ \tilde{\lambda}\tilde{D}e^{-\tilde{\kappa}_D\tilde{A}} & \zeta_2 - \zeta_1 \end{pmatrix}\begin{pmatrix} v_a \\ v_b \end{pmatrix} = \begin{pmatrix} 0 \\ 0 \end{pmatrix}$$
$$\begin{pmatrix} 0 & 0 \\ \tilde{\lambda}\tilde{D}e^{-\tilde{\kappa}_D\tilde{A}} & \zeta_2 - \zeta_1 \end{pmatrix}\begin{pmatrix} v_a \\ v_b \end{pmatrix} = \begin{pmatrix} 0 \\ 0 \end{pmatrix}$$

which implies,

(a) $0 = 0$.

(b) $v_a\tilde{\lambda}\tilde{D}e^{-\tilde{\kappa}_D\tilde{A}} + v_b\left(\zeta_2 - \zeta_1\right) = 0$.

and from (b) we have that,

$$v_b = \frac{\tilde{\lambda}\tilde{D}e^{-\tilde{\kappa}_D\tilde{A}}}{\zeta_1 - \zeta_2} v_a,$$

thus, an eigenvector corresponding to $L_1^{e_0}$ is,

$$\boldsymbol{v_1^{e_0}} = \begin{pmatrix} 1 \\ \frac{\tilde{\lambda}\tilde{D}e^{-\tilde{\kappa}_D\tilde{A}}}{\zeta_1 - \zeta_2} \end{pmatrix}.$$

2. $\boldsymbol{L_2^{e_0}}$ **:**

$$\begin{pmatrix} \zeta_1 - \zeta_2 & 0 \\ \tilde{\lambda}\tilde{D}e^{-\tilde{\kappa}_D\tilde{A}} & \zeta_2 - \zeta_2 \end{pmatrix} \begin{pmatrix} v_a \\ v_b \end{pmatrix} = \begin{pmatrix} 0 \\ 0 \end{pmatrix}$$
$$\begin{pmatrix} \zeta_1 - \zeta_2 & 0 \\ \tilde{\lambda}\tilde{D}e^{-\tilde{\kappa}_D\tilde{A}} & 0 \end{pmatrix} \begin{pmatrix} v_a \\ v_b \end{pmatrix} = \begin{pmatrix} 0 \\ 0 \end{pmatrix}$$

which implies,

(a) $v_a\,(\zeta_1 - \zeta_2) = 0.$

(b) $v_a\tilde{\lambda}\tilde{D}e^{-\tilde{\kappa}_D\tilde{A}} = 0.$

From this we obtain,

$$v_a = 0,$$

thus, an eigenvector corresponding to $L_2^{e_0}$ is,

$$\boldsymbol{v_2^{e_0}} = \begin{pmatrix} 0 \\ 1 \end{pmatrix}.$$

2. $\boldsymbol{e_1}$ **:**

The Jacobian matrix evaluated at e_1 is given by,

$$\boldsymbol{J}\Big|_{\left(\tilde{x}_1^{e_1}, \tilde{x}_2^{e_1}\right)} = \begin{pmatrix} \zeta_1 - \zeta_2 & 0 \\ \tilde{\lambda}\tilde{D}e^{-\tilde{\kappa}_D\tilde{A}} - \zeta_2 & -\zeta_2 \end{pmatrix},$$

which is a lower triangular matrix and thus the eigenvalues are just the diagonal entries,

$$L_1^{e_1} = \zeta_1 - \zeta_2 \quad \text{and} \quad L_2^{e_1} = -\zeta_2.$$

We can now obtain the eigenvectors by solving,

$$\left(\boldsymbol{J}\Big|_{\left(\tilde{x}_1^{e_1},\tilde{x}_2^{e_1}\right)} - L_{1,2}^{e_1}\boldsymbol{I}\right)\boldsymbol{v}_{\mathbf{1,2}}^{\boldsymbol{e_1}}.$$

1. $\boldsymbol{L_1^{e_1}}$ **:**

$$\begin{pmatrix} \zeta_1-\zeta_2-(\zeta_1-\zeta_2) & 0 \\ \tilde{\lambda}\tilde{D}e^{-\tilde{\kappa}_D\tilde{A}}-\zeta_2 & -\zeta_2-(\zeta_1-\zeta_2) \end{pmatrix}\begin{pmatrix} v_a \\ v_b \end{pmatrix} = \begin{pmatrix} 0 \\ 0 \end{pmatrix}$$
$$\begin{pmatrix} 0 & 0 \\ \tilde{\lambda}\tilde{D}e^{-\tilde{\kappa}_D\tilde{A}}-\zeta_2 & -\zeta_1 \end{pmatrix}\begin{pmatrix} v_a \\ v_b \end{pmatrix} = \begin{pmatrix} 0 \\ 0 \end{pmatrix}$$

which implies,

(a) $0 = 0$.

(b) $v_a\left(\tilde{\lambda}\tilde{D}e^{-\tilde{\kappa}_D\tilde{A}}-\zeta_2\right)-\zeta_1 v_b = 0$.

and from (b) we have that,

$$v_b = \frac{\tilde{\lambda}\tilde{D}e^{-\tilde{\kappa}_D\tilde{A}}-\zeta_2}{\zeta_1}v_a,$$

thus, an eigenvector corresponding to $L_1^{e_1}$ is,

$$\boldsymbol{v_1^{e_1}} = \begin{pmatrix} 1 \\ \frac{\tilde{\lambda}\tilde{D}e^{-\tilde{\kappa}_D\tilde{A}}-\zeta_2}{\zeta_1} \end{pmatrix}.$$

2. $\boldsymbol{L_2^{e_1}}$ **:**

$$\begin{pmatrix} \zeta_1-\zeta_2-(-\zeta_2) & 0 \\ \tilde{\lambda}\tilde{D}e^{-\tilde{\kappa}_D\tilde{A}}-\zeta_2 & -\zeta_2-(-\zeta_2) \end{pmatrix}\begin{pmatrix} v_a \\ v_b \end{pmatrix} = \begin{pmatrix} 0 \\ 0 \end{pmatrix}$$
$$\begin{pmatrix} \zeta_1 & 0 \\ \tilde{\lambda}\tilde{D}e^{-\tilde{\kappa}_D\tilde{A}}-\zeta_2 & 0 \end{pmatrix}\begin{pmatrix} v_a \\ v_b \end{pmatrix} = \begin{pmatrix} 0 \\ 0 \end{pmatrix}$$

which implies,

(a) $v_a\zeta_1 = 0$.

(b) $v_a\left(\tilde{\lambda}\tilde{D}e^{-\tilde{\kappa}_D\tilde{A}}-\zeta_2\right) = 0$.

From this we obtain,

$$v_a = 0,$$

thus, an eigenvector corresponding to $L_2^{e_1}$ is,

$$\boldsymbol{v_2^{e_1}} = \begin{pmatrix} 0 \\ 1 \end{pmatrix}.$$

3. $\boldsymbol{e_2}$ **:**

The Jacobian matrix evalueated at e_2 is given by,

$$\boldsymbol{J}\Big|_{(\tilde{x}_1^{e_2}, \tilde{x}_2^{e_2})} = \begin{pmatrix} \zeta_1 - 2\tilde{\gamma}\tilde{x}_1^{e_2} - \tilde{\gamma}\tilde{x}_2^{e_2} & -\tilde{\gamma}\tilde{x}_1^{e_2} \\ \tilde{\lambda}\tilde{D}e^{-\tilde{\kappa}_D\tilde{A}} - \tilde{\gamma}\tilde{x}_2^{e_2} & \zeta_2 - 2\tilde{\gamma}\tilde{x}_2^{e_2} - \tilde{\gamma}\tilde{x}_1^{e_2} \end{pmatrix}.$$

We can find the eigenvalues for this matrix using the formula,

$$L_{1,2}^{e_2} = \frac{1}{2}\left(Tr\left(\boldsymbol{J}\Big|_{(\tilde{x}_1^{e_2}, \tilde{x}_2^{e_2})}\right) \pm \sqrt{\left(Tr\left(\boldsymbol{J}\Big|_{(\tilde{x}_1^{e_2}, \tilde{x}_2)^{e_2}}\right)\right)^2 - 4Det\left(\boldsymbol{J}\Big|_{(\tilde{x}_1^{e_2}, \tilde{x}_2^{e_2})}\right)}\right)$$

where,

$$Tr\left(\boldsymbol{J}\Big|_{(\tilde{x}_1^{e_2}, \tilde{x}_2^{e_2})}\right) \quad \text{and} \quad Det\left(\boldsymbol{J}\Big|_{(\tilde{x}_1^{e_2}, \tilde{x}_2^{e_2})}\right),$$

are the trace and determinant of $\boldsymbol{J}\Big|_{(\tilde{x}_1^{e_2}, \tilde{x}_2^{e_2})}$ respectively.

The trace is computed by summing the diagonal entries of the matrix,

$$\begin{aligned} Tr\left(\boldsymbol{J}\Big|_{(\tilde{x}_1^{e_2}, \tilde{x}_2^{e_2})}\right) &= \zeta_1 + \zeta_2 - 2\tilde{\gamma}\left(\tilde{x}_1^{e_2} + \tilde{x}_2^{e_2}\right) - \tilde{\gamma}\left(\tilde{x}_2^{e_2} + \tilde{x}_1^{e_2}\right) \\ &= \zeta_1 + \zeta_2 - 2\zeta_1 - \zeta_1 \\ &= \zeta_2 - 2\zeta_1 \end{aligned}$$

We compute the determinant as follows,

$$
\begin{aligned}
Det\left(\boldsymbol{J}\Big|_{\left(\tilde{x}_1^{e_2},\tilde{x}_2^{e_2}\right)}\right) =& \left(\zeta_1 - 2\tilde{\gamma}\tilde{x}_1^{e_2} - \tilde{\gamma}\tilde{x}_2^{e_2}\right)\left(\zeta_2 - 2\tilde{\gamma}\tilde{x}_2^{e_2} - \tilde{\gamma}\tilde{x}_1^{e_2}\right) \\
&- \left(\tilde{\lambda}\tilde{D}e^{-\tilde{\kappa}_D\tilde{A}} - \tilde{\gamma}\tilde{x}_2^{e_2}\right)\left(-\tilde{\gamma}\tilde{x}_1^{e_2}\right) \\
=& \zeta_1\zeta_2 - 2\tilde{\gamma}\tilde{x}_2^{e_2}\zeta_1 - \tilde{\gamma}\tilde{x}_1^{e_2}\zeta_1 - 2\tilde{\gamma}\tilde{x}_1^{e_2}\zeta_2 - \tilde{\gamma}\tilde{x}_2^{e_2}\zeta_2 \\
&+ 4\tilde{\gamma}^2\tilde{x}_1^{e_2}\tilde{x}_2^{e_2} + 2\tilde{\gamma}^2\tilde{x}_1^{e_2 2} + 2\tilde{\gamma}^2\tilde{x}_2^{e_2 2} + \tilde{\gamma}^2\tilde{x}_1^{e_2}\tilde{x}_2^{e_2} \\
&+ \tilde{\gamma}\tilde{x}_1^{e_2}\tilde{\lambda}\tilde{D}e^{-\tilde{\kappa}_D\tilde{A}} - \tilde{\gamma}^2\tilde{x}_1^{e_2}\tilde{x}_2^{e_2} \\
=& \zeta_1\zeta_2 - 2\tilde{\gamma}\tilde{x}_2^{e_2}\zeta_1 - \tilde{\gamma}\tilde{x}_1^{e_2}\zeta_1 - 2\tilde{\gamma}\tilde{x}_1^{e_2}\zeta_2 - \tilde{\gamma}\tilde{x}_2^{e_2}\zeta_2 \\
&+ 2\tilde{\gamma}^2\left(\tilde{x}_1^{e_2} + \tilde{x}_2^{e_2}\right)^2 + \tilde{\gamma}\tilde{x}_1^{e_2}\tilde{\lambda}\tilde{D}e^{-\tilde{\kappa}_D\tilde{A}} \\
=& \zeta_1\zeta_2 - 2\zeta_1^2\left(\frac{\tilde{\lambda}\tilde{D}e^{-\tilde{\kappa}_D\tilde{A}}}{\zeta_1 + \tilde{\lambda}\tilde{D}e^{-\tilde{\kappa}_D\tilde{A}} - \zeta_2}\right) \\
&- \zeta_1^2\left(\frac{\zeta_1 - \zeta_2}{\zeta_1 + \tilde{\lambda}\tilde{D}e^{-\tilde{\kappa}_D\tilde{A}} - \zeta_2}\right) - 2\zeta_1\zeta_2\left(\frac{\zeta_1 - \zeta_2}{\zeta_1 + \tilde{\lambda}\tilde{D}e^{-\tilde{\kappa}_D\tilde{A}} - \zeta_2}\right) \\
&- \zeta_1\zeta_2\left(\frac{\tilde{\lambda}\tilde{D}e^{-\tilde{\kappa}_D\tilde{A}}}{\zeta_1 + \tilde{\lambda}\tilde{D}e^{-\tilde{\kappa}_D\tilde{A}} - \zeta_2}\right) + 2\zeta_1^2 \\
&+ \zeta_1\left(\frac{\zeta_1 - \zeta_2}{\zeta_1 + \tilde{\lambda}\tilde{D}e^{-\tilde{\kappa}_D\tilde{A}} - \zeta_2}\right)\tilde{\lambda}\tilde{D}e^{-\tilde{\kappa}_D\tilde{A}} \\
=& \zeta_1\zeta_2 - 2\zeta_1^2\left(\frac{\tilde{\lambda}\tilde{D}e^{-\tilde{\kappa}_D\tilde{A}}}{\zeta_1 + \tilde{\lambda}\tilde{D}e^{-\tilde{\kappa}_D\tilde{A}} - \zeta_2}\right) \\
&- \zeta_1^2\left(\frac{\zeta_1 - \zeta_2}{\zeta_1 + \tilde{\lambda}\tilde{D}e^{-\tilde{\kappa}_D\tilde{A}} - \zeta_2}\right) - 2\zeta_1\zeta_2\left(\frac{\zeta_1 - \zeta_2}{\zeta_1 + \tilde{\lambda}\tilde{D}e^{-\tilde{\kappa}_D\tilde{A}} - \zeta_2}\right) \\
&- \zeta_1\zeta_2\left(\frac{\tilde{\lambda}\tilde{D}e^{-\tilde{\kappa}_D\tilde{A}}}{\zeta_1 + \tilde{\lambda}\tilde{D}e^{-\tilde{\kappa}_D\tilde{A}} - \zeta_2}\right) + 2\zeta_1^2 \\
&+ \zeta_1^2\left(\frac{\tilde{\lambda}\tilde{D}e^{-\tilde{\kappa}_D\tilde{A}}}{\zeta_1 + \tilde{\lambda}\tilde{D}e^{-\tilde{\kappa}_D\tilde{A}} - \zeta_2}\right) - \zeta_1\zeta_2\left(\frac{\tilde{\lambda}\tilde{D}e^{-\tilde{\kappa}_D\tilde{A}}}{\zeta_1 + \tilde{\lambda}\tilde{D}e^{-\tilde{\kappa}_D\tilde{A}} - \zeta_2}\right) \\
=& \zeta_1\zeta_2 - \zeta_1^2\left(\frac{\tilde{\lambda}\tilde{D}e^{-\tilde{\kappa}_D\tilde{A}}}{\zeta_1 + \tilde{\lambda}\tilde{D}e^{-\tilde{\kappa}_D\tilde{A}} - \zeta_2}\right) \\
&- \zeta_1^2\left(\frac{\zeta_1 - \zeta_2}{\zeta_1 + \tilde{\lambda}\tilde{D}e^{-\tilde{\kappa}_D\tilde{A}} - \zeta_2}\right) - 2\zeta_1\zeta_2\left(\frac{\zeta_1 - \zeta_2}{\zeta_1 + \tilde{\lambda}\tilde{D}e^{-\tilde{\kappa}_D\tilde{A}} - \zeta_2}\right) \\
&- 2\zeta_1\zeta_2\left(\frac{\tilde{\lambda}\tilde{D}e^{-\tilde{\kappa}_D\tilde{A}}}{\zeta_1 + \tilde{\lambda}\tilde{D}e^{-\tilde{\kappa}_D\tilde{A}} - \zeta_2}\right) + 2\zeta_1^2 \\
=& \zeta_1\zeta_2 - \zeta_1^2 - 2\zeta_1\zeta_2 + 2\zeta_1^2 \\
=& \zeta_1^2 - \zeta_1\zeta_2.
\end{aligned}
$$

We can now compute the eigenvalues as follows,

$$\begin{aligned}
L_1^{e_2} =& \frac{1}{2}\left(\zeta_2 - 2\zeta_1 + \sqrt{\left(\zeta_2 - 2\zeta_1\right)^2 - 4\left(\zeta_1^2 - \zeta_1\zeta_2\right)}\right) \\
=& \frac{1}{2}\left(\zeta_2 - 2\zeta_1 + \sqrt{\zeta_2^2 - 4\zeta_1\zeta_2 + 4\zeta_1^2 - 4\zeta_1^2 + 4\zeta_1\zeta_2}\right) \\
=& \frac{1}{2}\left(\zeta_2 - 2\zeta_1 + \sqrt{\zeta_2^2}\right) \\
=& \frac{1}{2}\left(2\zeta_2 - 2\zeta_1\right) \\
=& \zeta_2 - \zeta_1 \\
L_2^{e_2} =& \frac{1}{2}\left(\zeta_2 - 2\zeta_1 - \sqrt{\zeta_2^2}\right) \\
=& \frac{1}{2}\left(-2\zeta_1\right) \\
=& -\zeta_1
\end{aligned}$$

We can now obtain the eigenvectors by solving,

$$\left(\boldsymbol{J}\Big|_{\left(\tilde{x}_1^{e_2}, \tilde{x}_2^{e_2}\right)} - L_{1,2}^{e_2}\boldsymbol{I}\right)\boldsymbol{v}_{\mathbf{1,2}}^{\boldsymbol{e_2}}.$$

1. $\boldsymbol{L_1^{e_2}}$ **:**

$$\begin{pmatrix} \zeta_1 - 2\tilde{\gamma}\tilde{x}_1^{e_2} - \tilde{\gamma}\tilde{x}_2^{e_2} - \left(\zeta_2 - \zeta_1\right) & -\tilde{\gamma}\tilde{x}_1^{e_2} \\ \tilde{\lambda}\tilde{D}e^{-\tilde{\kappa}_D\tilde{A}} - \tilde{\gamma}\tilde{x}_2^{e_2} & \zeta_2 - 2\tilde{\gamma}\tilde{x}_2^{e_2} - \tilde{\gamma}\tilde{x}_1^{e_2} - \left(\zeta_2 - \zeta_1\right) \end{pmatrix} \begin{pmatrix} v_a \\ v_b \end{pmatrix} = \begin{pmatrix} 0 \\ 0 \end{pmatrix}$$

$$\begin{pmatrix} 2\zeta_1 - \zeta_2 - 2\tilde{\gamma}\tilde{x}_1^{e_2} - \tilde{\gamma}\tilde{x}_2^{e_2} & -\tilde{\gamma}\tilde{x}_1^{e_2} \\ \tilde{\lambda}\tilde{D}e^{-\tilde{\kappa}_D\tilde{A}} - \tilde{\gamma}\tilde{x}_2^{e_2} & \zeta_1 - 2\tilde{\gamma}\tilde{x}_2^{e_2} - \tilde{\gamma}\tilde{x}_1^{e_2} \end{pmatrix} \begin{pmatrix} v_a \\ v_b \end{pmatrix} = \begin{pmatrix} 0 \\ 0 \end{pmatrix},$$

which implies,

(a)

$$v_a\left(2\zeta_1 - \zeta_2 - 2\tilde{\gamma}\tilde{x}_1^{e_2} - \tilde{\gamma}\tilde{x}_2^{e_2}\right) + v_b\left(-\tilde{\gamma}\tilde{x}_1^{e_2}\right) = 0.$$

(b)

$$v_a\left(\tilde{\lambda}\tilde{D}e^{-\tilde{\kappa}_D\tilde{A}} - \tilde{\gamma}\tilde{x}_2^{e_2}\right) + v_b\left(\zeta_1 - 2\tilde{\gamma}\tilde{x}_2^{e_2} - \tilde{\gamma}\tilde{x}_1^{e_2}\right) = 0.$$

From (a) we obtain,

$$
\begin{aligned}
0 =& v_a\left(2\zeta_1-\zeta_2-2\tilde{\gamma}\tilde{x}_1^{e_2}-\tilde{\gamma}\tilde{x}_2^{e_2}\right)+v_b\left(-\tilde{\gamma}\tilde{x}_1^{e_2}\right)\\
0 =& v_a\left(2\zeta_1-\zeta_2-2\zeta_1\left(\frac{\zeta_1-\zeta_2}{\zeta_1+\tilde{\lambda}\tilde{D}e^{-\tilde{\kappa}_D\tilde{A}}-\zeta_2}\right)-\zeta_1\left(\frac{\tilde{\lambda}\tilde{D}e^{-\tilde{\kappa}_D\tilde{A}}}{\zeta_1+\tilde{\lambda}\tilde{D}e^{-\tilde{\kappa}_D\tilde{A}}-\zeta_2}\right)\right)\\
&+v_b\left(-\zeta_1\left(\frac{\zeta_1-\zeta_2}{\zeta_1+\tilde{\lambda}\tilde{D}e^{-\tilde{\kappa}_D\tilde{A}}-\zeta_2}\right)\right)\\
v_b =& \left(\frac{2\zeta_1-\zeta_2-2\zeta_1\left(\frac{\zeta_1-\zeta_2}{\zeta_1+\tilde{\lambda}\tilde{D}e^{-\tilde{\kappa}_D\tilde{A}}-\zeta_2}\right)-\zeta_1\left(\frac{\tilde{\lambda}\tilde{D}e^{-\tilde{\kappa}_D\tilde{A}}}{\zeta_1+\tilde{\lambda}\tilde{D}e^{-\tilde{\kappa}_D\tilde{A}}-\zeta_2}\right)}{\zeta_1\left(\frac{\zeta_1-\zeta_2}{\zeta_1+\tilde{\lambda}\tilde{D}e^{-\tilde{\kappa}_D\tilde{A}}-\zeta_2}\right)}\right)v_a\\
v_b =& 2\left(\frac{\zeta_1+\tilde{\lambda}\tilde{D}e^{-\tilde{\kappa}_D\tilde{A}}-\zeta_2}{\zeta_1-\zeta_2}\right)-\frac{\zeta_2}{\zeta_1}\left(\frac{\zeta_1+\tilde{\lambda}\tilde{D}e^{-\tilde{\kappa}_D\tilde{A}}-\zeta_2}{\zeta_1-\zeta_2}\right)-2-\frac{\tilde{\lambda}\tilde{D}e^{-\tilde{\kappa}_D\tilde{A}}}{\zeta_1-\zeta_2}\\
v_b =& \left(\frac{\tilde{\lambda}\tilde{D}e^{-\tilde{\kappa}_D\tilde{A}}}{\zeta_1-\zeta_2}-\frac{\zeta_2}{\zeta_1}\left(\frac{\zeta_1+\tilde{\lambda}\tilde{D}e^{-\tilde{\kappa}_D\tilde{A}}-\zeta_2}{\zeta_1-\zeta_2}\right)\right)v_a\\
v_b =& \left(\frac{\zeta_1\tilde{\lambda}\tilde{D}e^{-\tilde{\kappa}_D\tilde{A}}-\zeta_2\zeta_1-\zeta_2\tilde{\lambda}\tilde{D}e^{-\tilde{\kappa}_D\tilde{A}}+\zeta_2^2}{\zeta_1\left(\zeta_1-\zeta_2\right)}\right)v_a\\
v_b =& \left(\frac{\tilde{\lambda}\tilde{D}e^{-\tilde{\kappa}_D\tilde{A}}\left(\zeta_1-\zeta_2\right)-\zeta_2\left(\zeta_1-\zeta_2\right)}{\zeta_1\left(\zeta_1-\zeta_2\right)}\right)v_a\\
v_b =& \left(\frac{\tilde{\lambda}\tilde{D}e^{-\tilde{\kappa}_D\tilde{A}}-\zeta_2}{\zeta_1}\right)v_a,
\end{aligned}
$$

thus, an eigenvector corresponding to $L_1^{e_2}$ is,

$$\boldsymbol{v_1^{e_2}}=\begin{pmatrix}1\\ \frac{\tilde{\lambda}\tilde{D}e^{-\tilde{\kappa}_D\tilde{A}}-\zeta_2}{\zeta_1}\end{pmatrix}.$$

2. $\boldsymbol{L_2^{e_2}}$:

$$
\begin{pmatrix}\zeta_1-2\tilde{\gamma}\tilde{x}_1^{e_2}-\tilde{\gamma}\tilde{x}_2^{e_2}-(-\zeta_1) & -\tilde{\gamma}\tilde{x}_1^{e_2}\\ \tilde{\lambda}\tilde{D}e^{-\tilde{\kappa}_D\tilde{A}}-\tilde{\gamma}\tilde{x}_2^{e_2} & \zeta_2-2\tilde{\gamma}\tilde{x}_2^{e_2}-\tilde{\gamma}\tilde{x}_1^{e_2}-(-\zeta_1)\end{pmatrix}\begin{pmatrix}v_a\\ v_b\end{pmatrix}=\begin{pmatrix}0\\0\end{pmatrix}
$$

$$
\begin{pmatrix}2\zeta_1-2\tilde{\gamma}\tilde{x}_1^{e_2}-\tilde{\gamma}\tilde{x}_2^{e_2} & -\tilde{\gamma}\tilde{x}_1^{e_2}\\ \tilde{\lambda}\tilde{D}e^{-\tilde{\kappa}_D\tilde{A}}-\tilde{\gamma}\tilde{x}_2^{e_2} & \zeta_2+\zeta_1-2\tilde{\gamma}\tilde{x}_2^{e_2}-\tilde{\gamma}\tilde{x}_1^{e_2}\end{pmatrix}\begin{pmatrix}v_a\\ v_b\end{pmatrix}=\begin{pmatrix}0\\0\end{pmatrix},
$$

which implies,

(a)

$$v_a\left(2\zeta_1-2\tilde{\gamma}\tilde{x}_1^{e_2}-\tilde{\gamma}\tilde{x}_2^{e_2}\right)+v_b\left(-\tilde{\gamma}\tilde{x}_1^{e_2}\right)=0.$$

(b)

$$v_a\left(\tilde{\lambda}\tilde{D}e^{-\tilde{\kappa}_D\tilde{A}}-\tilde{\gamma}\tilde{x}_2^{e_2}\right)+v_b\left(\zeta_2+\zeta_1-2\tilde{\gamma}\tilde{x}_2^{e_2}-\tilde{\gamma}\tilde{x}_1^{e_2}\right)=0.$$

From (a) we obtain,

$$\begin{aligned}
0=&v_a\left(2\zeta_1-2\tilde{\gamma}\tilde{x}_1^{e_2}-\tilde{\gamma}\tilde{x}_2^{e_2}\right)+v_b\left(-\tilde{\gamma}\tilde{x}_1^{e_2}\right)\\
0=&v_a\left(2\zeta_1-2\zeta_1\left(\frac{\zeta_1-\zeta_2}{\zeta_1+\tilde{\lambda}\tilde{D}e^{-\tilde{\kappa}_D\tilde{A}}-\zeta_2}\right)-\zeta_1\left(\frac{\tilde{\lambda}\tilde{D}e^{-\tilde{\kappa}_D\tilde{A}}}{\zeta_1+\tilde{\lambda}\tilde{D}e^{-\tilde{\kappa}_D\tilde{A}}-\zeta_2}\right)\right)\\
&+v_b\left(-\zeta_1\left(\frac{\zeta_1-\zeta_2}{\zeta_1+\tilde{\lambda}\tilde{D}e^{-\tilde{\kappa}_D\tilde{A}}-\zeta_2}\right)\right)\\
v_b=&\left(\frac{2\zeta_1-2\zeta_1\left(\frac{\zeta_1-\zeta_2}{\zeta_1+\tilde{\lambda}\tilde{D}e^{-\tilde{\kappa}_D\tilde{A}}-\zeta_2}\right)-\zeta_1\left(\frac{\tilde{\lambda}\tilde{D}e^{-\tilde{\kappa}_D\tilde{A}}}{\zeta_1+\tilde{\lambda}\tilde{D}e^{-\tilde{\kappa}_D\tilde{A}}-\zeta_2}\right)}{\zeta_1\left(\frac{\zeta_1-\zeta_2}{\zeta_1+\tilde{\lambda}\tilde{D}e^{-\tilde{\kappa}_D\tilde{A}}-\zeta_2}\right)}\right)v_a\\
v_b=&2\left(\frac{\zeta_1+\tilde{\lambda}\tilde{D}e^{-\tilde{\kappa}_D\tilde{A}}-\zeta_2}{\zeta_1-\zeta_2}\right)-2-\frac{\tilde{\lambda}\tilde{D}e^{-\tilde{\kappa}_D\tilde{A}}}{\zeta_1-\zeta_2}\\
v_b=&\left(\frac{\tilde{\lambda}\tilde{D}e^{-\tilde{\kappa}_D\tilde{A}}}{\zeta_1-\zeta_2}\right)v_a,
\end{aligned}$$

thus, an eigenvector corresponding to $L_2^{e_2}$ is,

$$\boldsymbol{v_2^{e_2}}=\begin{pmatrix}1\\ \frac{\tilde{\lambda}\tilde{D}e^{-\tilde{\kappa}_D\tilde{A}}}{\zeta_1-\zeta_2}\end{pmatrix}.$$

A.1.3 Proving that the lines passing through the points e_0 and e_1, e_0 and e_2, and e_1 and e_2 are invariant sets.

The system equations in terms of ζ_1 and ζ_2 are,

$$\frac{d\tilde{x}_1}{d\tilde{t}}=\zeta_1\tilde{x}_1-\tilde{\gamma}\tilde{x}_1\left[\tilde{x}_1+\tilde{x}_2\right] \tag{110}$$

$$\frac{d\tilde{x}_2}{d\tilde{t}}=\tilde{\lambda}\tilde{D}e^{-\tilde{\kappa}_D\tilde{A}}\tilde{x}_1+\zeta_2\tilde{x}_2-\tilde{\gamma}\tilde{x}_2\left[\tilde{x}_1+\tilde{x}_2\right] \tag{111}$$

The line passing through e_0 and e_1 is simply the $\tilde{x}_2$ axis of the phase space. Given any initial condition on this axis we have $\tilde{x}_1=0$ and thus,

$$\frac{d\tilde{x}_1}{d\tilde{t}}=0.$$

Therefore any trajectory that starts on the $\tilde{x}_2$ axis will remain there for all time and as such it is an invariant set.

The line passing through e_0 and e_2 is the span of the eigenvector $\boldsymbol{v_1^{e_0}}$. Let

$$\beta \boldsymbol{v_1^{e_0}} \quad \text{with} \quad \beta \in \mathbb{R}\backslash\{0\}, \tag{112}$$

be any non-zero initial condition on the line spanned by $\boldsymbol{v_1^{e_0}}$. We exclude $\beta = 0$ as this is a trivial case corresponding to an initial condition at the equilibrium point e_0, any trajectory starting here will obviously remain on the line for all time. To prove the line spanned by $\boldsymbol{v_1^{e_0}}$ is an invariant set, we will evaluate the system defined by [Eq. 110] and [Eq. 111] at the initial condition [Eq. 112], and show that the resulting flow is in the direction of $\boldsymbol{v_1^{e_0}}$.

$$\begin{aligned}
\left.\begin{pmatrix} \frac{d\tilde{x}_1}{d\tilde{t}} \\ \frac{d\tilde{x}_2}{d\tilde{t}} \end{pmatrix}\right|_{\beta \boldsymbol{v_1^{e_0}}} &= \begin{pmatrix} \zeta_1\beta - \tilde{\gamma}\beta\left[\beta + \frac{\beta\tilde{\lambda}\tilde{D}e^{-\tilde{\kappa}_D\tilde{A}}}{\zeta_1-\zeta_2}\right] \\ \beta\tilde{\lambda}\tilde{D}e^{-\tilde{\kappa}_D\tilde{A}} + \zeta_2\left(\frac{\beta\tilde{\lambda}\tilde{D}e^{-\tilde{\kappa}_D\tilde{A}}}{\zeta_1-\zeta_2}\right) - \tilde{\gamma}\left(\frac{\beta\tilde{\lambda}\tilde{D}e^{-\tilde{\kappa}_D\tilde{A}}}{\zeta_1-\zeta_2}\right)\left[\beta + \frac{\beta\tilde{\lambda}\tilde{D}e^{-\tilde{\kappa}_D\tilde{A}}}{\zeta_1-\zeta_2}\right] \end{pmatrix} \\
&= \begin{pmatrix} \zeta_1\beta - \tilde{\gamma}\beta^2\left[\frac{\zeta_1+\beta\tilde{\lambda}\tilde{D}e^{-\tilde{\kappa}_D\tilde{A}}-\zeta_2}{\zeta_1-\zeta_2}\right] \\ \frac{\tilde{\lambda}\tilde{D}e^{-\tilde{\kappa}_D\tilde{A}}}{\zeta_1-\zeta_2}\left(\beta\left(\zeta_1-\zeta_2\right) + \zeta_2\beta - \tilde{\gamma}\beta^2\left[\frac{\zeta_1+\beta\tilde{\lambda}\tilde{D}e^{-\tilde{\kappa}_D\tilde{A}}-\zeta_2}{\zeta_1-\zeta_2}\right]\right) \end{pmatrix} \\
&= \left(\zeta_1\beta - \tilde{\gamma}\beta^2\left[\frac{\zeta_1 + \beta\tilde{\lambda}\tilde{D}e^{-\tilde{\kappa}_D\tilde{A}} - \zeta_2}{\zeta_1 - \zeta_2}\right]\right)\begin{pmatrix} 1 \\ \frac{\tilde{\lambda}\tilde{D}e^{-\tilde{\kappa}_D\tilde{A}}}{\zeta_1-\zeta_2} \end{pmatrix} \\
&= \left(\zeta_1\beta - \tilde{\gamma}\beta^2\left[\frac{\zeta_1 + \beta\tilde{\lambda}\tilde{D}e^{-\tilde{\kappa}_D\tilde{A}} - \zeta_2}{\zeta_1 - \zeta_2}\right]\right)\boldsymbol{v_1^{e_0}}.
\end{aligned}$$

This shows that the flow at any point on the line spanned by $\boldsymbol{v_1^{e_0}}$ is in the direction of $\boldsymbol{v_1^{e_0}}$ and thus any trajectory whose initial condition is on this line, remains on it for all time. Therefore it is an invariant set.

We will use the same approach to show that the line passing through e_1 and e_2 is an invariant set. Any initial condition on this line can be described by,

$$\begin{pmatrix} 0 \\ \frac{\zeta_2}{\tilde{\gamma}} \end{pmatrix} + \beta \boldsymbol{v_1^{e_0}} \quad \text{with} \quad \beta \in \mathbb{R}\backslash\{0\}. \tag{113}$$

We again exclude the case $\beta = 0$ as it is the trivial case of an initial condition at the equilibrium point e_1. Evaluating [Eq. 110] and [Eq. 111] at the initial

condition [Eq. 113], we obtain,

$$
\begin{aligned}
\left(\begin{array}{c}\frac{d\tilde{x}_1}{d\tilde{t}}\\ \frac{d\tilde{x}_2}{d\tilde{t}}\end{array}\right)\Bigg|_{\beta \boldsymbol{v_1^{e_0}}} &= \begin{pmatrix} \zeta_1\beta - \tilde{\gamma}\beta\left[\beta + \frac{\zeta_2}{\tilde{\gamma}} + \beta\left(\frac{\tilde{\lambda}\tilde{D}e^{-\tilde{\kappa}_D\tilde{A}}-\zeta_2}{\zeta_1}\right)\right] \\ \tilde{\lambda}\tilde{D}e^{-\tilde{\kappa}_D\tilde{A}}\beta + \zeta_2\left(\frac{\zeta_2}{\tilde{\gamma}} + \beta\left(\frac{\tilde{\lambda}\tilde{D}e^{-\tilde{\kappa}_D\tilde{A}}-\zeta_2}{\zeta_1}\right)\right) \\ -\tilde{\gamma}\left(\frac{\zeta_2}{\tilde{\gamma}} + \beta\left(\frac{\tilde{\lambda}\tilde{D}e^{-\tilde{\kappa}_D\tilde{A}}-\zeta_2}{\zeta_1}\right)\right)\left[\beta + \frac{\zeta_2}{\tilde{\gamma}} + \beta\left(\frac{\tilde{\lambda}\tilde{D}e^{-\tilde{\kappa}_D\tilde{A}}-\zeta_2}{\zeta_1}\right)\right] \end{pmatrix} \\
&= \begin{pmatrix} \beta\left(\zeta_1-\zeta_2\right) - \tilde{\gamma}\beta\left[\frac{\beta}{\zeta_1}\left(\zeta_1 + \tilde{\lambda}\tilde{D}e^{-\tilde{\kappa}_D\tilde{A}} - \zeta_2\right)\right] \\ \tilde{\lambda}\tilde{D}e^{-\tilde{\kappa}_D\tilde{A}}\beta \\ -\tilde{\gamma}\left(\frac{\zeta_2}{\tilde{\gamma}} + \beta\left(\frac{\tilde{\lambda}\tilde{D}e^{-\tilde{\kappa}_D\tilde{A}}-\zeta_2}{\zeta_1}\right)\right)\left[\frac{\beta}{\zeta_1}\left(\zeta_1 + \tilde{\lambda}\tilde{D}e^{-\tilde{\kappa}_D\tilde{A}} - \zeta_2\right)\right] \end{pmatrix} \\
&= \begin{pmatrix} \beta\left(\zeta_1-\zeta_2\right) - \tilde{\gamma}\beta\left[\frac{\beta}{\zeta_1}\left(\zeta_1 + \tilde{\lambda}\tilde{D}e^{-\tilde{\kappa}_D\tilde{A}} - \zeta_2\right)\right] \\ \tilde{\lambda}\tilde{D}e^{-\tilde{\kappa}_D\tilde{A}}\beta - \zeta_2\left[\frac{\beta}{\zeta_1}\left(\zeta_1 + \tilde{\lambda}\tilde{D}e^{-\tilde{\kappa}_D\tilde{A}} - \zeta_2\right)\right] \\ -\tilde{\gamma}\beta\left(\frac{\tilde{\lambda}\tilde{D}e^{-\tilde{\kappa}_D\tilde{A}}-\zeta_2}{\zeta_1}\right)\left[\frac{\beta}{\zeta_1}\left(\zeta_1 + \tilde{\lambda}\tilde{D}e^{-\tilde{\kappa}_D\tilde{A}} - \zeta_2\right)\right] \end{pmatrix} \\
&= \begin{pmatrix} \beta\left(\zeta_1-\zeta_2\right) - \tilde{\gamma}\beta\left[\frac{\beta}{\zeta_1}\left(\zeta_1 + \tilde{\lambda}\tilde{D}e^{-\tilde{\kappa}_D\tilde{A}} - \zeta_2\right)\right] \\ \frac{\beta}{\zeta_1}\left(\tilde{\lambda}\tilde{D}e^{-\tilde{\kappa}_D\tilde{A}}\zeta_1 - \zeta_2\zeta_1 - \zeta_2\tilde{\lambda}\tilde{D}e^{-\tilde{\kappa}_D\tilde{A}} + \zeta_2^2\right) \\ -\tilde{\gamma}\beta\left(\frac{\tilde{\lambda}\tilde{D}e^{-\tilde{\kappa}_D\tilde{A}}-\zeta_2}{\zeta_1}\right)\left[\frac{\beta}{\zeta_1}\left(\zeta_1 + \tilde{\lambda}\tilde{D}e^{-\tilde{\kappa}_D\tilde{A}} - \zeta_2\right)\right] \end{pmatrix} \\
&= \begin{pmatrix} \beta\left(\zeta_1-\zeta_2\right) - \tilde{\gamma}\beta\left[\frac{\beta}{\zeta_1}\left(\zeta_1 + \tilde{\lambda}\tilde{D}e^{-\tilde{\kappa}_D\tilde{A}} - \zeta_2\right)\right] \\ \frac{\beta}{\zeta_1}\left(\tilde{\lambda}\tilde{D}e^{-\tilde{\kappa}_D\tilde{A}}\left(\zeta_1-\zeta_2\right) - \zeta_2\left(\zeta_1-\zeta_2\right)\right) \\ -\tilde{\gamma}\beta\left(\frac{\tilde{\lambda}\tilde{D}e^{-\tilde{\kappa}_D\tilde{A}}-\zeta_2}{\zeta_1}\right)\left[\frac{\beta}{\zeta_1}\left(\zeta_1 + \tilde{\lambda}\tilde{D}e^{-\tilde{\kappa}_D\tilde{A}} - \zeta_2\right)\right] \end{pmatrix} \\
&= \begin{pmatrix} \beta\left(\zeta_1-\zeta_2\right) - \tilde{\gamma}\beta\left[\frac{\beta}{\zeta_1}\left(\zeta_1 + \tilde{\lambda}\tilde{D}e^{-\tilde{\kappa}_D\tilde{A}} - \zeta_2\right)\right] \\ \beta\left(\zeta_1-\zeta_2\right)\left(\frac{\tilde{\lambda}\tilde{D}e^{-\tilde{\kappa}_D\tilde{A}}-\zeta_2}{\zeta_1}\right) \\ -\tilde{\gamma}\beta\left(\frac{\tilde{\lambda}\tilde{D}e^{-\tilde{\kappa}_D\tilde{A}}-\zeta_2}{\zeta_1}\right)\left[\frac{\beta}{\zeta_1}\left(\zeta_1 + \tilde{\lambda}\tilde{D}e^{-\tilde{\kappa}_D\tilde{A}} - \zeta_2\right)\right] \end{pmatrix} \\
&= \left(\beta\left(\zeta_1-\zeta_2\right) - \tilde{\gamma}\beta\left[\frac{\beta}{\zeta_1}\left(\zeta_1 + \tilde{\lambda}\tilde{D}e^{-\tilde{\kappa}_D\tilde{A}} - \zeta_2\right)\right]\right)\begin{pmatrix} 1 \\ \left(\frac{\tilde{\lambda}\tilde{D}e^{-\tilde{\kappa}_D\tilde{A}}-\zeta_2}{\zeta_1}\right)\end{pmatrix} \\
&= \left(\beta\left(\zeta_1-\zeta_2\right) - \tilde{\gamma}\beta\left[\frac{\beta}{\zeta_1}\left(\zeta_1 + \tilde{\lambda}\tilde{D}e^{-\tilde{\kappa}_D\tilde{A}} - \zeta_2\right)\right]\right)\boldsymbol{v_1^{e_1}}.
\end{aligned}
$$

Thus, we have shown that the flow at any arbitrary point on the line passing through e_1 and e_2, is along the line and hence any trajectory whose initial condition is on this line, remains on it for all time. Therefore it is also an invariant set.

A.2 Showing Conditions (1) and (2) Both Hold if $\frac{a_3}{e^{a_3}-1} < \frac{\delta_3}{\nu_3} < 1$.

Condition (1) holds if,

$$\begin{aligned}\frac{\nu_3}{2}\phi_3(1) &> \frac{\delta_3}{2}\\ \nu_3 &> \delta_3\\ \frac{\delta_3}{\nu_3} &< 1\end{aligned}$$

$\tilde{D}_{r3}$ is defined implicitly by,

$$\begin{aligned}\frac{\nu_3}{2}\phi_3(\tilde{D}_{r3}) - \frac{\delta_3}{2}\tilde{D}_{r3} &= 0\\ \frac{e^{a_3\tilde{D}_{r3}}-1}{e^{a_3}-1} - \frac{\delta_3}{\nu_3}\tilde{D}_{r3} &= 0\end{aligned}$$

Then, assuming (1) holds, we must derive a condition to ensure (2) also holds, i.e. that there exists $\tilde{D}_{r3} \in (0,1)$ such that $\frac{d\tilde{x}_3}{dt}\big|_{\tilde{x}_3=\frac{1}{2}} = 0$ if $\tilde{D} = \tilde{D}_{r3}$. Since both $\nu_3\phi_3(\tilde{D})$ and $\delta_3\tilde{D}$ are continuous, monotonically increasing functions of $\tilde{D}$, then there exists such a $\tilde{D}_{r3} \in (0,1)$ if,

$$\begin{aligned}\frac{d}{d\tilde{D}}\left(\frac{\nu_3}{2}\phi_3(\tilde{D})\right)\Big|_{\tilde{D}=0} &< \frac{d}{d\tilde{D}}\left(\frac{\delta_3}{2}\tilde{D}\right)\Big|_{\tilde{D}=0}\\ \left(\frac{\nu_3}{2}\frac{a_3 e^{a_3\tilde{D}}}{e^{a_3}-1}\right)\Big|_{\tilde{D}=0} &< \left(\frac{\delta_3}{2}\right)\Big|_{\tilde{D}=0}\\ \frac{\nu_3}{2}\frac{a_3}{e^{a_3}-1} &< \frac{\delta_3}{2}\\ \frac{a_3}{e^{a_3}-1} &< \frac{\delta_3}{\nu_3} < 1.\end{aligned}$$

A.3 Showing $\tilde{x}_3^e$ is non-decreasing when $\tilde{C} = 0$ or $\tilde{D} = 0$.

Here we show that [Eq. 49] and [Eq. 48] are both non-decresearing functions of $\tilde{D}$ and $\tilde{C}$ respectively.

(1) $\tilde{x}_3^e|_{\tilde{D}=0}$:

$$\frac{d\tilde{x}_3^e|_{D=0}}{d\tilde{C}} = \frac{\tilde{\rho}_{3C}\left(\tilde{\rho}_{3C}\tilde{C}+\tilde{\epsilon}\right) - \tilde{\rho}_{3C}\tilde{C}\left(\tilde{\rho}_{3C}\right)}{\left(\tilde{\rho}_{3C}\tilde{C}+\tilde{\epsilon}\right)^2}$$
$$= \frac{\tilde{\epsilon}}{\left(\tilde{\rho}_{3C}\tilde{C}+\tilde{\epsilon}\right)^2}$$

And since $\tilde{\epsilon} > 0$,

$$\frac{d\tilde{x}_3^e|_{\tilde{D}=0}}{d\tilde{C}} \geq 0$$

for all $\tilde{C} \geq 0$.

(2) $\tilde{x}_3^e|_{\tilde{C}=0}$:

$$\frac{d\tilde{x}_3^e|_{\tilde{C}=0}}{d\tilde{D}} = \frac{\tilde{\nu}_3\left(\frac{a_3 e^{a_3\tilde{D}}}{e^{a_3}-1}\right)\left(\tilde{\delta}_3\tilde{D}+\tilde{\epsilon}\right) - \tilde{\nu}_3\tilde{\delta}_3\left(\frac{e^{a_3\tilde{D}}-1}{e^{a_3}-1}\right)}{\left(\tilde{\nu}_3\left(\frac{e^{a_3\tilde{D}}-1}{e^{a_3}-1}\right)+\tilde{\delta}_3\tilde{D}+\tilde{\epsilon}\right)^2}$$

Then,

$$\frac{d\tilde{x}_3^e|_{\tilde{C}=0}}{d\tilde{D}} \geq 0$$

if,

$$\tilde{\delta}_3\left(e^{a_3\tilde{D}}-1\right) \leq \left(a_3 e^{a_3\tilde{D}}\right)\left(\tilde{\delta}_3\tilde{D}+\tilde{\epsilon}\right)$$
$$1 \geq e^{a_3\tilde{D}}\left(\left(1-\frac{a_3\tilde{\epsilon}}{\tilde{\delta}_3}\right)-a_3\tilde{D}\right)$$

Consider the coefficient of $e^{a_3\tilde{D}}$ above,

$$\left(\left(1-\frac{a_3\tilde{\epsilon}}{\tilde{\delta}_3}\right)-a_3\tilde{D}\right), \tag{114}$$

this is a linear function of $\tilde{D}$ with negative slope. The value of [Eq. 114] when $\tilde{D}=0$ is $(1-\frac{a_3\tilde{\epsilon}}{\tilde{\delta}_3})$ and we have that $(1-\frac{a_3\tilde{\epsilon}}{\tilde{\delta}_3}) < 1$, since all of the parameters are

positive. Therefore we have that,

$$e^{a_3\tilde{D}}\left(\left(1-\frac{a_3\tilde{\epsilon}}{\tilde{\delta}_3}\right)-a_3\tilde{D}\right)<e^{a_3\tilde{D}}\left(1-a_3\tilde{D}\right).$$

Hence it would be sufficient to show,

$$e^{a_3\tilde{D}}\left(1-a_3\tilde{D}\right)\leq 1 \tag{115}$$

for any $\tilde{D}\in[0,1]$ and $a_3>0$. To do this we will show that the maximum of [Eq. 115] occurs at $\tilde{D}=0$ and is equal to one.

$$\begin{aligned}
0&=\frac{d}{d\tilde{D}}\left(e^{a_3\tilde{D}}\left(1-a_3\tilde{D}\right)\right)\\
0&=-a_3e^{a_3\tilde{D}}+a_3e^{a_3\tilde{D}}\left(1-a_3\tilde{D}\right)\\
0&=-a_3\tilde{D}\\
\tilde{D}&=0,
\end{aligned}$$

Then evaluating [Eq. 115] at $\tilde{D}=0$ we have $e^0(1)=1$. We can be sure this is the maximum point of the function using the second derivative test,

$$\begin{aligned}
\frac{d^2}{d\tilde{D}^2}\left(e^{a_3\tilde{D}}\left(1-a_3\tilde{D}\right)\right)|_{\tilde{D}=0}&=\left(-a_3^2e^{a_3\tilde{D}}-a_3^2e^{a_3\tilde{D}}+a_3^2e^{a_3\tilde{D}}\left(1-a_3\tilde{D}\right)\right)|_{\tilde{D}=0}\\
&=-a_3^2<0
\end{aligned}$$

A.4 Solving for $\tilde{D}_{\mathbf{opt,5}}$.

Here we calculate the the expression for b in terms of $\tilde{D}_{\text{opt},5}$ [Eq. 54].

$$\begin{aligned}
\phi_{51}(\tilde{D}(t))&=\frac{e^{a_{51}b}+e^{-\eta a_{51}b}}{e^{-a_{51}(\tilde{D}(t)-b)}+e^{\eta a_{51}(\tilde{D}(t)-b)}}\\
\frac{d\phi_{51}}{d\tilde{D}(t)}&=\frac{-\left(e^{a_{51}b}+e^{-\eta a_{51}b}\right)\left(-a_{51}e^{-a_{51}(\tilde{D}(t)-b)}+\eta a_{51}e^{\eta a_{51}(\tilde{D}(t)-b)}\right)}{\left(e^{-a_{51}(\tilde{D}(t)-b)}+e^{\eta a_{51}(\tilde{D}(t)-b)}\right)^2}
\end{aligned}$$

Setting $\frac{d\phi_{51}}{d\tilde{D}(t)}=0$, we can solve for $\tilde{D}_{\text{opt},5}$ as follows,

$$
\begin{aligned}
0 &= \frac{-\left(e^{a_{51}b} + e^{-\eta a_{51}b}\right)\left(-a_{51}e^{-a_{51}(\tilde{D}(t)-b)} + \eta a_{51}e^{\eta a_{51}(\tilde{D}(t)-b)}\right)}{\left(e^{-a_{51}(\tilde{D}(t)-b)} + e^{\eta a_{51}(\tilde{D}(t)-b)}\right)^2} \\
0 &= -a_{51}e^{-a_{51}(\tilde{D}(t)-b)} + \eta a_{51}e^{\eta a_{51}(\tilde{D}(t)-b)} \\
\eta &= e^{\eta a_{51}(\tilde{D}(t)-b)+a_{51}(\tilde{D}(t)-b)} \\
\ln(\eta) &= (a_{51} + \eta a_{51})(\tilde{D}(t) - b) \\
\tilde{D}(t) &= \tilde{D}_{\text{opt},5} = b + \frac{\ln(\eta)}{a_{51} + \eta a_{51}}
\end{aligned}
$$

A.5 Reparameterising the Immune Response to Cancer.

Here we derive the forward [Eq. 60] and backward [Eq. 61] transformations that define the reparameterisation of the immune response to cancer.

Given [Eq. 59] as,

$$\rho_{5C}\left(\frac{C(t)}{a_{52} + C(t)}\right) - \sigma_{5C}C(t),$$

we can solve for the non-zero $C(t)$ such that [Eq. 59] is zero. We denote this value of $C(t)$ by C_r.

$$
\begin{aligned}
0 &= \rho_{5C}\left(\frac{C(t)}{a_{52} + C(t)}\right) - \sigma_{5C}C(t) \\
\sigma_{5C} &= \rho_{5C}\left(\frac{1}{a_{52} + C(t)}\right) \\
C(t) = C_r &= \frac{\rho_{5C}}{\sigma_{5C}} - a_{52}.
\end{aligned}
$$

To ensure $C_r > 0$ we enforce,

$$\frac{\rho_{5C}}{\sigma_{5C}} > a_{52}.$$

Next, we can solve for the non-zero $C(t)$ such that,

$$\frac{d}{dC(t)}\left(\rho_{5C}\left(\frac{C(t)}{a_{52} + C(t)}\right) - \sigma_{5C}C(t)\right) = 0.$$

We denote this value of $C(t)$ by C_{opt}.

$$\begin{aligned}
0 &= \frac{d}{dC(t)}\left(\rho_{5C}\frac{C(t)}{a_{52}+C(t)} - \sigma_{5C}C(t)\right) \\
\frac{\sigma_{5C}}{\rho_{5C}} &= \frac{a_{52}}{(a_{52}+C(t))^2} \\
(a_{52}+C(t))^2 &= \frac{\rho_{5C}a_{52}}{\sigma_{5C}} \\
C(t) &= -a_{52} \pm \sqrt{\frac{\rho_{5C}a_{52}}{\sigma_{5C}}} \\
&C(t) > 0 \text{ implies,} \\
C(t) &= C_{\text{opt}} = -a_{52} + \sqrt{\frac{\rho_{5C}a_{52}}{\sigma_{5C}}} \quad \text{with} \quad \frac{\rho_{5C}}{\sigma_{5C}} > a_{52}.
\end{aligned}$$

We denote by M the maximum value of [Eq. 59] with respect to $C(t)$, i.e.

$$\begin{aligned}
M &= \left(\rho_{5C}\left(\frac{C(t)}{a_{52}+C(t)}\right) - \sigma_{5C}C(t)\right)\Bigg|_{C(t)=C_{\text{opt}}} \\
&= \rho_{5C}\left(\frac{-a_{52}+\sqrt{\frac{\rho_{5C}a_{52}}{\sigma_{5C}}}}{a_{52}+\left(-a_{52}+\sqrt{\frac{\rho_{5C}a_{52}}{\sigma_{5C}}}\right)}\right) - \sigma_{5C}\left(-a_{52}+\sqrt{\frac{\rho_{5C}a_{52}}{\sigma_{5C}}}\right) \\
&= \frac{-\rho_{5C}a_{52}+\rho_{5C}\sqrt{\frac{\rho_{5C}a_{52}}{\sigma_{5C}}}+\sigma_{5C}a_{52}\sqrt{\frac{\rho_{5C}a_{52}}{\sigma_{5C}}}-\rho_{5C}a_{52}}{\sqrt{\frac{\rho_{5C}a_{52}}{\sigma_{5C}}}} \\
&= \rho_{5C} - \frac{2\rho_{5C}a_{52}}{\sqrt{\frac{\rho_{5C}a_{52}}{\sigma_{5C}}}} + \sigma_{5C}a_{52} \\
&= \rho_{5C} - 2\sqrt{\rho_{5C}\sigma_{5C}a_{52}} + \sigma_{5C}a_{52} \\
&= \left(\sqrt{\rho_{5C}} - \sqrt{\sigma_{5C}a_{52}}\right)^2 \quad \text{with} \quad \frac{\rho_{5C}}{\sigma_{5C}} > a_{52}.
\end{aligned}$$

In order to ensure $C_r, C_{\text{opt}}, M > 0$, we have the condition,

$$\frac{\rho_{5C}}{\sigma_{5C}} > a_{52}. \tag{116}$$

We can reparameterise [Eq. 59] in terms of C_r, C_{opt} and M as follows. We have that,

$$C_r = \frac{\rho_{5C}}{\sigma_{5C}} - a_{52}.$$

This implies,

$$\sigma_{5C} = \frac{\rho_{5C}}{C_r + a_{52}}. \tag{117}$$

We also have that,

$$C_{\text{opt}} = -a_{52} + \sqrt{\frac{\rho_{5C} a_{52}}{\sigma_{5C}}}.$$

We can rewrite C_{opt} in terms of C_r by replacing σ_{5C} using [Eq. 117] as follows,

$$C_{\text{opt}} = -a_{52} + \sqrt{a_{52}(C_r + a_{52})}.$$

Solving for a_{52} from this expression gives,

$$\begin{aligned} C_{\text{opt}}^2 + 2C_{\text{opt}} a_{52} + a_{52}^2 &= a_{52} C_r + a_{52}^2 \\ a_{52}(C_r - 2C_{\text{opt}}) &= C_{\text{opt}}^2 \\ a_{52} &= \frac{C_{\text{opt}}^2}{C_r - 2C_{\text{opt}}} \end{aligned} \tag{118}$$

Since $a_{52} > 0$, we must have $C_{\text{opt}} < \frac{C_r}{2}$.

We can now rewrite [Eq. 59] as,

$$\begin{aligned} &\rho_{5C} \frac{C(t)}{a_{52} + C(t)} - \sigma_{5C} C(t) \\ =&\rho_{5C} \left(\frac{C(t)}{a_{52} + C(t)} - \frac{C(t)}{C_r + a_{52}} \right) \\ =&\rho_{5C} C(t) \left(\frac{C_r - C(t)}{(a_{52} + C(t))(C_r + a_{52})} \right). \end{aligned} \tag{119}$$

For now we keep this expression in terms of a_{52} for the sake of simplicity.

We wish to write this expression in terms of its maximum value, M, thus we normalise by dividing [Eq. 119] by it's value at C_{opt}, which obtains,

$$\frac{C(t)}{C_{\text{opt}}} \left(\frac{(C_r - C(t))(a_{52} + C_{\text{opt}})}{(C_r - C_{\text{opt}})(a_{52} + C(t))} \right).$$

We then rescale by $M > 0$ which sucessfully expresses [Eq. 119] in terms of its maximum value.

$$M \frac{C(t)}{C_{\text{opt}}} \left(\frac{(C_r - C(t))(a_{52} + C_{\text{opt}})}{(C_r - C_{\text{opt}})(a_{52} + C(t))} \right). \tag{120}$$

This allows us to obtain an expression for ρ_{5C} by equating [Eq. 119] with [Eq. 120],

$$\rho_{5C} = \frac{M}{C_{\text{opt}}} \left(\frac{(a_{52} + C_{\text{opt}})(C_r + a_{52})}{C_r - C_{\text{opt}}} \right).$$

Now, using [Eq. 118] to replace a_{52}, we obtain,

$$\rho_{5C} = \frac{M}{C_{\text{opt}}} \left(\frac{\left(\frac{C_{\text{opt}}^2}{C_r - 2C_{\text{opt}}} + C_{\text{opt}} \right) \left(C_r + \frac{C_{\text{opt}}^2}{C_r - 2C_{\text{opt}}} \right)}{C_r - C_{\text{opt}}} \right)$$

$$\rho_{5C} = \frac{M}{C_{\text{opt}}} \left(\frac{\left(\frac{C_{\text{opt}}^2 + C_r C_{\text{opt}} - 2C_{opt}^2}{C_r - 2C_{\text{opt}}} \right) \left(\frac{C_r^2 - 2C_{\text{opt}} C_r + C_{\text{opt}}^2}{C_r - 2C_{\text{opt}}} \right)}{C_r - C_{\text{opt}}} \right)$$

$$\rho_{5C} = M \left(\frac{\left(\frac{C_r - C_{opt}}{C_r - 2C_{\text{opt}}} \right) \left(\frac{(C_r - C_{\text{opt}})^2}{C_r - 2C_{\text{opt}}} \right)}{C_r - C_{\text{opt}}} \right)$$

$$\rho_{5C} = M \left(\frac{C_r - C_{\text{opt}}}{C_r - 2C_{\text{opt}}} \right)^2. \tag{121}$$

Finally, replacing ρ_{5C} and a_{52} in [Eq. 117], using [Eq. 121] and [Eq. 118] respectively, we obtain,

$$\sigma_{5C} = M \left(\frac{\left(\frac{C_r - C_{\text{opt}}}{C_r - 2C_{\text{opt}}} \right)^2}{C_r + \frac{C_{\text{opt}}^2}{C_r - 2C_{\text{opt}}}} \right)$$

$$\sigma_{5C} = \frac{M}{C_r - 2C_{\text{opt}}}. \tag{122}$$

Under the change of parameters defined by [Eq. 118], [Eq. 121] and [Eq. 122], condition [Eq. 116] becomes,

$$\begin{aligned} \frac{(C_r - C_{\text{opt}})^2}{C_r - 2C_{\text{opt}}} &> \frac{C_{\text{opt}}^2}{C_r - 2C_{\text{opt}}} \\ (C_r - C_{\text{opt}})^2 - C_{\text{opt}}^2 &> 0 \\ C_r(C_r - 2C_{\text{opt}}) &> 0 \\ \text{since } C_r &> 0, \\ C_r - 2C_{\text{opt}} &> 0 \\ \frac{C_r}{2} &> C_{\text{opt}}. \end{aligned}$$

Using [Eq. 118], [Eq. 121] and [Eq. 122], we can rewrite [Eq. 59] as follows,

$$
\begin{aligned}
&\rho_{5C}\left(\frac{C(t)}{a+C(t)}-\sigma_{5C}C(t)\right)\\
=&C(t)\left(M\left(\frac{C_r-C_{\text{opt}}}{C_r-2C_{\text{opt}}}\right)^2\left(\frac{1}{\frac{C_{\text{opt}}^2}{C_r-2C_{\text{opt}}}+C(t)}\right)-\frac{M}{C_r-2C_{\text{opt}}}\right)\\
=&MC(t)\left(\left(\frac{C_r-C_{\text{opt}}}{C_r-2C_{\text{opt}}}\right)^2\left(\frac{C_r-2C_{\text{opt}}}{C_{\text{opt}}^2+C(t)\left(C_r-2C_{\text{opt}}\right)}\right)-\frac{1}{C_r-2C_{\text{opt}}}\right)\\
=&\frac{MC(t)}{C_r-2C_{\text{opt}}}\left(\frac{\left(C_r-C_{\text{opt}}\right)^2}{C_{\text{opt}}^2+C(t)\left(C_r-2C_{\text{opt}}\right)}-1\right)\\
=&\frac{MC(t)}{C_r-2C_{\text{opt}}}\left(\frac{\left(C_r-C(t)\right)\left(C_r-2C_{\text{opt}}\right)}{C_{\text{opt}}^2+C(t)\left(C_r-2C_{\text{opt}}\right)}\right)\\
=&MC(t)\left(\frac{C_r-C(t)}{C_{\text{opt}}^2+C(t)\left(C_r-2C_{\text{opt}}\right)}\right)
\end{aligned}
$$

A.6 Solving for the Condition that $\tilde{d} > \tilde{M}$ for the Existence of $\tilde{x}_5^e$.

Here we derive the condition $\tilde{d} > \tilde{M}$ [Eq. 71], which ensures that $\tilde{x}_5^e$ is positive and stable.

$\tilde{x}_5^e$ becomes undefined if the denominator of [Eq. 69] is equal to zero. Thus, we seek to identify ranges of parameter values such that there exist $\tilde{C} > 0$ for which this denominator becomes equal to zero.

$$
\begin{aligned}
\tilde{d}-\tilde{\rho}_{5C}\frac{\tilde{C}}{\tilde{a}_{52}+\tilde{C}}+\tilde{\sigma}_{5C}\tilde{C}&=0\\
\tilde{d}(\tilde{a}_{52}+\tilde{C})-\tilde{\rho}_{5C}\tilde{C}+\tilde{\sigma}_{5C}\tilde{C}(\tilde{a}_{52}+\tilde{C})&=0\\
\tilde{\sigma}_{5C}\tilde{C}^2+\left(\tilde{d}-\tilde{\rho}_{5C}+\tilde{\sigma}_{5C}\tilde{a}_{52}\right)\tilde{C}+\tilde{d}\tilde{a}_{52}&=0\\
\tilde{C}^2+\left(\frac{\tilde{d}-\tilde{\rho}_{5C}+\tilde{\sigma}_{5C}\tilde{a}_{52}}{\tilde{\sigma}_{5C}}\right)\tilde{C}+\frac{\tilde{d}\tilde{a}_{52}}{\tilde{\sigma}_{5C}}&=0
\end{aligned}
$$

Hence $\tilde{x}_5^e$ is undefined if,

$$
\tilde{C}_{1,2}=\frac{-\left(\frac{\tilde{d}-(\tilde{\rho}_{5C}-\tilde{\sigma}_{5C}\tilde{a}_{52})}{\tilde{\sigma}_{5C}}\right)\pm\sqrt{\left(\frac{\tilde{d}-(\tilde{\rho}_{5C}-\tilde{\sigma}_{5C}\tilde{a}_{52})}{\tilde{\sigma}_{5C}}\right)^2-\frac{4\tilde{d}\tilde{a}_{52}}{\tilde{\sigma}_{5C}}}}{2}
$$

Since we will only model physical solutions for the cancer equations, these values of $\tilde{C}$ are only problematic if they are both real and positive. Thus, we will now

identify the parameter value ranges for which these solutions, $\tilde{C}_{1,2}$, either do not exist (complex valued) or are nonphysical (negative).

$\tilde{C}_{1,2}$ do not exist if,

$$\left(\frac{\tilde{d}-(\tilde{\rho}_{5C}-\tilde{\sigma}_{5C}\tilde{a}_{52})}{\tilde{\sigma}_{5C}}\right)^2-\frac{4\tilde{d}\tilde{a}_{52}}{\tilde{\sigma}_{5C}}<0$$
$$\frac{\tilde{d}^2-2\tilde{d}\,(\tilde{\rho}_{5C}-\tilde{\sigma}_{5C}\tilde{a}_{52})+(\tilde{\rho}_{5C}-\tilde{\sigma}_{5C}\tilde{a}_{52})^2-4\tilde{d}\sigma_{5C}\tilde{a}_{52}}{\tilde{\sigma}_{5C}^2}<0$$
$$\tilde{d}^2-2\tilde{d}\,(\tilde{\rho}_{5C}+\tilde{\sigma}_{5C}\tilde{a}_{52})+(\tilde{\rho}_{5C}-\tilde{\sigma}_{5C}\tilde{a}_{52})^2<0$$

that is for,

$$\begin{aligned}\tilde{\rho}_{5C}+\tilde{\sigma}_{5C}\tilde{a}_{52}-2\sqrt{\tilde{\rho}_{5C}\tilde{\sigma}_{5C}\tilde{a}_{52}}<&\tilde{d}<\tilde{\rho}_{5C}+\tilde{\sigma}_{5C}\tilde{a}_{52}+2\sqrt{\tilde{\rho}_{5C}\tilde{\sigma}_{5C}\tilde{a}_{52}}\\ \left(\sqrt{\tilde{\rho}_{5C}}-\sqrt{\tilde{\sigma}_{5C}\tilde{a}_{52}}\right)^2<&d<\left(\sqrt{\tilde{\rho}_{5C}}+\sqrt{\tilde{\sigma}_{5C}\tilde{a}_{52}}\right)^2\\ \tilde{M}(\tilde{\rho}_{5C},\tilde{\sigma}_{5C},\tilde{a}_{52})<&\tilde{d}<\left(\sqrt{\tilde{\rho}_{5C}}+\sqrt{\tilde{\sigma}_{5C}\tilde{a}_{52}}\right)^2.\end{aligned}\tag{123}$$

Hence $\tilde{C}_{1,2}$ are real for values for values of d outside the range specified in [Eq. 123]. There are two possible cases to consider,

1. $\tilde{d}>\left(\sqrt{\tilde{\rho}_{5C}}+\sqrt{\tilde{\sigma}_{5C}\tilde{a}_{52}}\right)^2$.
2. $\tilde{d}<\tilde{M}=\left(\sqrt{\tilde{\rho}_{5C}}-\sqrt{\tilde{\sigma}_{5C}\tilde{a}_{52}}\right)^2$.

Case 1: We will show that in the case where,

$$\tilde{d}>\left(\sqrt{\tilde{\rho}_{5C}}+\sqrt{\tilde{\sigma}_{5C}\tilde{a}_{52}}\right)^2$$

then $\tilde{C}_{1,2}$ are both negative. In order to show this we will use the fact that, in this case, $\tilde{d}>\tilde{\rho}_{5C}-\tilde{\sigma}_{5C}\tilde{a}_{52}$. This is derived as follows,

$$\begin{aligned}&\tilde{d}>\tilde{\rho}_{5C}+2\sqrt{\tilde{\rho}_{5C}\tilde{\sigma}_{5C}\tilde{a}_{52}}+\tilde{\sigma}_{5C}\tilde{a}_{52}\\ &\tilde{d}>\tilde{\rho}_{5C}+\tilde{\sigma}_{5C}\tilde{a}_{52}\\ &\tilde{d}>\tilde{\rho}_{5C}-\tilde{\sigma}_{5C}\tilde{a}_{52}\quad\text{since}\quad\tilde{\sigma}_{5C}\tilde{a}_{52}>0\end{aligned}$$

Now $\tilde{C}_1<0$ if,

$$\frac{-\left(\frac{\tilde{d}-(\tilde{\rho}_{5C}-\tilde{\sigma}_{5C}\tilde{a}_{52})}{\tilde{\sigma}_{5C}}\right)+\sqrt{\left(\frac{\tilde{d}-(\tilde{\rho}_{5C}-\tilde{\sigma}_{5C}\tilde{a}_{52})}{\tilde{\sigma}_{5C}}\right)^2-\frac{4\tilde{d}\tilde{a}_{52}}{\tilde{\sigma}_{5C}}}}{2}<0$$
$$\sqrt{\left(\frac{\tilde{d}-(\tilde{\rho}_{5C}-\tilde{\sigma}_{5C}\tilde{a}_{52})}{\tilde{\sigma}_{5C}}\right)^2-\frac{4\tilde{d}\tilde{a}_{52}}{\tilde{\sigma}_{5C}}}<\frac{\tilde{d}-(\tilde{\rho}_{5C}-\tilde{\sigma}_{5C}\tilde{a}_{52})}{\tilde{\sigma}_{5C}}$$

We now use the fact that $\tilde{d} > \tilde{\rho}_{5C} - \tilde{\sigma}_{5C}\tilde{a}_{52}$, which allows us to square both sides giving,

$$-\frac{4\tilde{d}\tilde{a}_{52}}{\tilde{\sigma}_{5C}} < 0,$$

which is always true since $\tilde{d}, \tilde{a}_{52}, \tilde{\sigma}_{5C} > 0$. Similarly $\tilde{C}_2 < 0$ if,

$$\frac{-\left(\frac{\tilde{d}-(\tilde{\rho}_{5C}-\tilde{\sigma}_{5C}\tilde{a}_{52})}{\tilde{\sigma}_{5C}}\right) - \sqrt{\left(\frac{\tilde{d}-(\tilde{\rho}_{5C}-\tilde{\sigma}_{5C}\tilde{a}_{52})}{\tilde{\sigma}_{5C}}\right)^2 - \frac{4\tilde{d}\tilde{a}_{52}}{\tilde{\sigma}_{5C}}}}{2} < 0$$

$$-\sqrt{\left(\frac{\tilde{d}-(\tilde{\rho}_{5C}-\tilde{\sigma}_{5C}\tilde{a}_{52})}{\tilde{\sigma}_{5C}}\right)^2 - \frac{4\tilde{d}\tilde{a}_{52}}{\tilde{\sigma}_{5C}}} < \frac{\tilde{d}-(\tilde{\rho}_{5C}-\tilde{\sigma}_{5C}\tilde{a}_{52})}{\tilde{\sigma}_{5C}},$$

which must be true since $\tilde{d} > \tilde{\rho}_{5C} - \tilde{\sigma}_{5C}\tilde{a}_{52}$ and the square root of a positive number is always positive. Thus, $\tilde{C}_{1,2}$ are both nonphysical (negative) for $\tilde{d} > \left(\sqrt{\tilde{\rho}_{5C}} + \sqrt{\tilde{\sigma}_{5C}\tilde{a}_{52}}\right)^2$.

Case 2: We will show that in the case where,

$$\tilde{d} < \tilde{M} = \left(\sqrt{\tilde{\rho}_{5C}} - \sqrt{\tilde{\sigma}_{5C}\tilde{a}_{52}}\right)^2$$

then $\tilde{C}_{1,2}$ are both positive. In order to show this we will use the fact that, in this case, $\tilde{d} < \tilde{\rho}_{5C} - \tilde{\sigma}_{5C}\tilde{a}_{52}$. This is derived as follows,

we have that,

$$\tilde{d} < \tilde{\rho}_{5C} - 2\sqrt{\tilde{\rho}_{5C}\tilde{\sigma}_{5C}\tilde{a}_{52}} + \tilde{\sigma}_{5C}\tilde{a}_{52}$$

now recall,

$$\begin{aligned}
\tilde{\rho}_{5C} &> \tilde{\sigma}_{5C}\tilde{a}_{52} \\
\sqrt{\rho_{5C}} &> \sqrt{\sigma_{5C}a52} \\
-2\sqrt{\tilde{\rho}_{5C}\tilde{\sigma}_{5C}\tilde{a}_{52}} &< -2\tilde{\sigma}_{5C}\tilde{a}_{52}
\end{aligned}$$

thus,

$$\begin{aligned}
d &< \tilde{\rho}_{5C} - 2\tilde{\sigma}_{5C}\tilde{a}_{52} + \tilde{\sigma}_{5C}\tilde{a}_{52} \\
d &< \tilde{\rho}_{5C} - \tilde{\sigma}_{5C}\tilde{a}_{52}
\end{aligned}$$

Now, $\tilde{C}_1 < 0$ if,

$$\frac{-\left(\frac{\tilde{d}-(\tilde{\rho}_{5C}-\tilde{\sigma}_{5C}\tilde{a}_{52})}{\tilde{\sigma}_{5C}}\right)+\sqrt{\left(\frac{\tilde{d}-(\tilde{\rho}_{5C}-\tilde{\sigma}_{5C}\tilde{a}_{52})}{\tilde{\sigma}_{5C}}\right)^2-\frac{4\tilde{d}\tilde{a}_{52}}{\tilde{\sigma}_{5C}}}}{2}<0$$

$$\sqrt{\left(\frac{\tilde{d}-(\tilde{\rho}_{5C}-\tilde{\sigma}_{5C}\tilde{a}_{52})}{\tilde{\sigma}_{5C}}\right)^2-\frac{4\tilde{d}\tilde{a}_{52}}{\tilde{\sigma}_{5C}}}<\frac{\tilde{d}-(\tilde{\rho}_{5C}-\tilde{\sigma}_{5C}\tilde{a}_{52})}{\tilde{\sigma}_{5C}},$$

which cannot be true since $\tilde{d} < \tilde{\rho}_{5C} - \tilde{\sigma}_{5C}\tilde{a}_{52}$ and the square root of a positive number is positive. Similarly, $\tilde{C}_2 < 0$ if,

$$\frac{-\left(\frac{\tilde{d}-(\tilde{\rho}_{5C}-\tilde{\sigma}_{5C}\tilde{a}_{52})}{\tilde{\sigma}_{5C}}\right)-\sqrt{\left(\frac{\tilde{d}-(\tilde{\rho}_{5C}-\tilde{\sigma}_{5C}\tilde{a}_{52})}{\tilde{\sigma}_{5C}}\right)^2-\frac{4\tilde{d}\tilde{a}_{52}}{\tilde{\sigma}_{5C}}}}{2}<0$$

$$-\sqrt{\left(\frac{\tilde{d}-(\tilde{\rho}_{5C}-\tilde{\sigma}_{5C}\tilde{a}_{52})}{\tilde{\sigma}_{5C}}\right)^2-\frac{4\tilde{d}\tilde{a}_{52}}{\tilde{\sigma}_{5C}}}<\frac{\tilde{d}-(\tilde{\rho}_{5C}-\tilde{\sigma}_{5C}\tilde{a}_{52})}{\tilde{\sigma}_{5C}}$$

$$\sqrt{\left(\frac{\tilde{d}-(\tilde{\rho}_{5C}-\tilde{\sigma}_{5C}\tilde{a}_{52})}{\tilde{\sigma}_{5C}}\right)^2-\frac{4\tilde{d}\tilde{a}_{52}}{\tilde{\sigma}_{5C}}}>-\left(\frac{\tilde{d}-(\tilde{\rho}_{5C}-\tilde{\sigma}_{5C}\tilde{a}_{52})}{\tilde{\sigma}_{5C}}\right)$$

Both sides of this equation are positive since, $\tilde{d} < \tilde{\rho}_{5C} - \tilde{\sigma}_{5C}\tilde{a}_{52}$, so we can square both sides to obtain,

$$-\frac{4\tilde{d}\tilde{a}_{52}}{\tilde{\sigma}_{5C}} > 0$$

Which cannot be true since, $\tilde{d}, \tilde{a}_{52}, \tilde{\sigma}_{5C} > 0$.

Thus, $\tilde{C}_{1,2}$ exist and are positive for $0 < \tilde{d} < \tilde{M}$. Therefore, to ensure that there is no $\tilde{C} > 0$ for which the equilibrium is undefined, we only require,

$$\tilde{d} > \tilde{M} = \left(\sqrt{\tilde{\rho}_{5C}} - \sqrt{\tilde{\sigma}_{5C}\tilde{a}_{52}}\right)^2.$$

A.7 Behaviour of $\tilde{x}_5^e$ on separate intervals of $\tilde{C}$.

We have already established that if $\tilde{x}_5^e > 0$ then $\tilde{x}_5^e$ is stable, and if $\tilde{x}_5^e < 0$ then $\tilde{x}_5^e$ is unstable. We simply need to compute the sign of [Eq. 70],

$$-\left(\frac{d}{d\tilde{x}_5}\frac{d\tilde{x}_5^e}{d\tilde{t}}\right)\Bigg|_{\tilde{x}_5=\tilde{x}_5^e} = \tilde{d} - \tilde{\rho}_{5C}\frac{\tilde{C}}{\tilde{a}_{52}+\tilde{C}} + \tilde{\sigma}_{5C}\tilde{C} \tag{124}$$

on the each of the intervals: $[0, \tilde{C}_1)$, $(\tilde{C}_1, \tilde{C}_2)$ and $(\tilde{C}_2, \infty)$. The approach we will take will be to show that [Eq. 124] is a continuous function of $\tilde{C}$ over the

interval $[0, \infty)$, and that it's sign is positive at $\tilde{C} = 0$. Then, since the function is continuous and only has the non-repeated roots $\tilde{C}_1$ and $\tilde{C}_2$, the sign will be negative for $\tilde{C} \in (\tilde{C}_1, \tilde{C}_2)$ and positive for $\tilde{C} \in [0, \infty) \backslash [\tilde{C}_1, \tilde{C}_2]$.

$$\begin{aligned}
&\frac{d}{d\tilde{C}}\left(\tilde{d} - \tilde{\rho}_{5C}\frac{\tilde{C}}{\tilde{a}_{52}+\tilde{C}} + \tilde{\sigma}_{5C}\tilde{C}\right) \\
=&\tilde{\rho}_{5C}\left(\frac{1}{\tilde{a}_{52}+\tilde{C}} - \frac{\tilde{C}}{(\tilde{a}_{52}+\tilde{C})^2}\right) + \tilde{\sigma}_{5C} \\
=&\tilde{\rho}_{5C}\frac{\tilde{a}_{52}}{(\tilde{a}_{52}+\tilde{C})^2} + \tilde{\sigma}_{5C}.
\end{aligned}$$

Hence, [Eq. 124] has a well defined derivative everywhere except for $\tilde{C} = -\tilde{a}_{52} < 0$. Thus, it is differentiable on $[0, \infty)$ and therefore continuous on $[0, \infty)$. We also have that,

$$\begin{aligned}
&\left(\tilde{d} - \tilde{\rho}_{5C}\frac{\tilde{C}}{\tilde{a}_{52}+\tilde{C}} + \tilde{\sigma}_{5C}\tilde{C}\right)\Bigg|_{\tilde{C}=0} \\
=&\tilde{d} > 0,
\end{aligned}$$

therefore the argument holds and we have: $\tilde{x}_5^e > 0$ and stable for $\tilde{C} \in [0, \tilde{C}_1)$, $\tilde{x}_5^e < 0$ and unstable for $\tilde{C} \in (\tilde{C}_1, \tilde{C}_2)$ and $\tilde{x}_5^e > 0$ and stable for $\tilde{C} \in (\tilde{C}_2, \infty)$.

A.8 Solving for $\psi_{0,1,2,3}$.

Substituting [Eq. 84] into [Eq. 74] and setting $\frac{d\tilde{x}_1}{d\tilde{t}} = 0$ we obtain,

$$\begin{aligned}
0 = &\left(1 + \tilde{\rho}_{C3}\frac{\tilde{A}\,(1+a_C)}{\tilde{A}+a_C} - \tilde{\gamma}_T\right)\tilde{x}_1 - \tilde{\gamma}\tilde{x}_1^2 \\
&- \tilde{\sigma}_{15}e^{-\tilde{\kappa}_5\tilde{A}}\tilde{x}_1\left(\frac{\tilde{d}}{\tilde{d} - \tilde{\rho}_{5C}\left(\frac{\tilde{x}_1}{\tilde{a}_{52}+\tilde{x}_1}\right) + \tilde{\sigma}_{5C}\tilde{x}_1}\right)
\end{aligned}$$

We already have the solution for $\tilde{x}_1 = 0$, so we will assume $\tilde{x}_1 \neq 0$,

$$\begin{aligned}
= &\left(1 + \tilde{\rho}_{C3}\frac{\tilde{A}\,(1+a_C)}{\tilde{A}+a_C} - \tilde{\gamma}_T\right) - \tilde{\gamma}\tilde{x}_1 \\
&- \tilde{\sigma}_{15}e^{-\tilde{\kappa}_5\tilde{A}}\left(\frac{\tilde{d}}{\tilde{d} - \tilde{\rho}_{5C}\left(\frac{\tilde{x}_1}{\tilde{a}_{52}+\tilde{x}_1}\right) + \tilde{\sigma}_{5C}\tilde{x}_1}\right)
\end{aligned}$$

let,

$$\zeta_3 = 1 + \tilde{\rho}_{C3}\frac{\tilde{A}\,(1+a_C)}{\tilde{A}+a_C} - \tilde{\gamma}_T$$

then,

$$\begin{aligned}
0 =& \zeta_3 - \tilde{\gamma}\tilde{x}_1 - \tilde{\sigma}_{15}e^{-\tilde{\kappa}_5\tilde{A}}\left(\frac{\tilde{d}}{\tilde{d}-\tilde{\rho}_{5C}\left(\frac{\tilde{x}_1}{\tilde{a}_{52}+\tilde{x}_1}\right)+\tilde{\sigma}_{5C}\tilde{x}_1}\right)\\
=& \zeta_3\left(\tilde{d}-\tilde{\rho}_{5C}\left(\frac{\tilde{x}_1}{\tilde{a}_{52}+\tilde{x}_1}\right)+\tilde{\sigma}_{5C}\tilde{x}_1\right)-\tilde{\gamma}\tilde{x}_1\left(\tilde{d}-\tilde{\rho}_{5C}\left(\frac{\tilde{x}_1}{\tilde{a}_{52}+\tilde{x}_1}\right)+\tilde{\sigma}_{5C}\tilde{x}_1\right)\\
&-\tilde{\sigma}_{15}\tilde{d}e^{-\tilde{\kappa}_5\tilde{A}}\\
=& \underbrace{\left[-\tilde{\gamma}\tilde{\sigma}_{5C}\right]}_{\psi_3}\tilde{x}_1^3+\underbrace{\left[\zeta_3\tilde{\sigma}_{5C}-\tilde{\gamma}\tilde{d}+\tilde{\gamma}\tilde{\rho}_{5C}-\tilde{\gamma}\tilde{a}_{52}\tilde{\sigma}_{5C}\right]}_{\psi_2}\tilde{x}_1^2\\
&\underbrace{\left[\zeta_3\tilde{d}-\zeta_3\tilde{\rho}_{5C}+\zeta_3\tilde{a}_{52}\tilde{\sigma}_{5C}-\tilde{\gamma}\tilde{a}_{52}\tilde{d}-\tilde{\sigma}_{15}\tilde{a}_{52}\tilde{d}e^{-\tilde{\kappa}_5\tilde{A}}\right]}_{\psi_1}\tilde{x}_1\\
&+\underbrace{\left[\zeta_3\tilde{a}_{52}\tilde{d}-\tilde{\sigma}_{15}\tilde{a}_{52}\tilde{d}e^{-\tilde{\kappa}_5\tilde{A}}\right]}_{\psi_0}
\end{aligned}$$

Following the approach of Kuznetsov et al. [38] and using Descartes' rule of signs, we can produce the following table which describes the number of positive, real roots of [Eq. 85] for different combinations of the signs of the coefficients ψ_0, ψ_1, ψ_2 and ψ_3. Note that we must have $\psi_3 < 0$ in each case since $\tilde{\gamma} > 0$ and $\tilde{\sigma}_{5C} > 0$.

# of Positive Real Roots	Sign of ...			
	ψ_3	ψ_2	ψ_1	ψ_0
0	−	−	−	−
0 or 2	−	+	−	−
	−	−	+	−
	−	+	+	−
1	−	−	−	+
	−	−	+	+
	−	+	+	+
1 or 3	−	+	−	+

Table 1: Table providing the possible number of positive, real roots of [Eq. 85] for different combinations of signs of the coefficients ψ_3, ψ_2, ψ_1 and ψ_0

B Complete Model Equations Prior to Any Rescalings.

The model equations prior to any variable rescalings, and in terms of $D(t)$, are given by,

$$\begin{aligned}
\dot{x}_1 &= \left(r_1 - \frac{\lambda}{D_{\text{MTD}}} D(t) e^{-\kappa_D x_3} + \rho_{13} \frac{x_3(1+a_1)}{x_3 + a_1 T}\right) x_1 - x_1\left[\gamma_{11} x_1 + \gamma_{12} x_2 + \gamma_{1T} T\right] \\
&\quad - \frac{\delta_1}{D_{\text{MTD}}} D(t) e^{-\kappa_D x_3} x_1 - \sigma_{15} x_5 e^{-\kappa_5 x_3} x_1 \\
\dot{x}_2 &= \frac{\lambda}{D_{\text{MTD}}} D(t) e^{-\kappa_D x_3} x_1 + \left(r_2 + \rho_{23} \frac{x_3(1+a_2)}{x_3 + a_2 T}\right) x_2 - x_2\left[\gamma_{21} x_1 + \gamma_{22} x_2 + \gamma_{2T} T\right] \\
&\quad - \frac{\delta_2}{D_{\text{MTD}}} D(t) e^{-\kappa_D x_3} x_2 - \sigma_{25} x_5 e^{-\kappa_5 x_3} x_2 \\
\dot{x}_3 &= \nu_3 \left(\frac{e^{\frac{a_3 D(t)}{D_{\text{MTD}}}} - 1}{e^{a_3} - 1}\right)(T - x_3) - \frac{\delta_3 D(t)}{D_{\text{MTD}}} x_3 + \rho_{31} x_1 (T - x_3) \\
&\quad + \rho_{32} x_2 (T - x_3) - \epsilon x_3 \\
x_4 &= T - x_3 \\
\dot{x}_5 &= s\Phi_{51}(D(t)) - d x_5 + \rho_{5C} \left(\frac{x_1 + x_2}{a_{52} + x_1 + x_2}\right) x_5 - \sigma_{5C}(x_1 + x_2) x_5
\end{aligned}$$

where,

$$\Phi_{51}(D(t)) = \frac{e^{a_{51} b} + e^{-\eta a_{51} b}}{e^{-\left(\frac{a_{51}}{D_{\text{MTD}}}\right)(D(t) - b D_{\text{MTD}})} + e^{\eta\left(\frac{a_{51}}{D_{\text{MTD}}}\right)(D(t) - b D_{\text{MTD}})}}$$

with,

$$\begin{aligned}
b D_{\text{MTD}} &= \tilde{D}_{\text{opt},5} D_{\text{MTD}} + \frac{\ln(\eta)}{\frac{a_{51}}{D_{\text{MTD}}} + \eta \frac{a_{51}}{D_{\text{MTD}}}} \\
&= D_{\text{opt},5} + \frac{\ln(\eta)}{\frac{a_{51}}{D_{\text{MTD}}} + \eta \frac{a_{51}}{D_{\text{MTD}}}}
\end{aligned}$$

C Code Availability Statement

The Python code used to generate the figures in this thesis may be found at `https://github.com/Thomas-28/Masters-by-Research`.

References

[1] Bruce Alberts, Alexander Johnson, Julian Lewis, Martin Raff, Keith Roberts, and Peter Walter. Cancer as a microevolutionary process. In *Molecular Biology of the Cell. 4th edition*. Garland Science, 2002.

[2] Bruce Alberts, Alexander Johnson, Julian Lewis, Martin Raff, Keith Roberts, and Peter Walter. Pathogens, infection and innate immunity. In *Molecular Biology of the Cell. 4th edition*. Garland Science, 2002.

[3] Philipp M Altrock, Lin L Liu, and Franziska Michor. The mathematics of cancer: integrating quantitative models. *Nature Reviews Cancer*, 15(12):730–745, 2015.

[4] Giulia Biffi and David A Tuveson. Diversity and biology of cancer-associated fibroblasts. *Physiological reviews*, 2020.

[5] Padmini Bisoyi. Malignant tumors–as cancer. In *Understanding Cancer*, pages 21–36. Elsevier, 2022.

[6] Hossein Borghaei, Mitchell R Smith, and Kerry S Campbell. Immunotherapy of cancer. *European journal of pharmacology*, 625(1-3):41–54, 2009.

[7] L Bracci, G Schiavoni, A Sistigu, and F Belardelli. Immune-based mechanisms of cytotoxic chemotherapy: implications for the design of novel and rationale-based combined treatments against cancer. *Cell Death & Differentiation*, 21(1):15–25, 2014.

[8] Roy M Bremnes, Tom Dønnem, Samer Al-Saad, Khalid Al-Shibli, Sigve Andersen, Rafael Sirera, Carlos Camps, Inigo Marinez, and Lill-Tove Busund. The role of tumor stroma in cancer progression and prognosis: emphasis on carcinoma-associated fibroblasts and non-small cell lung cancer. *Journal of thoracic oncology*, 6(1):209–217, 2011.

[9] Petter Brodin and Mark M Davis. Human immune system variation. *Nature reviews immunology*, 17(1):21–29, 2017.

[10] Karol Bukowski, Mateusz Kciuk, and Renata Kontek. Mechanisms of multidrug resistance in cancer chemotherapy. *International journal of molecular sciences*, 21(9):3233, 2020.

[11] HM Byrne, T Alarcon, MR Owen, SD Webb, and PK Maini. Modelling aspects of cancer dynamics: a review. *Philosophical Transactions*

of the Royal Society A: Mathematical, Physical and Engineering Sciences, 364(1843):1563–1578, 2006.

[12] Alessandro Caporale, Anna Rita Vestri, Eugenio Benvenuto, Mauro Mariotti, Umile Michele Cosenza, Massimo Scarpini, Andrea Giuliani, Pietro Mingazzini, and Francesco Angelico. Is desmoplasia a protective factor for survival in patients with colorectal carcinoma? *Clinical Gastroenterology and Hepatology*, 3(4):370–375, 2005.

[13] Tze-Sian Chan, Chung-Chi Hsu, Vincent C Pai, Wen-Ying Liao, Shenq-Shyang Huang, Kok-Tong Tan, Chia-Jui Yen, Shu-Ching Hsu, Wei-Yu Chen, Yan-Shen Shan, et al. Metronomic chemotherapy prevents therapy-induced stromal activation and induction of tumor-initiating cells. *Journal of Experimental Medicine*, 213(13):2967–2988, 2016.

[14] Gerald C Chu, Alec C Kimmelman, Aram F Hezel, and Ronald A DePinho. Stromal biology of pancreatic cancer. *Journal of cellular biochemistry*, 101(4):887–907, 2007.

[15] European Commission. Europe's beating cancer plan. `https://commission.europa.eu/strategy-and-policy/priorities-2019-2024/promoting-our-european-way-life/european-health-union/cancer-plan-europe_en`, Feb 2021.

[16] Ralf-Peter Czekay, Dong-Joo Cheon, Rohan Samarakoon, Stacie M Kutz, and Paul J Higgins. Cancer-associated fibroblasts: mechanisms of tumor progression and novel therapeutic targets. *Cancers*, 14(5):1231, 2022.

[17] Ian A Darby, Betty Laverdet, Frédéric Bonté, and Alexis Desmoulière. Fibroblasts and myofibroblasts in wound healing. *Clinical, cosmetic and investigational dermatology*, pages 301–311, 2014.

[18] PW Dempsey, SA Vaidya, and G Cheng. The art of war: Innate and adaptive immune responses. *Cellular and Molecular Life Sciences CMLS*, 60:2604–2621, 2003.

[19] Pinky Dua, Vivek Dua, and Efstratios N Pistikopoulos. Optimal delivery of chemotherapeutic agents in cancer. *Computers & Chemical Engineering*, 32(1-2):99–107, 2008.

[20] Werner Dubitzky, Olaf Wolkenhauer, Kwang-Hyun Cho, and Hiroki Yokota. *Encyclopedia of systems biology*, volume 402. Springer New York, NY, USA:, 2013.

[21] Elisa D'Arcangelo, Nila C Wu, Jose L Cadavid, and Alison P McGuigan. The life cycle of cancer-associated fibroblasts within the tumour stroma and its importance in disease outcome. *British journal of cancer*, 122(7):931–942, 2020.

[22] Pedro M Enriquez-Navas, Jonathan W Wojtkowiak, and Robert A Gatenby. Application of evolutionary principles to cancer therapy. *Cancer research*, 75(22):4675–4680, 2015.

[23] Christine E Eyler and Jeremy N Rich. Survival of the fittest: cancer stem cells in therapeutic resistance and angiogenesis. *Journal of Clinical Oncology*, 26(17):2839–2845, 2008.

[24] Bing Feng, Jianzhong Wu, Bo Shen, Feng Jiang, and Jifeng Feng. Cancer-associated fibroblasts and resistance to anticancer therapies: Status, mechanisms, and countermeasures. *Cancer Cell International*, 22(1):166, 2022.

[25] Edward H Flach, Vito W Rebecca, Meenhard Herlyn, Keiran SM Smalley, and Alexander RA Anderson. Fibroblasts contribute to melanoma tumor growth and drug resistance. *Molecular pharmaceutics*, 8(6):2039–2049, 2011.

[26] EA Gaffney. The mathematical modelling of adjuvant chemotherapy scheduling: incorporating the effects of protocol rest phases and pharmacokinetics. *Bulletin of mathematical biology*, 67:563–611, 2005.

[27] Lorenzo Galluzzi, Juliette Humeau, Aitziber Buqué, Laurence Zitvogel, and Guido Kroemer. Immunostimulation with chemotherapy in the era of immune checkpoint inhibitors. *Nature reviews Clinical oncology*, 17(12):725–741, 2020.

[28] Sara Hamis, Gibin G Powathil, and Mark AJ Chaplain. Blackboard to bedside: a mathematical modeling bottom-up approach toward personalized cancer treatments. *JCO clinical cancer informatics*, 3:1–11, 2019.

[29] Danielle M Hari, Anna M Leung, Ji-Hey Lee, Myung-Shin Sim, Brooke Vuong, Connie G Chiu, and Anton J Bilchik. Ajcc cancer staging manual 7th edition criteria for colon cancer: do the complex modifications improve prognostic assessment? *Journal of the American College of Surgeons*, 217(2):181–190, 2013.

[30] James Harper and Richard CA Sainson. Regulation of the anti-tumour immune response by cancer-associated fibroblasts. In *Seminars in cancer biology*, volume 25, pages 69–77. Elsevier, 2014.

[31] Bikash Chandra Jena, Chandan Kanta Das, Deblina Bharadwaj, and Mahitosh Mandal. Cancer associated fibroblast mediated chemoresistance: A paradigm shift in understanding the mechanism of tumor progression. *Biochimica et Biophysica Acta (BBA)-Reviews on Cancer*, 1874(2):188416, 2020.

[32] Peter AS Johnstone, Marilyn S Norton, and Robert H Riffenburgh. Survival of patients with untreated breast cancer. *Journal of surgical oncology*, 73(4):273–277, 2000.

[33] Kevin J Kaczorowski, Karthik Shekhar, Dieudonné Nkulikiyimfura, Cornelia L Dekker, Holden Maecker, Mark M Davis, Arup K Chakraborty, and Petter Brodin. Continuous immunotypes describe human immune variation and predict diverse responses. *Proceedings of the National Academy of Sciences*, 114(30):E6097–E6106, 2017.

[34] Raghu Kalluri. The biology and function of fibroblasts in cancer. *Nature Reviews Cancer*, 16(9):582–598, 2016.

[35] Raghu Kalluri and Michael Zeisberg. Fibroblasts in cancer. *Nature reviews cancer*, 6(5):392–401, 2006.

[36] Emilia Kozłowska, Anniina Färkkilä, Tuulia Vallius, Olli Carpén, Jukka Kemppainen, Seija Grénman, Rainer Lehtonen, Johanna Hynninen, Sakari Hietanen, and Sampsa Hautaniemi. Mathematical modeling predicts response to chemotherapy and drug combinations in ovarian cancer. *Cancer research*, 78(14):4036–4044, 2018.

[37] Masaru Kubota, Ying-Wei Lin, Keigo Hamahata, Machiko Sawada, Seiji Koishi, Haruyo Hirota, and Yoshihiro Wakazono. Cancer chemotherapy and somatic cell mutation. *Mutation Research/Genetic Toxicology and Environmental Mutagenesis*, 470(2):93–102, 2000.

[38] Vladimir A Kuznetsov, Iliya A Makalkin, Mark A Taylor, and Alan S Perelson. Nonlinear dynamics of immunogenic tumors: parameter estimation and global bifurcation analysis. *Bulletin of mathematical biology*, 56(2):295–321, 1994.

[39] Matthew A Lakins, Ehsan Ghorani, Hafsa Munir, Carla P Martins, and Jacqueline D Shields. Cancer-associated fibroblasts induce antigen-specific deletion of cd8+ t cells to protect tumour cells. *Nature communications*, 9(1):948, 2018.

[40] Lucie Laplane, Dorothée Duluc, Andreas Bikfalvi, Nicolas Larmonier, and Thomas Pradeu. Beyond the tumour microenvironment. *International journal of cancer*, 145(10):2611–2618, 2019.

[41] Xu Lei, Yu Lei, Jin-Ke Li, Wei-Xing Du, Ru-Gui Li, Jing Yang, Jian Li, Fang Li, and Hua-Bing Tan. Immune cells within the tumor microenvironment: Biological functions and roles in cancer immunotherapy. *Cancer letters*, 470:126–133, 2020.

[42] Ana Maia and Stefan Wiemann. Cancer-associated fibroblasts: implications for cancer therapy. *Cancers*, 13(14):3526, 2021.

[43] Rituparna Maiti. Metronomic chemotherapy. *Journal of pharmacology and pharmacotherapeutics*, 5(3):186–192, 2014.

[44] Alberto Mantovani, Paola Allavena, Federica Marchesi, and Cecilia Garlanda. Macrophages as tools and targets in cancer therapy. *Nature reviews Drug discovery*, 21(11):799–820, 2022.

[45] Xiaoqi Mao, Jin Xu, Wei Wang, Chen Liang, Jie Hua, Jiang Liu, Bo Zhang, Qingcai Meng, Xianjun Yu, and Si Shi. Crosstalk between cancer-associated fibroblasts and immune cells in the tumor microenvironment: new findings and future perspectives. *Molecular cancer*, 20(1):1–30, 2021.

[46] Yan Mao, Evan T Keller, David H Garfield, Kunwei Shen, and Jianhua Wang. Stromal cells in tumor microenvironment and breast cancer. *Cancer and Metastasis Reviews*, 32:303–315, 2013.

[47] Ariel E Marciscano and Niroshana Anandasabapathy. The role of dendritic cells in cancer and anti-tumor immunity. In *Seminars in immunology*, volume 52, page 101481. Elsevier, 2021.

[48] RB Martin, ME Fisher, RF Minchin, and KL Teo. A mathematical model of cancer chemotherapy with an optimal selection of parameters. *Mathematical biosciences*, 99(2):205–230, 1990.

[49] RB Martin, ME Fisher, RF Minchin, and KL Teo. Optimal control of tumor size used to maximize survival time when cells are resistant to chemotherapy. *Mathematical biosciences*, 110(2):201–219, 1992.

[50] Luis Martínez-Lostao, Alberto Anel, and Julián Pardo. How do cytotoxic lymphocytes kill cancer cells? *Clinical cancer research*, 21(22):5047–5056, 2015.

[51] Scott McComb, Aude Thiriot, Bassel Akache, Lakshmi Krishnan, and Felicity Stark. Introduction to the immune system. *Immunoproteomics: methods and protocols*, pages 1–24, 2019.

[52] Matthew L Meizlish, Ruth A Franklin, Xu Zhou, and Ruslan Medzhitov. Tissue homeostasis and inflammation. *Annual review of immunology*, 39:557–581, 2021.

[53] Marco Carlo Merlano, Nerina Denaro, Danilo Galizia, Fiorella Ruatta, Marcella Occelli, Silvia Minei, Andrea Abbona, Matteo Paccagnella, Michele Ghidini, and Ornella Garrone. How chemotherapy affects the tumor immune microenvironment: a narrative review. *Biomedicines*, 10(8):1822, 2022.

[54] AM Moorman, R Vink, HJ Heijmans, J Van Der Palen, and EA Kouwenhoven. The prognostic value of tumour-stroma ratio in triple-negative breast cancer. *European Journal of Surgical Oncology (EJSO)*, 38(4):307–313, 2012.

[55] Larry Norton[1]. The norton-simon hypothesis revisited. *Cancer treatment reports*, 70(1):163, 1986.

[56] Peter Nygren. What is cancer chemotherapy? *Acta Oncologica*, 40(2-3):166–174, 2001.

[57] J Tinsley Oden, Ernesto ABF Lima, Regina C Almeida, Yusheng Feng, Marissa Nichole Rylander, David Fuentes, Danial Faghihi, Mohammad M Rahman, Matthew DeWitt, Manasa Gadde, et al. Toward predictive multiscale modeling of vascular tumor growth: computational and experimental oncology for tumor prediction. *Archives of Computational Methods in Engineering*, 23:735–779, 2016.

[58] Central Statistics Office. Vital statistics yearly summary 2022. `https://www.cso.ie/en/releasesandpublications/ep/p-vsys/vitalstatisticsyearlysummary2022/`, May 2023.

[59] Akira Orimo, Piyush B Gupta, Dennis C Sgroi, Fernando Arenzana-Seisdedos, Thierry Delaunay, Rizwan Naeem, Vincent J Carey, Andrea L Richardson, and Robert A Weinberg. Stromal fibroblasts present in invasive human breast carcinomas promote tumor growth and angiogenesis through elevated sdf-1/cxcl12 secretion. *Cell*, 121(3):335–348, 2005.

[60] Eoin O'Sullivan, Kieran Mulchrone, and Sebastian Wieczorek. Rate-induced tipping to metastable zombie fires. *Proceedings of the Royal Society A*, 479(2275):20220647, 2023.

[61] Derek S Park, Mark Robertson-Tessi, Kimberly A Luddy, Philip K Maini, Michael B Bonsall, Robert A Gatenby, and Alexander RA Anderson. The goldilocks window of personalized chemotherapy: getting the immune response just right. *Cancer research*, 79(20):5302–5315, 2019.

[62] Yeon Hee Park, Samir Lal, Jeong Eon Lee, Yoon-La Choi, Ji Wen, Sripad Ram, Ying Ding, Soo-Hyeon Lee, Eric Powell, Se Kyung Lee, et al. Chemotherapy induces dynamic immune responses in breast cancers that impact treatment outcome. *Nature communications*, 11(1):6175, 2020.

[63] Maria Peiris-Pagès, Federica Sotgia, and Michael P Lisanti. Chemotherapy induces the cancer-associated fibroblast phenotype, activating paracrine hedgehog-gli signalling in breast cancer cells. *Oncotarget*, 6(13):10728, 2015.

[64] Noemi Picco, Erik Sahai, Philip K Maini, and Alexander RA Anderson. Integrating models to quantify environment-mediated drug resistance. *Cancer research*, 77(19):5409–5418, 2017.

[65] Qinrong Ping, Ruping Yan, Xin Cheng, Wenju Wang, Yiming Zhong, Zongliu Hou, Yunqiang Shi, Chunhui Wang, and Ruhong Li. Cancer-associated fibroblasts: Overview, progress, challenges, and directions. *Cancer gene therapy*, 28(9):984–999, 2021.

[66] Isabel Prager and Carsten Watzl. Mechanisms of natural killer cell-mediated cellular cytotoxicity. *Journal of leukocyte biology*, 105(6):1319–1329, 2019.

[67] Lucy Rasmussen and Ann Arvin. Chemotherapy-induced immunosuppression. *Environmental health perspectives*, 43:21–25, 1982.

[68] Cédric Rébé and François Ghiringhelli. Cytotoxic effects of chemotherapy on cancer and immune cells: how can it be modulated to generate novel therapeutic strategies? *Future Oncology*, 11(19):2645–2654, 2015.

[69] Chiara Riganti and Marialessandra Contino. New strategies to overcome resistance to chemotherapy and immune system in cancer, 2019.

[70] Erik Sahai, Igor Astsaturov, Edna Cukierman, David G DeNardo, Mikala Egeblad, Ronald M Evans, Douglas Fearon, Florian R Greten, Sunil R Hingorani, Tony Hunter, et al. A framework for advancing our understanding of cancer-associated fibroblasts. *Nature Reviews Cancer*, 20(3):174–186, 2020.

[71] Manfred Schwab. *Encyclopedia of cancer*. Springer, 2017.

[72] Robert J Seager, Cynthia Hajal, Fabian Spill, Roger D Kamm, and Muhammad H Zaman. Dynamic interplay between tumour, stroma and immune system can drive or prevent tumour progression. *Convergent science physical oncology*, 3(3):034002, 2017.

[73] Howard E Skipper, Frank M Schabel, and William S Wilcox. Experimental evaluation of potential anticancer agents. xiii. on the criteria and kinetics associated with "curability" of experimental leukemia. *Cancer Chemotherapy Reports*, 35, Feb 1964.

[74] Maike Sonnenberg, Heiko van der Kuip, Silke Haubeiß, Peter Fritz, Werner Schroth, Godehard Friedel, Wolfgang Simon, Thomas E Mürdter, and Walter E Aulitzky. Highly variable response to cytotoxic chemotherapy in carcinoma-associated fibroblasts (cafs) from lung and breast. *BMC cancer*, 8(1):1–13, 2008.

[75] Victoria Sopik and Steven A Narod. The relationship between tumour size, nodal status and distant metastases: on the origins of breast cancer. *Breast cancer research and treatment*, 170:647–656, 2018.

[76] John S Spratt, John S Meyer, and John A Spratt. Rates of growth of human neoplasms: Part ii. *Journal of surgical oncology*, 61(1):68–83, 1996.

[77] Kateřina Staňková, Joel S Brown, William S Dalton, and Robert A Gatenby. Optimizing cancer treatment using game theory: A review. *JAMA oncology*, 5(1):96–103, 2019.

[78] Triantafyllos Stylianopoulos, John D Martin, Vikash P Chauhan, Saloni R Jain, Benjamin Diop-Frimpong, Nabeel Bardeesy, Barbara L Smith, Cristina R Ferrone, Francis J Hornicek, Yves Boucher, et al. Causes, consequences, and remedies for growth-induced solid stress in murine and human tumors. *Proceedings of the National Academy of Sciences*, 109(38):15101–15108, 2012.

[79] Stuart E Turvey and David H Broide. Innate immunity. *Journal of Allergy and Clinical Immunology*, 125(2):S24–S32, 2010.

[80] Cancer Research UK. Your chemotherapy plan - length of treatment. `https://www.cancerresearchuk.org/about-cancer/treatment/chemotherapy/planning/your-chemotherapy-plan`, Dec 2023.

[81] Cristina Vaghi, Anne Rodallec, Raphaëlle Fanciullino, Joseph Ciccolini, Jonathan P Mochel, Michalis Mastri, Clair Poignard, John ML Ebos, and

Sébastien Benzekry. Population modeling of tumor growth curves and the reduced gompertz model improve prediction of the age of experimental tumors. *PLoS computational biology*, 16(2):e1007178, 2020.

[82] Matthew D Vesely, Michael H Kershaw, Robert D Schreiber, and Mark J Smyth. Natural innate and adaptive immunity to cancer. *Annual review of immunology*, 29(1):235–271, 2011.

[83] Dass S Vinay, Elizabeth P Ryan, Graham Pawelec, Wamidh H Talib, John Stagg, Eyad Elkord, Terry Lichtor, William K Decker, Richard L Whelan, HMC Shantha Kumara, et al. Immune evasion in cancer: Mechanistic basis and therapeutic strategies. In *Seminars in cancer biology*, volume 35, pages S185–S198. Elsevier, 2015.

[84] Yannick Viossat and Robert Noble. A theoretical analysis of tumour containment. *Nature ecology & evolution*, 5(6):826–835, 2021.

[85] Xuan Wang, Haiyun Zhang, and Xiaozhuo Chen. Drug resistance and combating drug resistance in cancer. *Cancer Drug Resistance*, 2(2):141, 2019.

[86] Robert A Weinberg. How cancer arises. *Scientific American*, 275(3):62–70, 1996.

[87] E John Wherry and Makoto Kurachi. Molecular and cellular insights into t cell exhaustion. *Nature reviews immunology*, 15(8):486–499, 2015.

[88] Yanpeng Yang, Yongchen Ma, Shen Yan, Pengyuan Wang, Jianwen Hu, Shanwen Chen, Jing Zhu, Jingui Wang, Guowei Chen, and Yucun Liu. Caf promotes chemoresistance through nrp2 in gastric cancer. *Gastric Cancer*, pages 1–12, 2022.

[89] Laurence Zitvogel, Lionel Apetoh, François Ghiringhelli, and Guido Kroemer. Immunological aspects of cancer chemotherapy. *Nature reviews immunology*, 8(1):59–73, 2008.